The role of Neuron Navigator 1 in vascular development

Dissertation

zur Erlangung des akademischen Grades

doctor rerum naturalium
(Dr. rer. nat.)

im Fach Biologie

eingereicht an der
Mathematisch-Naturwissenschaftlichen Fakultät I
der Humboldt-Universität zu Berlin

von

Stefan Kunert, M.Sc.

Präsident der Humboldt-Universität zu Berlin
Prof. Dr. Jan-Hendrik Olbertz

Dekan der Mathematisch-Naturwissenschaftlichen Fakultät I
Prof. Dr. Stefan Hecht

Gutachter/innen: 1. Prof. Dr. H. Saumweber
2. Prof. Dr. F. le Noblé
3. Prof. Dr. P. Knaus

Tag der mündlichen Prüfung: 22.05.2014

Acknowledgment

An dieser Stelle möchte ich mich bei allen bedanken, die zum Gelingen dieser Arbeit beigetragen haben.
Herrn Prof. Dr. Ferdinand le Noble danke ich für die Überlassung eines spannenden Promotionsthemas, sowie meiner Betreuung.
Mein aufrichtiger Dank gilt allen Mitarbeitern der AG le Noble, insbesondere Anja Zimmer, Janine Mikutta und Katja Meyer für tatkräftige Unterstützung und einen reibungslosen Arbeitsablauf im Labor. Außerdem allen für eine angenehme und fröhliche Arbeitsatmosphäre.
Insbesondere möchte ich Janna Krüger für wiederholtes Korrekturlesen sowie Raphael Wild, Anna Katharina Klaus, Alina Klems, Giulia Caglio und Qiu Jiang für produktive Diskussionen als auch unproduktive Gespräche und Kaffeerunden danken.
Christian Klein danke ich für die anfänglichen Arbeiten an diesem Projekt und weiterführendes Interesse, auch nach seinem Ausscheiden aus unserer Arbeitsgruppe.

Ich danke Herrn Prof. Dr. Saumweber für die Übernahme meiner Betreuung an der Humbold-Universität zu Berlin sowie den Mitgliedern meiner Promotions-kommission.

Harald Schulze und Imke Meyer gilt mein Dank für ihre Hilfe in der Endphase des Schreibprozesses.
Weiterhin vielen Dank meinen Freunden für all die nötige (und unnötige…) Ablenkung zwischen durch.
Mein besonderer Dank gilt meiner Familie:
Meine Eltern, die mich durch alle Zeiten begleitet, unterstützt, gefördert und nie den Glauben an mich verloren haben.
Meiner Schwester für das Korrekturlesen unter erschwerten Bedingungen.
Meinen Großeltern.
Anni und Wolfgang für die zeitweilige Unterkunft zur Überbrückung schweren Seegangs.

Chantal. Für alles. Danke.

Table of Contents

List of abbreviations

This abbreviation index contains no SI or therefrom derived units. Scientifically usual abbreviations are not indicated and plural forms are labeled by suffixed “s”.

AAA	ATPase Associated with diverse cellular Activities
ABI-1	Abelson Kinase Interactor 1
α-SMA	α-Smooth Muscle Actin
Alk	Activin receptor-like
Ang	Angiopoietin
AV	Arterio-Venous
β-gal	β-galactosidase
BM	Basement Membrane
CC	Coiled Coil
CH	Calponin Homology
Col IV	Collagen IV
CtA	Central Arteries
DCC	Deleted in Colorectal Cancer
DIG	Digoxigenin
DMEM	Dulbeccos Modified Eagle Medium
E	Embryonic day
EC	Endothelial Cell
ECM	Extra Cellular Matrix
EGFP	Enhanced Green Fluorescent Protein
ES	Embryonic Stem Cell
FA	Focal Adhesion
GFP	Green Fluorescent Protein
hpf	Hours post fertilization
IB4	Isolectin B4
Jag	Jagged
MO	Morpholino antisense Oligonucleotide
MT	Microtubule
NAV	Neuron Navigator
NG2	Nerve/Glial 2
P	Postnatal day
PDGF	Platelet Derived Growth Factor
PFA	Paraformaldehyd
PMHC	Primordial Hindbrain Channel
Tg	Transgenic
TGF-β	Transforming Growth Factor-β
UNC	Uncoordinated
VEGF	Vascular Endothelial Growth Factor
vSMC	Vascular Smooth Muscle Cell
WISH	Whole mount In Situ Hybridization
X-gal	5-bromo-4-chloro-3-indolyl-β-D-galactopyranoside

1. Introduction

1.1 Blood vessel formation

The cardiovascular system is the first organ system that develops during vertebrate embryogenesis. It consists of arteries and veins that are connected with an elaborate network of capillaries, enabling blood flow through the developing embryo. It accomplishes the transport of oxygen, nutrients and hormones, as well as the removal of waste products, thereby allowing growth and differentiation of the developing organs. The generation of a properly branched vascular system is essential for embryo development and its survival, as mouse mutants with defective arterial-venous (AV) differentiation or capillary organization are embryonal lethal. In adults, vessels are usually in a quiescent state but vessel growth can be initiated in response to a variety of physiological and pathological conditions like tissue repair, tumor growth and cardiovascular insults. Based on genetic analysis in mouse and zebrafish it is believed that the initial specification of endothelial cells (ECs) into an artery or venous phenotype is genetically hardwired. After the start of the heart beat and blood flow hemodynamic factors, most notably shear stress, contribute to AV remodeling and patterning of developing vascular networks. In the adult hemodynamic driven vascular remodeling is essential to trigger arteriogenesis, the development of collateral networks, in arterial occlusive disease. Thus, vessel remodeling is controlled by a combination of genetic and haemodynamic forces [1]. Here, we will mainly focus on the embryonic aspects of vessel formation, vasculogenesis and angiogenesis, and will address the contribution of mural cells in vascular remodeling events.

1.1.1 Vasculogenesis and Angiogenesis

During embryogenesis *de novo* assembly of precursor cells forms the central axial vessels and a meshwork of capillaries. Mesodermal cells give rise to angioblasts and endothelial cells (ECs). These coalesce to form lumenized tubes that build an initial vessel network. This *de novo* assembly of a primitive vascular plexus from precursor cells is defined as vasculogenesis. (Fig. 1) [2]. The expansion of vascular networks

from pre-existing vessel segments is defined as angiogenesis. During embryogenesis this process contributes to extensive expansion of the vasculature (Fig. 1) [3].

Based on differences in morphology and underlying cellular mechanisms, the process of angiogenesis can be classified into two distinct forms: sprouting and intussusception angiogenesis. Sprouting angiogenesis involves the budding and extension of vessel segments into avascular areas. Over the last decades substantial progress has been made to unravel the mechanisms underlying sprouting angiogenesis. It is thought to account for the substantial fraction of vessel formation processes [4–6]. A more detailed description of the molecular mediators is presented in paragraph 1.1.2

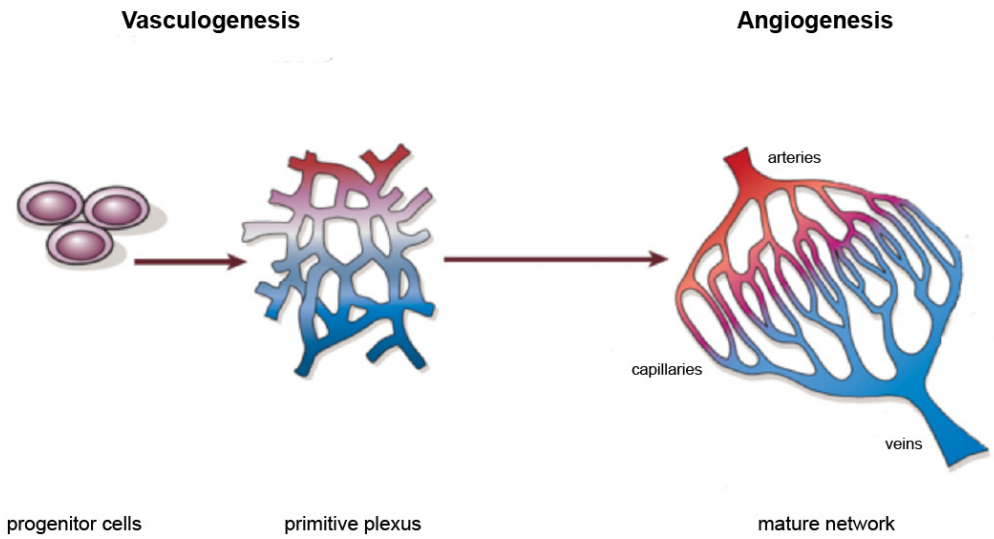

Figure 1. Blood vessel formation mechanisms.

Vasculogenesis is a process where endothelial precursors (left panel) assemble *de novo* to form a primitive vascular plexus (middle panel). Enlargement and remodeling of the initial vessel network occurs during angiogenesis resulting in a mature vascular network (left panel). Modified from [7].

The process of intussusceptive angiogenesis was first described in 1986. Transluminar tissue pillars develop within a plexus of small vessels and subsequently fuse, resulting in vessel remodeling and composing of new vessel entities. Compared to sprouting angiogenesis, intussusceptive proceeds fast. Within four hours new segments can be generated. Furthermore, this process does not seem to require EC proliferation, and due to the unique rearrangements of the pillars, vascular leakage is effectively prevented – as often associated with angiogenic sprouting processes [8].

1.1.2 Cellular mechanisms of sprouting angiogenesis

A mismatch between tissue metabolic demand and oxygen supply by the surrounding vascular network is believed to be the primary stimulus for sprouting angiogenesis. The resulting local hypoxic environment triggers secretion of growth factors and chemokines, which drives the dynamic EC rearrangements underlying the morphogenic process of sprouting.

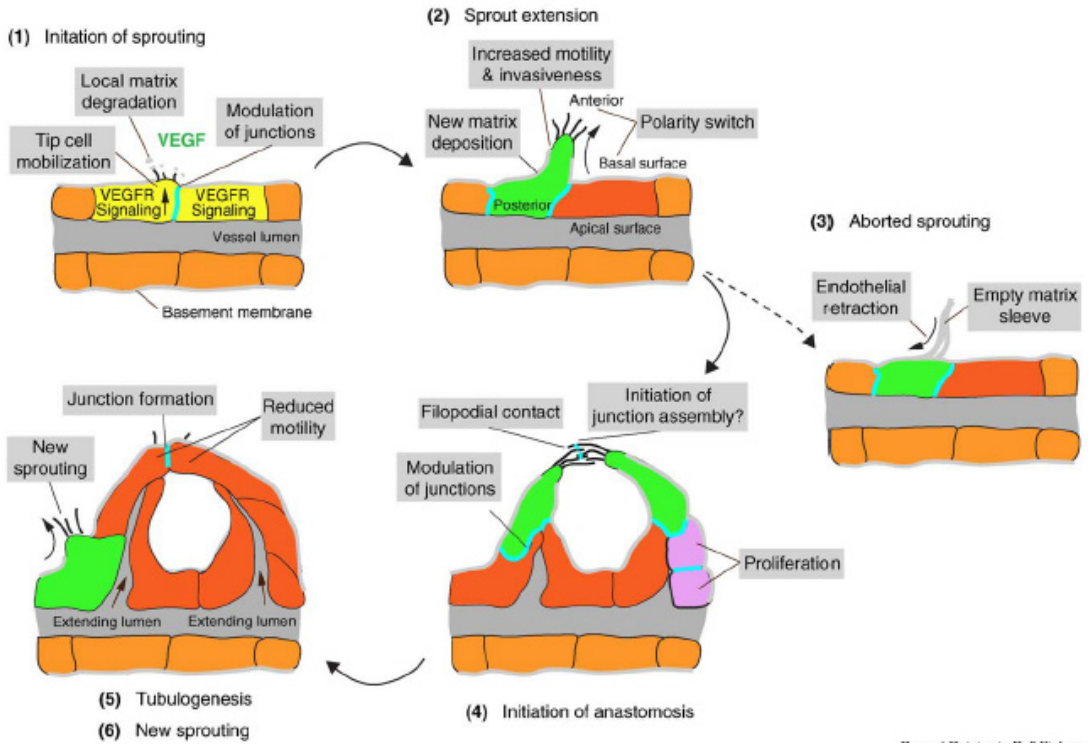

Figure 2. Overview of processes involved in sprouting angiogenesis.
(1) Initiation of endothelial cell sprouting. A new tip cell (yellow to green conversion from 1 to 2) is mobilized and invades the environment. The endothelial basement membrane and extracellular matrix components are degraded. Inter-endothelial junctions are modulated to allow sprout extension **(2)** The tip cell changes apical-basal polarity and migrates towards guidance cues. Local breakdown of the basement membrane is required for sprout extension, as well as new matrix deposition. **(3)** The sprouting process can be aborted leading to endothelial regression and a remaining matrix sleeve. **(4)** The contact of sprouting endothelial cells leads to initiation of new inter-cellular junctions and the connection of two sprouts. **(5)** The ECs of the newly connected tubule reduce their motility and a lumen is formed, enabling blood flow. **(6)** A new round of sprouting angiogenesis can take place. The scheme was modified from [4].

In growing tissues the initial generation of a functional vessel network is mainly dependent on coordinated EC behavior (Fig. 2) [4, 6]. Activation of ECs in quiescent blood vessels is driven by a gradient of the vascular endothelial growth factor (VEGF)-A and induces a motile and invasive EC behavior resulting in the formation

of a sprout [9, 10]. The growing angiogenic sprout consists of distinct cell populations; called the tip and stalk cell. The tip cell senses the local environment for guidance cues and migrates toward or away from them. The stalk cell follows, can proliferate and forms the lumen of emerging vessel sprouts [10, 11]. Recently, it has been shown that both cell types dynamically compete for the leading position [12].

The basal part of ECs is covered by a basement membrane whose components are degraded by matrix metalloproteinases prior to the onset of sprouting [13]. Finally, the outgrowth of endothelial sprouts is achieved by activation of signaling pathways, leading to loosening of cell-cell junctions [14, 15].

The pro-angiogenic signal VEGF selects a defined fraction of ECs to become a tip cell that guides the sprout outgrowth (Fig. 2, Panels 1 and 2). The elongation of the EC sprout takes place subsequently to tip cell selection (Fig 2 Panel 2) [9–11]. Once the tip cell of a newly developing sprout contacts an adjacent sprout, these two sprouts connect through establishment of tight EC-EC junctions and fuse to form a continuous patent lumen (Fig. 2 Panel 4) [6].

ECs loose then their motile behavior and reach a quiescent state (Fig. 2 Panel 5). If this state cannot be stabilized the newly formed angiogenic sprout regresses. As a result an empty sleeve of basement membrane components is left behind at the position where once a vessel developed (Fig. 2 panel 3) [14, 16]. Staining for such "empty sleeves" may thus help to identify sites of vessel regression.

Taken together, the process of sprouting angiogenesis is largely dependent on EC migration, orchestrated by multiple juxtacrine and paracrine signaling pathways.

1.1.3 Vessel network remodeling and maturation

Vessel segments of the initially formed capillary plexus need to be remodeled into an arterial and venous tree. Seminal work by the group of David Anderson has shown that neural guidance genes of the ephrin family mediate the specification of AV identity in blood vessels. Mouse mutants for ephrinB2 or its receptor EphB4 show an inability for capillaries to remodel into arteries or veins [1, 17]. Interestingly, mouse mutants for neuropilin 1 harbor differentiation defects suggesting that neural guidance genes – besides their impact on guidance for axonal growth cones – actually play an important role in establishing arterial and venous domains in growing vascular

networks (see Section 1.4 for more details on the neuro-vascular link) [18–21]. Analyses during recent years have further identified the Dll4-Notch-VEGF receptor-signaling pathway to be essential for AV differentiation in early developmental stages. In zebrafish AV specification seems to be completely genetically hardwired [22]. In the developing mouse embryo, however, heart beat and blood flow are essential to drive AV differentiation. It is therefore believed that the genetically hardwired programs are essential for generating the axial vessels relevant for accommodating the first cardiac output, whereas during later stages hemodynamic factors and probably oxygen metabolism fine-tune AV remodeling [23–25]. Interestingly, while zebrafish do not require blood flow for the major vessels to develop during early stages, at later time points formation of cerebral vessel clearly requires a hemodynamic component [26]. This suggests certain heterogeneity in the control of AV differentiation that is still only partly understood.

The recruitment of mural cells to the vessel wall is furthermore important for stabilization and maturation of a newly formed vessel network. General characteristics and the influence of mural cells on vessel remodeling and development are delineated in Section 1.2.

1.2 The mural cell

After formation of a capillary plexus, expansion through angiogenesis and formation of arteries and veins, the vascular network can be perfused with blood. The heart acts as pump and generates pressure in the vascular network. In order to accommodate the pressure in the system, the primitive vascular network, that initially consists of ECs only, starts to recruit mural cells. Besides making vessels more stable, mural cells can also exhibit contractile or relaxation behavior influencing vessel diameter. In this way they contribute to the distribution of blood flow toward tissues that require oxygen. Several types of mural cells can be distinguished and are discussed below.

Blood vessels are composed of an inner line of ECs surrounded by perivascular cells, the mural cells, and an extracellular matrix (ECM). Depending on their morphology, anatomical position and molecular signature mural cells are commonly subdivided into pericytes and vascular smooth muscle cells (vSMC) (Fig. 3). This simple classification is far from being complete.

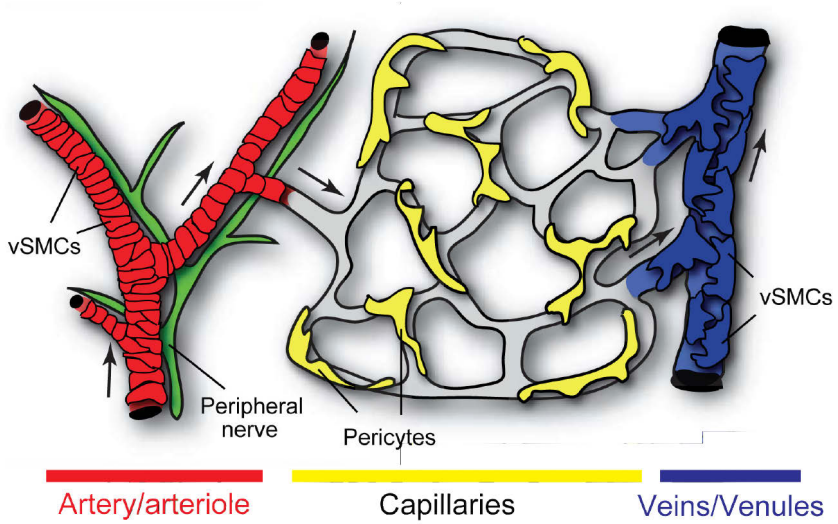

Figure 3. Blood vessels are covered by mural cells.

Blood flows through arteries and arterioles (red) into capillaries (grey). Venules and veins (blue) collect the blood from the capillary bed. Peripheral nerves (green) are often aligned with arteries. Perivascular cells, also designated 'mural cells', cover the vessels. Mural cells can be subdivided into vascular smooth muscle cells (vSMCs) that cover arteries and veins and pericytes (yellow) that are confined to capillaries. Modified from [27].

It is generally believed that pericytes and vSMC belong to the same cell lineage, but no specific marker exists that can unambiguously identify, and thus distinguish them [28]. Furthermore, it is assumed that pericytes are able to differentiate into vSMC and

vice versa [29]. At present, it is still not clear if they share the same or different progenitor cells and if pericytes are just cells with vSMC characteristics or the other way around [28, 30, 31].
In the next sections, detailed overview of vSMC and pericyte characteristics are given.

1.2.1 The vascular smooth muscle cell (vSMC)

The vSMCs are specialized cells embedded in the tunica media of the vessel wall with no direct cell-cell contact to neighboring ECs. Their principal role is regulation of vascular tone, blood pressure and blood flow distribution by their contractile function. They exhibit a wide range of different phenotypes at different stages of vascular development, as well as in physiologic and pathologic conditions [32].
The vSMC phenotype can be subdivided into “contractile” or “synthetic”. The differentiated “contractile” vSMC performs its contractile function in the vessel wall, exhibits nonmigratory behavior and a low rate of proliferation. This differentiated state is not definite. Changes in the local environment, due to developmental processes or after vascular injury, can lead to a reversible phenotypic switch. In contrast, the “synthetic” vSMC exhibits high rates of migration, proliferation and production of extracellular matrix components [34, 36]. Each of the different phenotypic state has different marker expression indicative for its relative differentiation state, but no single marker exists that can exclusively identify one type to the exclusion of the other one [32].
The heterogeneity of the vSMC cell population is further underlined by recent cell fate mapping studies. It was shown that the vascular smooth muscle of a common arterial tree is a mosaic tissue produced from several unique origins [35].
The classical vSMCs are associated with larger vessels. In contrast, cells associated with the microvasculature are defined as pericytes.

1.2.2 The pericyte

Pericytes are cells located within the basement membrane of capillary and post-capillary arterioles and venules (Fig. 4A). First description of this cell type dates back

to 1871. Zimmermann coined the term ‘pericyte’ in 1923 and demonstrated their presence around capillaries in a variety of vertebrate species [36].

The current accepted definition of a mature pericyte as a cell embedded within the vascular basement membrane (BM) emerged with the application of electron microscopy for ultrastructure analysis [37]. However, this definition is difficult to apply for situations of active angiogenesis, given that in pathological situations or embryonic tissues the relationship between the pericyte and the microvascular BM is hard to observe, as BM is in a state of synthesis or turnover [38].

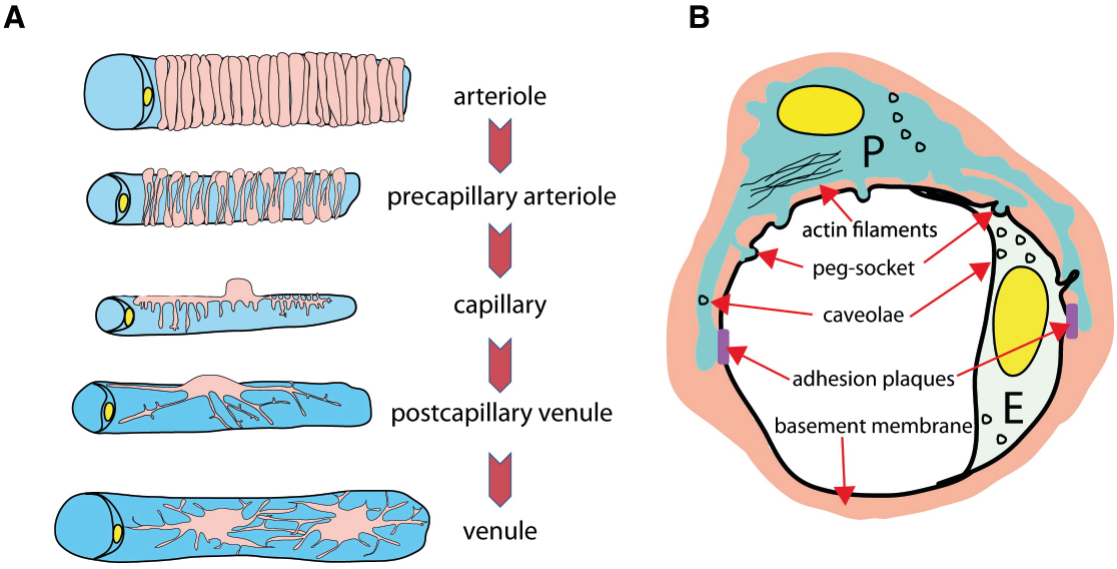

Figure 4. Mural cell anatomy.

(A) A continuum of mural cell architecture from arterioles to venules is depicted. Mural cells at arterioles have a flattened, spindle-shaped appereance, surrounding the entire endothelial surface. At precapillary arterioles cell bodies extend several protrusions, encircling the endothelium. Pericytes located at capillaries have characteristic rounded cell bodies with few protrusions located around the endothelium. At postcapillary venules and venules the mural cell body flattens and changes to a relative big and stellar shaped appereance. **(B)** Pericytes (P) and ECs (E) are seperated by a shared basement membrane. Nevertheless, they make direct contacts of different type: adhesion plaques and peg-socket connections. Scheme was taken from [38].

Pericytes do not only serve as a scaffold with ECs, but also communicate with them by direct physical contacts. They are connected to each other by holes in the BM (Fig 4B). Several morphologies of these contacts have been described. Pericyte cytoplasmic fingers (pegs) are inserted into endothelial invaginations (sockets) in the “peg-socket” type connection that contains tight, gap and adherens junctions (Fig. 4B) [39], [40]. Another contact morphology is described as adhesion plaques (Fig. 4B), which resemble adherence junctions at the ultrastructural level.

The cytoplasmic extrusions of one pericyte usually span over several ECs and can encircle a whole vessel (Fig. 4A), suggesting the facilitation of cell-cell communication. In contrast, vSMCs are not in direct cell-cell contact with the endothelium. When cultured *in vitro*, pericytes are able to contract comparable to vSMCs [41]. But to what extent this characteristic is important *in vivo* is still not clear [38].

Pericytes are commonly identified by molecular markers, like α-smooth muscle actin (α-SMA) [29], desmin [42], nerve/glial antigen 2 (NG2 also chondroitin sulfate proteoglycan 4) [43] and platelet derived growth factor-β (PDGFR-β) [44]. Unfortunately, none of these markers are exclusively specific for pericytes and/or are dynamic in their expression profile [31, 32]. Pericytes and vSMCs belong to the same cell lineage and category, sharing some of those cellular markers like α-SMA. The expression of specific markers varies between species, tissues and developmental time points examined.

It can be summarized that the mural cell population is heterogenous; pericytes and vSMCs show profound anatomical and functional differences (direct vs. no direct EC contact) but also harbor similarities (identical molecular marker expression, like α-SMA) [45]. The definition as 'mural cells' will be used consistently throughout this thesis, unless otherwise specified. In the next section the involvement of mural cells in vessel development and remodeling will be described.

1.2.3 Influence of mural cells on vessel network development and remodeling

The canonical view of mural cell function in angiogenesis holds that mural cells contribute mainly to vascular stabilization and maturation (Fig. 5) [16, 46]. The definite molecular mechanisms by which mural cells mediate vascular stabilization are so far not well understood. Several studies demonstrate that vessels covered by mural cells are protected from regression (Fig. 5 II.) [47–49]. In contrast to these studies, recent experiments suggest that mural cells may also be capable to promote selective vessel regression (Fig. 5 III.) [50]. *In vivo* mural cells are present in active angiogenic sprouts, pointing toward a potential role in sprouting angiogenesis [51–53]. In addition, studies in human fetal brain indicate that ECs and mural cells

cooperate to disassemble vascular BM which is the prerequisite for sprout initiation of ECs (Fig. 5 I.) [54].

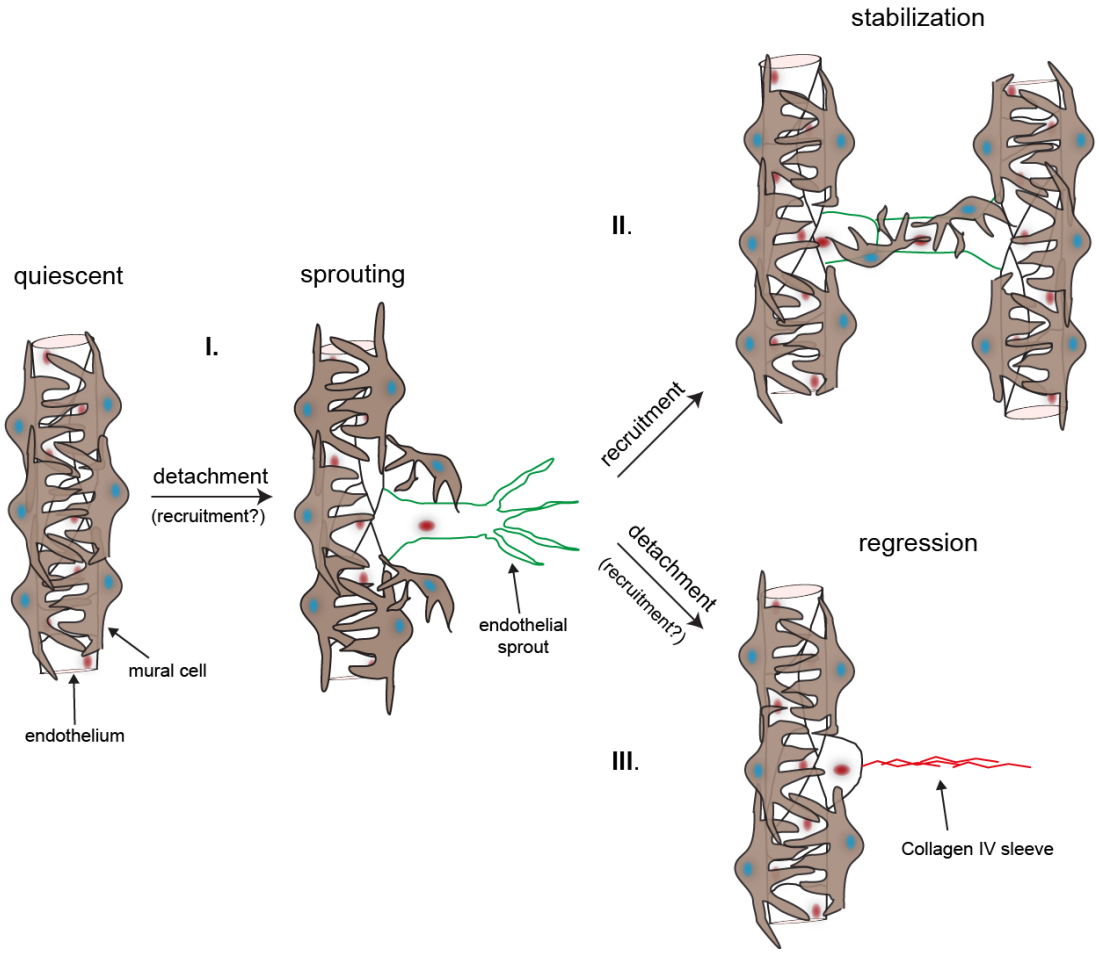

Figure 5. Mural cell impact on vascular remodeling processes.

Schematic view of vascular remodeling processes influenced by mural cell behavior is depicted. **I.** In a quiescent state of a vessel the mural cell (brown) encircles the endothelium (white). Sprouting angiogenesis is accompanied with mural cell detachment (detachment). It is uncertain whether the recruitment of mural cells to the endothelial sprout influences angiogenesis (recruitment?). **II.** The newly formed vessel can be stabilized after the process of angiogenic sprouting. Mural cell recruitment to the endothelium is thought to be most important for the stabilization process (recruitment). **III.** Alternatively, newly formed vessels can undergo regression. Sleeves of basement membrane components, like collagen IV, are left behind and are devoid of endothelial cells. It is believed that loss of mural cells (detachment) promote this event, although recently it was shown that mural cells can selectively promote regression (recruitment?).

These findings provide a line of evidence that the role of mural cells in vessel development is diverse and its distinct roles and functions should be objective of thorough investigation. The identification of underlying signaling pathways involved in mural cell behaviors and ECs-mural cell interactions are thus of major interest to unravel the definite role of mural cells during vessel development and remodeling.

1.3 Endothelial-mural cell signaling

The spatial proximity of endothelial and mural cells suggests cellular interactions that involve paracrine or juxtacrine signaling. Recent advances in the field has given insights into signaling pathways and mechanisms related to mural cell specification, differentiation, recruitment and attachment to ECs, as well as their relationship to vascular development and stability. In the following paragraphs main mural cell/endothelial cell signaling pathways are summarized.

1.3.1 PDGF-B/PDGFR-β signaling

The platelet derived growth factor (PDGF) family was identified more than three decades ago. PDGFs are dimers of disulfide-linked polypeptide chains and the PDGF family consists of four members: PDGF-A, -B, -C and –D. They act via two different receptor tyrosine kinases: PDGF receptor-α (PDGFR-α) and PDGF receptor-β (PDGFR-β). For cardiovascular development a major role of PDGF-B/PDGFR-β signaling has been described [55, 56].

PDGF-B is expressed by ECs and secreted as a homodimer [44], whereas PDGFR-β is expressed by mural cells [57]. Once secreted PDGF-B is bound by extracellular matrix proteins or on the cell surface by heparan sulfate proteoglycans, thereby limiting the range of action [55, 58]. PDGF-B expression is stronger in the tip cells of growing endothelial sprouts. As a result co-migrating mural cells are attracted toward the endothelium of growing vessels. Furthermore, PDGF-B-PDGFR-β signaling seems to promote proliferation of mural cell progenitors during their recruitment to the vessel wall [10, 57]. In addition, mural cell fate can be induced in mesenchymal progenitor cells by addition of PDGF-B *in vitro* [59].

The general knockout of PDGF-B or PDGFR-β in mice results in similar phenotypes: widespread microvascular bleedings leading to perinatal lethality [60, 61]. The cause of the vascular dysfunction in the absence of PDGF-B or PDGFR-β is attributed to the reduction of mural cell coverage of vessels [45, 57, 60, 61]. The endothelial-specific knockout of PDGF-B confirmed the essential role for recruitment and proliferation of mural cells [49, 62]. Interestingly, the degree of mural cell deficiency in PDGF-B/PDGFR-β mutant mice varies extensively between different organs. For example,

mural cells in the kidney are almost totally missing, leading to defective formation of glomerular tufts, whereas the mural cells in the liver appear unaffected [45, 57]. Thus, one main regulator of EC and mural cell interaction influencing correct vessel morphogenesis is the PDGF-B/PDGFR-β signaling pathway, but it is suggested that other pathways play a similar role during mural cell recruitment [56].

1.3.2 Angiopoietin and Tie receptor tyrosine signaling

The EC secreted ligand PDGF-B attracts mural cells via their receptor PDGFR-β to the endothelium. The angiopoietin (ANG)/ TIE receptor tyrosine signaling pathway acts mainly in the opposite direction regulating vascular morphogenesis [63].

The angiopoietins (ANG1, ANG2 and ANG4) are secreted glycoproteins binding their corresponding tyrosine kinase receptors (TIE1 and TIE2). ANG1 is expressed in mural cells of vessels and capillaries [64, 65], whereas ANG2, TIE1 and TIE2 are mainly expressed in ECs [32, 66].

TIE2 and TIE1 ablation lead to embryonic lethality in mice [63]. In *TIE2*-deficient mice the primary capillary plexus fail to remodel and vessels are less covered with mural cells. TIE1 has thus far not been implicated in mural cell recruitment but seems to be important for vessel integrity [67–70].

ANG1-deficient mice phenocopy the early embryonic lethal phenotype of *TIE2*-deficient mice [71], whereas ANG2 is dispensable for embryonic angiogenesis. However, at later stages the loss of ANG2 leads to severe vascular remodeling defects in the murine retina [72]. Interestingly, transgenic overexpression of ANG2 leads to embryonic lethality due to perturbed vessel formation similar to the ANG1-deficient phenotype [71, 73]. These observations have led to the concept that ANG2 acts as a natural antagonist of ANG1.

The ANG-TIE-signaling pathway is an important regulator of vessel remodeling. ANG1 is suggested to be important for vessel stabilization and ANG2 seems to promote vessel plasticity [63, 66].

1.3.3 Other signaling components

The overview of the PDGF/PDGFR-β and ANG/TIE signaling pathways mark the diversity of mural/endothelial cell interaction. In the following insights into three additional pathways important for this complex cellular interplay influencing vessel development are given.

The process of mural cell differentiation is still incompletely understood, but several studies argue for an important role of the transforming growth factor-β (TGF-β) signaling pathway [45]. TGF- β signals via two distinct receptors in ECs and mural cells – activin receptor-like 1 (Alk1) and 5 (Alk5). Both receptors seem to trigger different and opposing intracellular signaling pathways [74]. The activation of Alk-5 in mesenchymal cells promotes differentiation into mural cells. In contrast, Alk-1 activation enhances cell migration and proliferation opposing the differentiation process. Thus, it is difficult to sort out the primary roles of TGF-β in vascular development. Overall, it seems that Alk5 promotes vessel maturation, whereas Alk1 has the opposing effect [45].

Notch signaling has major role in ECs and is essential for angiogenic sprouting. Recently, it was demonstrated that Notch signaling is also important for EC-mural cell interactions. Adult Notch3-knockout mice exhibit improper maturation of vSMCs [75] involving the Notch-ligand Jagged-1 (Jag-1) [76]. Analysis of retinal angiogenesis demonstrated the importance of Notch3 signaling for mural cell recruitment and proper angiogenesis [77]. Mutations in the human Notch3 cause CADASIL (cerebral autosomal dominant arteriopathy with subcortical infarcts and leukoencephelopathy), a disorder causing stroke and dementia, which arises from systemic vascular lesions finally resulting in degeneration of mural cells [78].

Ephrin-Eph signaling axis is known to play an important role in AV differentiation of ECs [17]. Interestingly, mural-cell specific ablation of Ephrin-B2 resulted in poor mural cell recruitment of vessels and vascular defects leading to embryonic lethality in mice [79]. However, the precise mechanism how mural cell recruitment is affected is unclear. At least, *in vitro* work suggests that cell-autonomous functions connected with the formation of focal adhesions may play a role [80].

1.4 The neuro-vascular link

Formation of vascular networks requires capillary plexus formation, expansion via angiogenesis, AV differentiation and stabilization by recruitment of mural cells, but it is still not clear how tissue specific vascular patterns are achieved. In peripheral tissues blood vessels are often aligned with nerves and display similar branching patterns [81]. It has recently become clear that developing nerves can secrete factors that influence arterial specification and patterning. It was shown that peripheral nerve derived VEGF promotes arterial differentiation of the primitive capillary plexus via neuropilin-1 in the developing murine limb skin [21, 82]. Conversely, developing sympathetic nerves are guided toward their target by nerve growth factors secreted by smooth muscle cells derived from the major arteries [83]. At the cellular level the developing neuronal growth cone shows many similarities with the angiogenic sprout. Both contain specialized cells that display filopodia extensions, which sense gradient cues and direct movement. It was demonstrated that the neuronal growth cone and the angiogenic sprout utilize same ligands and receptors, including Uncoordinated (UNC)5 and Plexin family [27]. These observations led to the suggestion that during evolution the developing blood vessels have co-opted growth control mechanisms from the nervous system. It is believed that the intimate cross-talk between developing nerves and vessels is relevant for establishing functional branched vascular networks.
Neural guidance has been well studied in the model organism *C. elegans*. Based on chemical-induced mutations, nematodes with movement defects in sensory-nerve induced locomotion screens were identified. Subsequently, the affected genes in these "uncoordinated" (UNC) mutants were determined [84]. In this screens the factors UNC5 and UNC6 were discovered and subsequently shown to be important for guidance of cell migration and pioneering axons [85]. The vertebrate homologues of these genes were *UNC5* and *Netrin-1*. Netrin-1 belongs to a family of secreted proteins, which are structurally related to laminins. Netrin-1-deficient mice exhibit shortened commissural axons [86]. It was shown that it is a bifunctional axonal guidance cues, capable of repelling and attracting axons [27, 87]. Moreover, it was demonstrated that Netrin-1 acts as repulsive cue during angiogenesis remodeling processes via its EC specific receptor UNC5B [88, 89].

This is the proof of principle that it is a valid approach to investigate genes, derived from locomotion screens in *C. elegans*, to score for angiogenic remodeling defects in higher vertebrates. Neural guidance genes important for vascular patterning described so far are receptors or ligands important for determining the directionality of the migrating cell. However, the guidance signal has to be transduced into cell movement, which is strictly dependent on cytoskeletal remodeling. The mechanisms by which guidance cues are interpreted, to produce organized rearrangements of the cytoskeleton and hence directional movement are not fully understood. One particular interest is in neural genes that actually regulate cell locomotion and attracted our attention to the neuron navigator (NAV) family.

1.5 The Neuron Navigator protein family

The Neuron Navigators (NAVs) are novel modulators of axon guidance and cell migration events. This protein family seems to act cell autonomously on cell locomotion by interacting with cytoskeleton dynamics [90, 100]. The family member NAV1 has been linked to Netrin-1 signaling [92] and Netrin-1 is known to inhibit angiogenic sprouting [89]. We postulated therefore that NAV1 is a promising candidate to analyze for its role in cell migration events of vascular development. In the following we give an overview about the NAV family members and their identification history.

The NAV family consist of three members (NAV-1, -2 and -3) and were identified as homologues of the gene uncoordinated (*unc*)-*53* of the nematode *C. elegans* [93]. The gene *unc-53* encodes for a cytoplasmic protein that is a novel component of a signal transduction pathway controlling cell locomotion in the developing nervous system of *C. elegans* [91]. UNC-53 functions cell autonomously to control cell migration. Mutations in the *unc-53* gene affect axonal guidance [94] and cause defective sex myoblast migration [95]. It was proposed that UNC-53 acts cell autonomously on cell migration by interfering with actin cytoskeleton dynamics [96].

The mammalian homologues to UNC-53 were identified in 2002 and were coined Neuron Navigators [93]. NAV proteins belong to the AAA (ATPases Associated with diverse cellular Activities) group of ATPases. Members of this superfamily of proteins were shown to be involved in a variety of cellular processes, including signal transduction, regulation of gene expression, membrane fusion, microtubule severing, and microtubule-mediated transport [97]. Aside from the AAA domain the NAVs consist of a calponin homology (CH) and several coiled coil (CC) domains, as well as actin binding motifs. Interestingly, only NAV1 has undergone several deletions during evolution and lacks the CH domain (Fig. 6) [93].

NAV1 exhibits microtubule binding capacity and plays a role in neurite outgrowth *in vitro* [92]. The same was shown for NAV2 [98]. *In vitro* experiments with rhombic lip explants linked NAV1 downstream to Netrin-1 signaling [92]. Mammalian cell culture experiments showed that all three Navigators are plus-end-tracking-proteins (+-TIP) localized at the end of growing microtubules. It was proposed that all Navigators are involved in the organization of the cytoskeleton [90, 98].

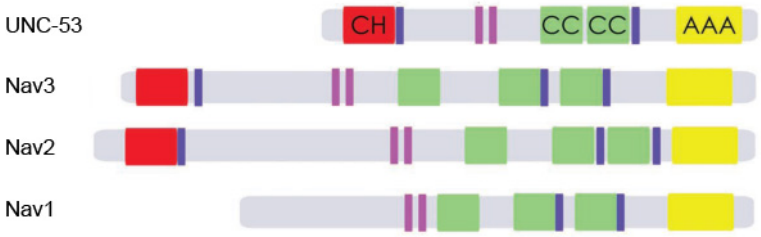

Figure 6. The neuron navigator protein family.

Protein domain schemes of UNC-53 (*C. elegans*) and the three different neuron navigators (NAV) are depicted. Domains include a calponin homology domain (CH, red), coiled coiled domain (CC, green), LKK acting-binding motifs (blue), polyproline rich SH3 binding motifs (purple) and an AAA domain (yellow). NAV1 lacks the CH domain. Modified from [91].

UNC-53 contains several domains observed in actin binding properties [100]. It was demonstrated furthermore that UNC-53 interacts with abelson kinase interactor (ABI-1) mediated by the N-terminal CH-domain in *C. elegans* [96]. Similar function has been described for zebrafish Nav3 in our laboratory. Here, it was shown *in vitro* that one isoform of Nav3 (Nav3a) associates with ABI-1 in lamellopodia of moving hepatocytes, acting as positive modulator of actin polymerization dynamics. Loss-of-function experiments during zebrafish embryogenesis resulted in strikingly reduced liver size. This phenotype was attributed to reduced movement of hepatoblasts out from the gut endoderm. This implicates that Nav3a is essential for movement of liver stem cells *in vivo* [90]. Hence, these data support the concept that the NAV family is a promising protein family to analyze for its influence on cell locomotion beyond the neuronal system.

To investigate the role of NAV1 in vertebrates we performed loss- and gain-of-function studies in a zebrafish and mouse model supplemented with *in vitro* angiogenesis assays. The generation of the NAV1-knockout mice is described in detail in section 2.2.1.1 and an overview of the used angiogenesis assays in mouse and zebrafish are given in the next section.

1.6 Angiogenesis assays

Excessive angiogenesis is a hallmark for numerous disease states including cancer, whereas reduced angiogenic potential associates with ischemic cardiovascular diseases [101]. Therefore, understanding of angiogenic processes is fundamental for treatment of angiogenesis-dependent diseases. The use of different *in vivo* and *in vitro* angiogenesis assays has lead to substantial progress in the understanding of angiogenic processes. In the following sections typical assays to study angiogenesis and that we used to unravel NAV1 function are outlined.

1.6.1 The mouse retina model

The murine retina is an established and reliable model to analyze vessel development. Intraretinal vessel development occurs postnatally in mice. The formation of the retinal vasculature is tightly regulated resulting in specific vessel patterns. Vascular growth progression and correct vessel formation can be easily observed at different time points of postnatal development.

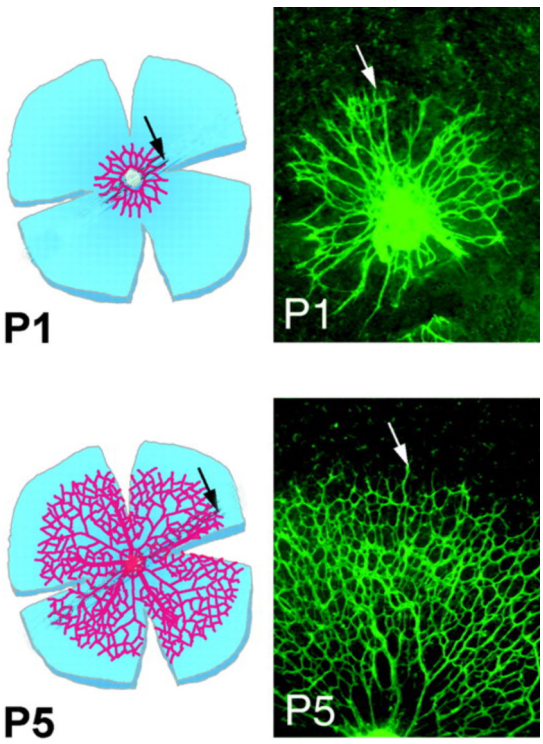

Figure 7. Schematic presentation of murine retinal vessel development.
Right panels depict flat-mounted retina, immunofluorescently labeled for endothelium (green) at postnatal day (P)1 and P5. Corresponding schemes on the left shows the vascular plexus (purple) schematically. Arrows indicate the vascular growth front. Modified from [10].

The retinal vasculature emerges from the optic disc and growth radially by angiogenic sprouting, reaching the peripheral boundaries approximately at postnatal day 8 (P8) (Fig. 7). This two-dimensional vascular growth process undergoes substantial remodeling. It matures into a hierarchical blood vessel network of arteries, veins and capillaries. The growth and remodeling process is dependent on several cellular interactions, including mural cell recruitment and guidance by astrocytes, but is also influenced by blood flow. This well-defined sequence of events has been studied extensively and had significantly advanced the understanding of angiogenic processes in the last decades [10, 102–104].

The simultaneous appearance of sprouting and vessel remodeling events allows for analysis of different parameters in a single flat-mounted retina preparation. For instance, the radial expansion of the vasculature can be measured as an indicator of angiogenic sprouting behavior. Furthermore, the amount of endothelial tip cells at the vascular growth front (Fig. 7) can be counted to analyze vessel sprouting in more detail. Vascular remodeling properties are determined by counting the branch points of the capillary network. An easy to follow manual for retinal vessel analysis protocol was published recently [105].

1.6.2 The murine aortic ring assay

The murine aortic ring assay is a versatile *ex vivo*/*in vitro* assay to study angiogenesis under defined conditions without a total loss of physiological parameters. It was originally developed in the rat [106, 107]. The principle is based on injury-induced outgrowth of vessels from aortic rings.

The thoracic aortae of mice are dissected and cut into rings. Subsequently, single rings are embedded in ECM components (like Collagen I) and cultured in growth medium for several days. First, adventitial macrophages and fibroblasts grow into the gel environment followed by formation of blood vessel sprouts at day 2-3 (Fig. 8). These neovessels arise from ECs and mural cells from the intimal layer of the artery. Therefore, mural cell recruitment to the abluminal surface of the endothelium can be analyzed. The vessels form networks by elongation and branching. The growth and remodeling process stops after approximately one week and the formed blood vessels are then readsorbed into the matrix.

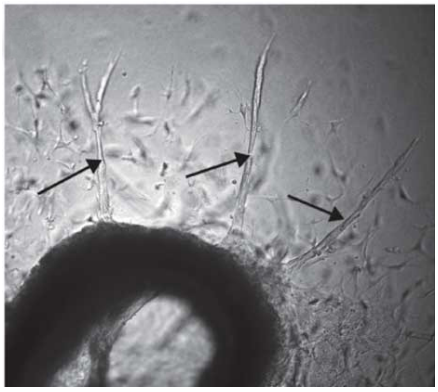

Figure 8. The mouse aortic ring assay.
Phase contrast image of an aortic ring embedded in collagen I matrix. Microvessel outgrowth is marked with black arrows. Modified from [108].

The *in vitro* culture allows direct manipulation by addition of chemical inhibitors and growth factors to analyze desired signaling pathways in more detail. Furthermore, blood flow and neural cell influences on the vessel growth process can be excluded [109]. Recently, a standardized protocol for the mouse was established [108].

1.6.3 The zebrafish model

The zebrafish (Danio rerio) is a small tropical fresh water fish with a rapid generation time. It is a genetically tractable model for studying angiogenesis and vascular remodeling events *in vivo*. The embryos are transparent, so that the direct *in vivo* observation of tissue and organ growth in the living animal is feasible. Moreover, using specific genetic approaches it is possible to express fluorescent marker proteins selectively in distinct tissues and cells. The analysis of early blood vessel development has been well characterized by the use of transgenic fish lines like Tg(fli1a:egfp)^{y1} or Tg(flk1:EGFP)^{s483}. Both lines express the enhanced green fluorescent protein (eGFP) under an endothelial specific promoter [110]–[114].

Loss of function studies can be executed easily by antisense morpholino oligonucleotide (MOs). MOs are designed to bind to the translation start site or a splice site of a desired mRNA, thereby inhibiting proper translation and depleting protein levels.

The development of blood vessels in zebrafish follows a dynamic and spatiotemporally conserved pattern [112]. The signaling pathways during vascular

development are often conserved throughout vertebrates, as shown by loss-of-function experiments for the Notch-pathway in mouse and zebrafish [115]. Therefore, insights about the function of specific genes in zebrafish will be applicable for future research in other vertebrates.

1.7 Aim of the study

Vessel development is a multistep process orchestrated by different cellular and signaling mechanisms. In the past it could be shown that signaling molecules playing a role in axon growth have also a function in angiogenesis. Based on the evolutionary conserved molecular and cellular mechanisms governing growth of vessels and nerves, we postulated that genes relevant for neural guidance in *C. elegans* may have a role in vascular development in higher vertebrates. We focused on the UNC53/NAV family, because it has been implicated to influence guidance events of neurons in both, *C. elegans* and mouse. The NAV family consists of three members. Our group recently showed that zebrafish Nav3a modulated cell movement of hepatoblasts by influencing actin dynamics. Here, we focus on NAV1 and hypothesize that NAV1 plays a role in vascular development in vertebrates. The analysis of NAV1 by loss-of-function studies in mouse and zebrafish is expected to reveal a new modulator of vessel developmental processes.

We generated a *NAV1*-knockout mouse by a gene-trap-approach and want to verify the null mutation on protein and mRNA level with immunoblot and qRT-PCR, respectively. Taking advantage of the β-gal activity expressed under the endogenous *NAV1* promotor, due to the inserted gene trap vector, we aim to characterize embryonic and adult tissue expression domains. Furthermore, *NAV1* localization is analyzed on a cellular level in the neonatal retina and the murine aortic ring assay. The vascular development in the retina will be analyzed by immunostaining of the endothelium and the vascular phenotype is substantiated by the murine aortic ring assay. Additionally, in both assays the mural cell recruitment is studied by counting the amount of mural cells located at distinct vessels. Mural cell behavior will be analyzed in cell migration and adhesion assays of primary vSMCs.

The murine loss-of-function data are supplemented with data of the zebrafish model. Molecular characterization of *nav1* isoforms will be performed and their spatio-temporal expression pattern analyzed by WISH and qRT-PCR. Morpholino-induced depletion of NAV1 in transgenic reporter fish lines, expressing GFP in the endothelium, is performed and subsequent analysis of the vessel network will give us insights into conserved functions of Nav1 on vascular development.

2. Material and Methods

2.1 Material

2.1.1 Chemicals and Kits

All chemicals were obtained from Sigma-Aldrich unless otherwise noted.

Ethanol	Merck
Ethidium bromide	Serva
Goat serum	Invitrogen
Isopropanol	Roth
Proteinase K	Roche
TRIzol reagent	PeqLab

SMARTer® RACE cDNA Amplification Kit	Clontech
TaqMan® Gene Expression Assay	Life Technologies
Tyramide Signal Amplification TM	PerkinElmer
ThermoScriptTM First-Strand System	Invitrogen
Pierce®BCA Protein Assay Kit	Thermo Scientific

2.1.2 Buffers and Solutions

Inmunofluorescence

Blocking buffer

1x PBS (pH 7.4)
1% BSA or 3% goat serum
0.5% Triton X-100

Incubation buffer

1x PBS

0.5% BSA or 1.5 % goat serum

0.25% Triton X-100

Pblec buffer

1x PBS (pH 6.8)

1mM $CaCl_2$

1mM $MgCl_2$

0.1 mM $MnCl_2$

1% Triton X-100

X-gal staining

Detergent rinse

1M NaH_2PO_4

1M Na_2HPO_4

1M $MgCl_2$

5% Sodium deoxycholat

10% NP-40

Staining solution

1M Na_2HPO_4

1M $MgCl_2$

5% $C_{24}H_{39}NaO_4$

10% NP-40

100 mM $K_3[Fe(CN)_6]$

100 mM $K_4[Fe(CN)_6] \cdot 3H_2O$

0.5 M Tris-HCl (pH 7.3)

Zebrafish handling

Egg water

60^{-4} % red sea salt

10^{-5} % methylene blue

VE-water

Danieau buffer (10x)

174 mM NaCl
2.1 mM KCl
1.2 mM $MgSO_4$
1.8 mM $Ca(NO_3)$
15mM HEPES
pH 7.6, used at 1x

In situ hybridization

Hybridization buffer

50% formamide
5 x SSC
100 µg/ml yeast RNA (tRNA)
0.1% tween-20
50 µg/ml heparin
4.6 µM citric acid (pH 6)

RNase buffer

0.1M hepes (pH7.5)
0.15 M NaCl
0.1% tween-20

MABT

100 mM maleic acid
150 mM NaCl,
0.1% tween-20
pH 7.5 buffered with NaOH

NTMT

0.1 M tris-HCl (pH 9.5)
0.1 M NaCl
1% tween-20
50 mM $MgCl_2$

2.1.3 Antibodies and Proteins

Description	Manufacturer
Alexa Fluor 568 goat anti rabbit IgG	Invitrogen
Alexa Fluor 488 donkey anti rat IgG	Invitrogen
Anti beta galactosidase	Abcam
Anti-Collagen IV	Abcam
Anti-NG2 Chondroitin Sulfate Proteoglycan	Millipore
CD31/PECAM-1 rat-anti-mouse	Millipore
Collagen I from rat tail	Millipore
Donkey anti chicken HRP	Dako
Isolectin B4-lectin 1 biotinylated	VectorLabs
NAV1 rabbit-anti-mouse	Abcam
murine Netrin-1	R&D Systems
murine PDGF-B	Peprotech
Streptavidine Alexa Fluor 488	Invitrogen
murine VEGF-165	Peprotech

2.1.4 Equipment

CoolSnapTM color camera	Visitron Systems
Leica TCS SP5 microscope	Leica microsystems
Microinjector MPPI-2	ASI
MZ16FA microscope	Leica microsystems
MZ75 stereomicroscope	Leica microsystems
NanoDrop ND-1000	Thermo Scientific
ABI Prism 7000 Thermo Cyler	Applied Biosystems
Thermocycler Tgradient	Biometra
Zeiss LSM 510 microscope	Carl Zeiss MicroImaging

2.2 Methods

2.2.1 Mouse procedures

2.2.1.1 Generation of NAV1-knockout mice and general mice husbandry

NAV1-knockout mice were generated by a gene trap approach. The gene trap method is a randomized approach, where a gene trap vector is randomly inserted into the genome of a mouse embryonic stem (ES) cell by electroporation or retroviral infection. The insertion leads to the mutation of an endogenous gene. The gene trap vector consists of a splice acceptor site, a promotorless reporter gene (in general β-galactosidase), neomycin resistance gene and a polyadenylation signal. The presence of the neomycin resistance gene allows the selective growth of mutated ES cells. The activation of the endogenous, gene specific promotor leads to the generation of a fusion transcript, due to the splice acceptor site of the gene trap vector. This fusion transcript is non-functional for the endogenous protein, but exhibits β -galactosidase (β -gal) activity. Therefore, enabling detection of expression domains by this reporter gene [117, 118]. The generation of transgenic ES cells is mostly conducted by so called gene trap consortia and facilitated in databases for interested scientists. The desired ES cell line is injected into the blastocyst of a pseudopregnant mother, which give birth to chimeric mice. Subsequently, these are mated with the inbred mice strain C57/BL6 to monitor germline transmission [119] and to obtain transgenic mice harboring a heterozygous mutation of the desired gene..

For generation of NAV1-deficient mice we used the ES cell clone D062H05 from the german gene trap consortium (GGTC). Here, the gene trap inserted into the intronic region after exon 3 of the *NAV1* gene.

Heterozygous mice were back bred to C57/BL6 strain. Animal care and all experiments were performed according to institutional guidelines. For generation of embryos of defined gestation day one male mice was bred with two female mice for two days. Day 1 of breeding was set as gestation day 0.5 (E 0.5).

2.2.1.2 Genotyping

Tissues of desired mice was digested with lysis buffer and Proteinase K (20 mg/ml) overnight at 55°C on a shaker. Digested samples were centrifuged at 8000 g for 10 min at room temperature (RT). The supernatant was removed and isopropanol added. After 10 min centrifugation (8000 g, RT) the supernatant was discarded and the pelleted DNA was washed with 70% ethanol and centrifuged again for 5 min (8000 g). DNA was dissolved in 50 µL H_2O for 20 min at 55°C and stored at 4°C.
The isolated genomic DNA was used for genotyping of mice by PCR. Standard conditions for PCR reaction are listed in Table 1.

Table 1. Polymerase chain reaction.

PCR reaction	**PCR cycle conditions**		
	Step	**Temperature**	**and Time**
1x *Taq* DNA polymerase buffer	1. First denaturation	94°C	3 min
20 ng cDNA	2. Denaturation	94°C	30 s
0.4 µM primers mix	3. Annealing	60°C	30 s
0.2 mM dNTP	4. Elongation	68°C	2 min
0.02 U/µl *Taq* DNA polymerase	5. Storage	4°C	∞
ad 20 µl H_2O	Repeated steps: 2-4, 25 x		

2.2.1.3 Organ, embryo and retina preparation

Neonatal mice at postnatal day (P)5 to P7 or adult mice were sacrificed and brain, heart, lung, kidney, thoracic aorta, retina and/or embryos were isolated. Time mated pregnant mothers were sacrificed and embryos isolated. Retina dissection was performed as described previously and is illustrated in Figure 1. Briefly, incisions were made over the skin covering the eye with a scissor. By compressing a pair of tweezers under the eye the optic nerve and other tissues were cut and the eye was taken out of the eye-socket. The whole eye was fixed in 4% paraformaldehyde (PFA) for 20 min at room temperature. Pre-fixed eyes were transferred to a petri dish in PBS under a stereomicroscope. Fat and surrounding tissue was removed and incisions in the cornea were made, followed by peeling off the outer layer, as well as the sclera and pigmented retina layer. Next, the hyaloids vessels were detached carefully from the inner side of the eye.

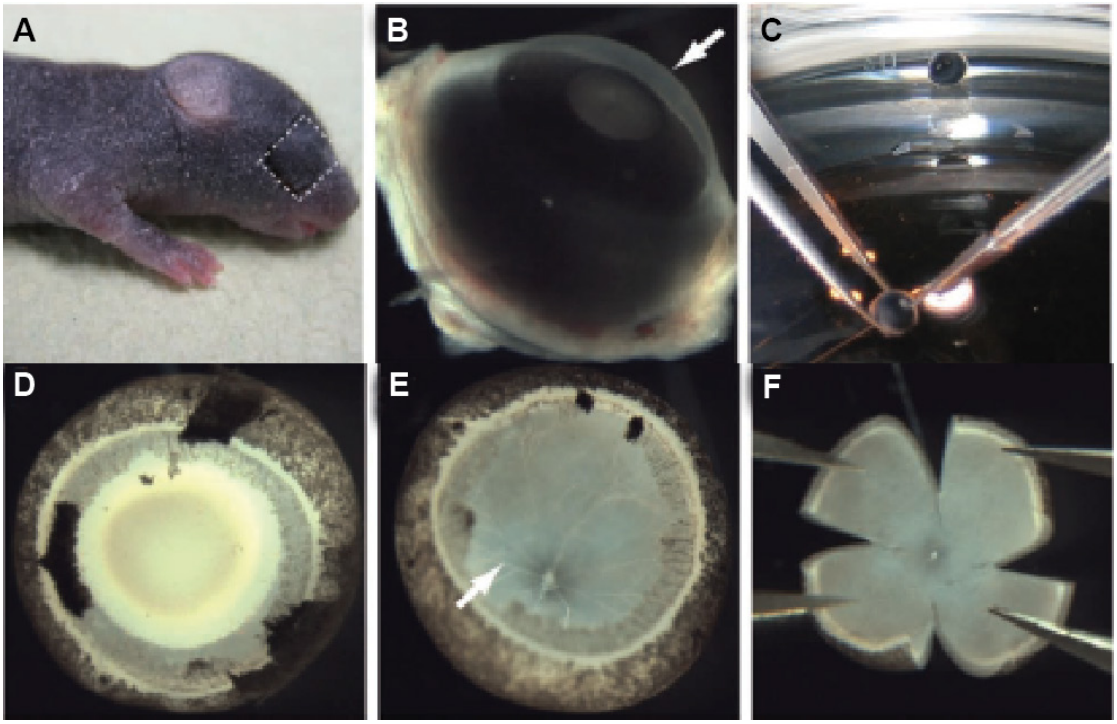

Figure 9. Overview of retina preparation.
(A) The skin covering the eye (dot-lined box) is cut to reach the eyeball. **(B)** The dissected eyeball. White arrow indicates the cornea. **(C)** Overview of removal of fat- and surrounding tissues. **(D)** Eye without cornea and pigmented layers **(E)** Lens is removed. Hyaloid vessels (denoted by white arrow) are detached by forceps. **(F)** Immunostained retina is cut at four positions and flat-mounted at glass slides. Modified from [105].

Dissected retinas, organs or embryos were fixed for 10 min (RT) or over night (4°C) depending on subsequent staining methods.

2.2.1.4 Mouse aortic ring assay

Thoracic aorta was isolated from neonatal mice and processed for an aortic ring assay as described [108]. Briefly, for each genotype 30 rings of two individuals were collected and embedded in 50 µL Collagen type I diluted in DMEM (final concentration c= 1 mg/mL). 150 µL Opti-MEM containing murine VEGF-165 (final concentration 1.5 ng/µL) and 2.5% FBS was added. Aortic rings were incubated in a humidified incubator for six days at 37 °C and 5% CO_2. Medium was exchanged at day 3. Analysis of endothelial sprouts was performed at day 6.

2.2.2 Zebrafish procedures

2.2.2.1 Zebrafish husbandry

Zebrafish were kept under standard conditions as described [120]. Briefly, they were maintained at 26°C on a 10 hrs light and 14 hrs dark cycle and fed four times daily with brine shrimp. Transgenic zebrafish line Tg(flk1:EGFP)^{s483} was used for analysis of the vasculature [113].
Fertilized zebrafish eggs were generated by pair-wise mating of adult fish. Eggs were collected and kept at 28°C in egg water. Embryos were staged according to hours post fertilization (hpf).
To prevent pigmentation 0.003% 1-phenyl-2-thiourea was added at around 24 hpf. Living embryos were anesthetized with 0.016% tricaine for phenotype analysis at desired developmental stage. Subsequently, embryos were embedded in 0.8% low-melting agarose for imaging.

2.2.2.2 Zebrafish loss-of-function experiments

Gene knockdown *in vivo* was achieved by injecting morpholino antisense olionucleotides (MOs, GeneTools) into the yolk of one-cell stage embryos. Beforehand, fertilized eggs were set in an agarose ramp. Subsequently, injection was performed with a glass micropipette through a microinjector.
MOs are blockers of mRNA translation or splicing, depending on designated effect. All injected morpholinos were diluted in Danieau Buffer to finally used concentration, according to manufactures protocol.
We used following MOs targeting *nav1*:

MO1 5′-AGACTTGCCCCTCTTGGCAGCCATG-3′
MO2 5′-TGGGCTACCCCCAAGCATTCCTCCT-3′
control MO: 5′-CTCTTACCTCAGTTACAATTTATA-3′

2.2.2.3 Whole Mount In Situ Hybridization (WISH) of zebrafish embryos

WISH was performed as described elsewhere [121]. Briefly, zebrafish embryos were fixed in 4% PFA at the desired developmental stage and dehydrated in 100% methanol. Rehydration in 75%, 50%, 25% methanol/PBT (PBS with 0.1% Tween) followed by proteinase K (c= 2.5 µg/µl) treatment, permeabilized the embryos. After re-fixation in 4% PFA for 20 min and three washing steps in PBT, the embryos were pre-hybridized with pre-warmed hybridization buffer at least 2 h at 65°C. Subsequently, hybridization with the appropriate Digoxigenin (DIG)-labeled RNA (500 ng) probe (see 2.2.4.5 for generation procedure) was performed for 16 h at 65°C. Next, the probe and the hybridization buffer were removed via washing and RNase (100 µg/ml, Roche) digestion. Embryos were incubated in 2% Boehringer blocking reagent (2 h RT), before it was replaced with an antibody directed against DIG for at least 12 h at 4°C. The embryos were then rinsed with MABT and washed with substrate buffer NTMT. The staining was performed with BM purple at 37°C and was stopped when desired staining level was reached by removal of the substrate. The stained embryos were finally conserved in 80% glycerol/PBS.

2.2.3 Biochemical techniques

2.2.3.1 Protein isolation

Embryos at desired stage were dechorionated, in order to isolate proteins and subsequently homogenized with a pestle in lysis buffer.

Confluent grown murine primary vSMCs (see section 2.2.5.1 for generation) were first rinsed with ice-cold PBS and then harvested from a 10 cm dish with a cell scratcher on ice. The harvested cells were pelleted and the cell pellet lysed in M2 buffer for 30 min at 4°C.

Lysed proteins were centrifuged at 8000 g (20 min/4°C). The supernatant contained proteins and was transferred into a new tube. The protein concentration was determined by using the Pierce®BCA Protein Assay Kit.

2.2.3.2 Immunoprecipitation and immunoblot

Endogenous murine NAV1 was immunoprecipated with NAV1-antibody from primary vSMCs with the Immunoprecipitation Kit Dynabeads® Protein G (Invitrogen) according to manufacturers protocol.
Immunoprecipated protein or whole protein lysates were loaded onto SDS-polyacrylamid gel and separated by electrophoresis. For detection of endogenous NAV1 protein, the antibody was used in 1:500 dilution for immunoblot. As loading control anti-beta-tubulin was used in 1:1000 dilution.
A custom made polyclonal antibody against zebrafish nav1 was generated, affinity purified (KSDDDILSSKAKAS ; Eurogentec, Belgium) and used in a 1:500 dilution for verification of the functionality of MOs by immunoblot.

2.2.4 Molecular biology techniques

2.2.4.1 RNA isolation

RNA was separated from tissues, cells or whole zebrafish by Trizol® reagent according to manufacturers instructions. The quantity and quality of extracted RNA was measured photometrically using NanoDrop. Total RNA samples were stored at -80°C.

2.2.4.2 Generation of cDNA

Complementary DNA (cDNA) was generated by reverse transcription using First Strand cDNA Synthesis Kit (Thermo Scientific) following manufacturers protocol. 1 µg RNA and random hexamer primer mix or oligodT primer dependent on subsequent processing steps were used. cDNA was stored at -20°C

2.2.4.3 rapid amplification of cDNA ends (RACE)-PCR

RACE-PCR is a technique for identifying unknown 5´- and 3´-end sequences from cDNA. During the procedure nucleic acid sequences between a defined internal site and an unknown 5´- or 3´-end are amplified [122].
Rapid amplification of cDNA ends (RACE) – polymerase chain reaction (PCR) was performed by the use of the SMARTer® RACE cDNA Amplification Kit (Clontech) according to manufacturer instructions. Primer used for identification of 5´- and 3´-ends of zebrafish *nav1* are listed in Table 2. PCR products were cloned into the pGEM-T easy vector (Promega) and sequenced.

Table 2. Primer for zebrafish nav1 RACE-PCR.

Gene specific primer	Sequence (5´→3´-end)
5´-RACE 1	TGGCTGATCCCGAAGTACCACTCAAA
5´-RACE 2	TCTGACCACTTGGGCTGGTACAGGTG
5´-RACE 3	CTTTTCGCAGCCATGCCTCCAACT
3´-RACE 1	TGGCAGGGGTATCCCTCTTTCCAAG
3´-RACE 2	GAAAACCTCCATCCGGGCTTGTCC
3´-RACE 3	CAGTCCCTCCAATCAGCCGTCTCCT

2.2.4.4 quantitative realtime PCR (qRT-PCR)

In order to analyze the expression levels of specific genes we performed quantitative real-time PCR using TaqMan® Gene Expression Assay. The principle relies on the 5' – 3' exonuclease activity of Taq polymerase that cleaves the double-labeled probe (fluorophore and quencher) during hybridization to the complementary target sequence and its fluorophore-based detection. The reaction mix was prepared according to the manufacturers instruction. Primers and the probes were designed individually (FAM and TAMRA labeled, Biotez, Berlin) or commercially available assays (Life Technolgies) were used. Primer and probes for individually designed assays are listed in Table 3.

Table 3. Primer and probes for quantitative real-time PCR (qRT-PCR).

Gene	Forward primer 5` - 3`/reverse primer 5` - 3` Probe 5´ - 3´
mGAPDH	GGCAAATTCAACGGCACAGT / AGATGGTGATGGGCTTCCC FAM- AGGCCGAGAATGGGAAGCTTGTCATC –TAMRA
Nav1	TCCTAGTGGCCGCTTTCG / AGTCTATAGTTTCTCGCAAATCCAA FAM- CCTGGTGAATATGACATCCCGCC –TAMRA
ef1α	GTTGCCTTCGTCCCAATTTC/ CAATCTTCCATCCCTTGAACCA FAM- ATGTTTGAGCTGGCCTCCAGCATGTT -TAMRA

FAM: 6-carboxyfluorescein; TAMRA: 6-carboxytetramethylrhodamin

Each gene was analyzed in triplicates. The amplification was carried out in the ABI Prism 7000 thermo cycler.

Gene expression data were normalized against ubiquitously expressed housekeeping genes. Relative expression levels were calculated by the ΔΔct comparative method.

2.2.4.5 Generation of DIG-labeled RNA

DIG-labeled RNA was generated by *in vitro* transcription of linearized template DNA. Gene specific sequences were amplified first by PCR of cDNA and cloned into the pGEM®-T Easy vector (Promega) and subsequently sequenced to identify the orientation of the insert. Primers used for generation of RNA probes are listed in Table 4.

Table 4. Primer for WISH probe generation.

RNA probe	**Forward primer**	**Reverse primer**
nav1A	TGCCACCATGAGTGGGGGAGT	GCTGGGCCAGGCCTCAAGTT
nav1B	TGCGAAAGACACCAGGCACACG	TACCCCTGCCAATGCTCCCTCC
PDFGFR-β	GTGTCCTGCTCTAGAAGAAAGC	TCTCGTACAGCGTGACGTTT

20 µg of plasmid DNA was linearized with desired restriction endonucleases (NEB) according to manufacturers instruction. Linearization was verified by agarose gel electrophoresis and purified with GeneJet Gel extraction kit (Thermo Scientific). 1 µg linearized template DNA was *in vitro* transcribed using SP6 or T7 polymerase (Promega) for 2 hours at 37°C to generate an DIG-labeled antisense or sense RNA

probe, dependent on orientation of the gene insert. After DNase digestion the DIG-labelled RNA was purified and measured by NanoDrop. Correct fragment size was analysed by agarose gel electrophoresis. Antisense probes contained the complementary counterpart of the particular mRNA, used therefore to detect endogenous mRNAs and the sense probes was used as negative control.

2.2.4.6 Molecular cloning

Full length cloning of nav1B isoforms was conducted by nested PCR. Primers used are listed in Table 5.

Table 5. Primer for zebrafish nav1 full length cloning.

Primer	Sequence (5´→3´-end)
nav1BA_33_for	GCAGCGAGACACTCCGCTGAAG
nav1BA_2868_rev	GTCTGGGCGCATGACAATCGCA
nav1BB__17_for	GCGAGACACTCCGCTGAAGGG
nav1BB_6069_rev	GTCTGCCCCGACCTGGATGT
nav1BA_start_for	ATGCTTGGGGGTAGCCCAAG
nav1BA_stop_rev	TTAATTTTCTGACCTGTGAGAGTTTGGA
nav1BB_start_rev	ATGCTTGGGGGTAGCCCAAG
nav1BB_stop_rev	CCTAGAAAGTGGGGTTGCCTGAAA

In a first amplification step primers lying in the untranslated regions of the mRNA based on information obtained by RACE-PCR were used. Subsequently, primers starting at translation start site and ending at translation stop site were used. PCR products were verified by agarose gel electrophoresis, purified with the GeneJet Gel extraction kit and subsequently cloned into the pCR8/GW/TOPO (Invitrogen) and/or pGEM®T-Easy vector (Promega).

2.2.5 Cell biology techniques

2.2.5.1 primary vSMC isolation and culture

Isolation of vSMC of the thoracic aorta is based on a protocol from [79]. Briefly, thoracic aorta from adult mice was isolated. Then, adventitia was removed and the

aorta was sliced and digested in a Collagenase F/H (30/70%) mixture at 37°C for 30 min. Obtained single cell suspension was seeded on uncoated 6-well plates and cultured in DMEM with 20% FBS and Penicillin/Streptomycin as antibiotics in a humidified incubator at 37 °C and 5% CO_2. Cells between passage 3 and 7 were used for experiments. vSMC showed typical morphology and immunofluorescent staining against α-SMA and NG2 demonstrated that cells were vSMCs.

2.2.5.2 vSMC migration and adhesion assay

The vSMC migration assay was performed as described previously [90]. Briefly, cells were seeded on 24-well plates or 8-well chambers (Ibidi) and grown until they were confluent. A scratch was made with a plastic 200 µL plastic pipette. After washing twice with DMEM to get rid of cell debris, cells were cultured under standard conditions as in 2.2.5.1 described. Images of the migration front were taken immediately after the scratch (0 hours) and after three, six and 24 hours. Calculation of the migration area was done by first determining the cell-free area for each time point. The first time point was set as 0 % and the following decrease in cell-free area was calculated as increase in migration area.

For single cell migration analysis sub-confluent cells were fluorescently labeled with Calcein (1:1000 dilution from stock solution, Invitrogen) for 2 hours prior to scratching the cell layer. Then, every 5 min an image was acquired with a Leica TCS SP5 (Leica microsystems) and a 10x objective for 3 hours. In addition to standard culture conditions 30 ng/mL PDGF-B or 50 ng/mL Netrin-1 were added. Cell tracking was performed with ManuelCellTracking plugin of Fiji (Image J software).

The adhesion assay was performed in 96-well plates. The plastic surface was coated with BSA (3% in PBS), Collagen I (c=1mg/mL) , PDGF-B (30 ng/mL) and Netrin-1 (50 ng/mL) for 16 hours at 4°C. The supernatant was removed and unspecific binding to the plastic surface was blocked with BSA (3% in PBS) for 1 hour at RT. The vSMCs were harvested and 50000 cell per well were allowed to adhere for 30 min at 37°C. Washing with pre-warmed PBS removed not adhered cells. After fixation with 4% PFA for 30 min at RT the nuclei of the adhered cells were stained with DAPI. Subsequently, fluorescent images of the adhered cells were acquired and cell number

per visual field was manually counted. Each condition was performed in triplicates. The experiments were repeated three times.

2.2.5.3 Immunofluorescence and 5-bromo-4-chloro-3-indolyl-β-D-galactopyranoside (X-gal) staining

Aortic rings and neonatal retina were fixed for 20 min at room temperature in 4 % PFA/PBS for X-gal staining and accordingly over night at 4°C for immunofluorescence staining. All stainings were performed as previously described [105, 108]. In retinas, β-galactosidase signal was detected and amplified by tyramid signal amplification kit (TSA Cyanin 3 System, Perkin Elmer).

We followed standard protocols for immunofluorescence staining of retina and aortic rings. Briefly, unspecific binding sides were blocked with blocking buffer for 1 hour at room temperature before the primary antibody were added and incubated o/n at 4°C. Unbound primary antibody was removed by 5 washes with PBT or Pblec for 10 min. Subsequently, probes were incubated with desired fluorescent-labeled secondary antibody for 1 hour. After washing 3 x 10 min with PBT, samples were blocked again and, when necessary, incubated with a new first antibody following the same conditions as before.

Antibody and protein dilutions used for immunofluorescence stainings are listed: biotinylated griffonia simplicifolia Lectin I isolectin-B4 (1:25), anti-NG2 (1:250), anti-beta-galactosidase (1:250), anti-collagen IV (1:200), Streptavidin Alexa Fluor 488 (1:500), goat-anti-rabbit- IgG Alexa Flour 568 (1:500) and anti-chicken IgY-PO (1:1000).

Whole organs or tissues were fixed for 15 min (RT) in 4% PFA/PBS and washed three times for 10 min in detergent rinse. Incubation with the staining solution and its substrate 5-bromo-4-chloro-3-indolyl-β-D-galactopyranoside (Xgal) was performed in the dark at room temperature (10µl Xgal/1ml staining solution). Re-fixation in 4% PFA stopped the staining process. Subsequently, samples were imaged, sectioned or further immunofluorescently labeled.

2.2.6 Imaging and Data Analysis

Confocal imaging of agarose embedded Tg(flk1:GFP)^{la116} zebrafish embryos, flat mounted murine retinas or mounted aortic rings was performed with a Zeiss LSM 510 or Leica TCS SP5 microscope with a 20x (NA= 0,7 oil immersion), 25x (NA=0.8 water immersion) or 63x (NA=1.2 oil immersion) objective. Images were acquired with LAS AF software. Images were further analyzed and processed with ImageJ software or Adobe Photoshop CS5.

Images of X-gal stained whole organs and sections were performed with the Leica MZ 16 FA microscope or Leica MZ75 stereomicroscope and a CoolSnapTM color camera from Visitron Systems.

Analysis of retina vessel architecture was performed as described [105].

Analysis of mural coverage was performed as follows: manual mural cell counting at arteries was done by scrolling through z-stacks of acquired images to unambiguously identify single cells. For determination of vessel and mural cell density the fluorescence threshold of identical acquired images was set manually and percentage of fluorescence area per 250μm^2 capillary area was measured automatically by ImageJ software. Then, mural cell to vascular density ratio was calculated.

Statistical analysis was performed using student´s unpaired two tailed t-test (*, $p<0.05$).

3. Results

It is postulated that during evolution the blood vessel system has co-opted growth control mechanisms from the nervous system in order to shape its structure. The Neuron Navigator (NAV) protein family is a novel factor involved in neuronal growth and cell migration events. We hypothesized that NAV1 may influence cell migration events during angiogenesis. In order to investigate the impact of NAV1 on vascular development in higher vertebrates we used two different loss-of-function models. Special focus was given to the murine model. The zebrafish model was used to complement and substantiate obtained results of the mouse.

3.1 The role of murine NAV1 in vascular development

3.1.1 Characterization of NAV1-mutant mice

The loss-of-function mouse model was generated using a gene trap approach. The ES stem cell D062H05 was used in which a gene trap cassette (β-geo) was inserted into the intronic region after exon 3 of the *NAV1* gene (see chapter 2.2.1.1 for details). The insertion leads to a non-functional fusion protein with β-galactosidase (β-gal) activity (Fig. 10A), due to the strong splice acceptor site of the β-geo cassette. The β-gal activity can be used to identify *NAV1* expression domains using specific staining protocols. Genotype identification was accomplished routinely by PCR using genomic DNA.

To test whether the β-geo vector inserted only once into the genome of the transgenic mice we performed a Southern blot (performed by C. Klein). Based on genomic integration site information provided by the embryonic stem cell clone distributor (GGTC) we used a radioactive labeled probe directed against the β-geo cassette of the vector (Fig. 10B). Digestion of genomic DNA of all three genotypes with the restriction endonuclease XmnI, and detection of the digested fragments with the radioactive labeled β-geo specific probe, results in a single 6 kb sized band in *NAV1*-heterozygous and –knockout mice as expected (Fig. 10C, performed by C. Klein). This confirmed the single integration site of the gene trap vector.

The integration of the β-geo cassette into the intronic region after exon 3 of the *NAV1* gene should lead to the ablation of endogenous mRNA and protein levels. We used quantitative real-time PCR (qRT-PCR) and immunoblot to test for mRNA and protein levels, respectively. The immunoblot was performed with protein lysates of primary vascular smooth muscle cell (vSMCs) cultures. NAV1 protein was enriched by immunoprecipitation. Only in *NAV1*-knockout mice no NAV1 protein was detectable (Fig. 10D). Furthermore, qRT-PCR of endogenous mRNA levels in primary vSMCs verified the efficient ablation of *NAV1* in mutant mice (Fig. 10E).

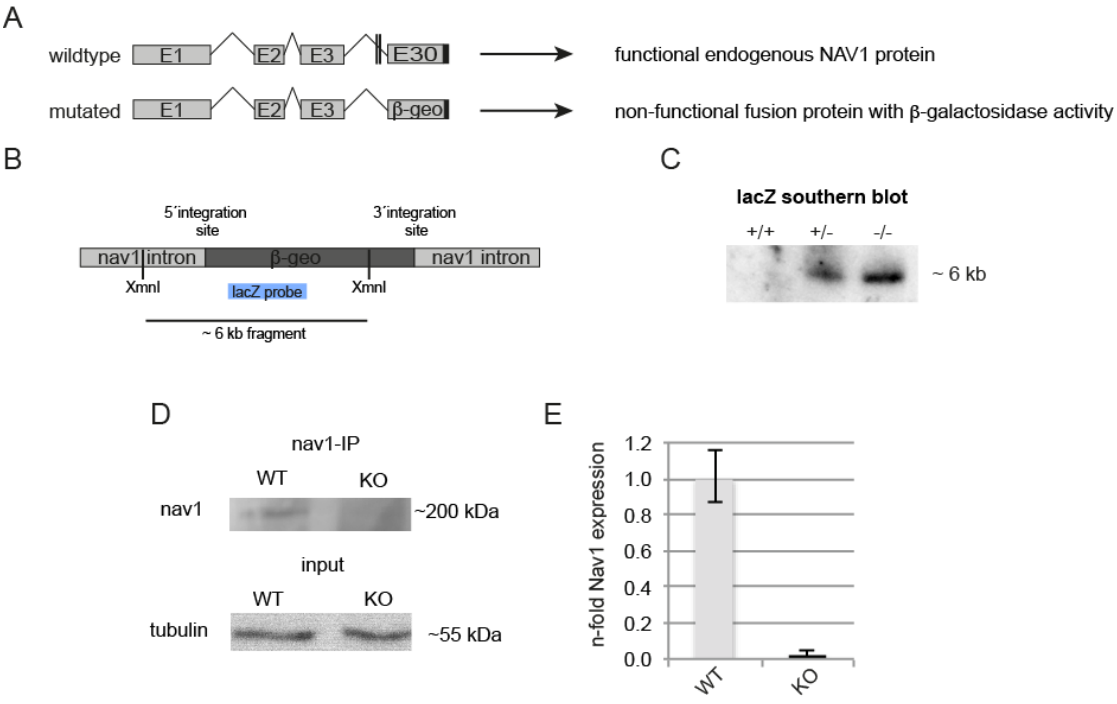

Figure 10. Generation of *NAV1*-knockout mice.

(A) *NAV1*-knockout mice were generated by a gene trap approach. Scheme of gene trap insertion into the genome is depicted. Wildtype shows the exon structure leading to endogenous *nav1*. The integration of the gene trap cassette (β-geo) into the intronic region after exon 3 leads to a non-functional fusion protein with β-galactosidase activity (β-gal). **(B)** Scheme of single integration site verification by southern blot. Genomic DNA was digested with XmnI leading to a 6 kb fragment when the β-geo cassette is present. A radioactive labeled lacZ probe was used to detect the 6 kb fragment. **(C)** Only in *NAV1*-heterozygous (+/-) and –knockout (-/-) mice one 6 kb sized product could be detected with the lacZ probe by a Southern blot. Wildtype (+/+) showed no product. **(D)** NAV1-protein was enriched by immunoprecipitation of primary vSMC protein lysates. Only in WT an approximately 200 kDa protein can be detected by an immunoblot. **(E)** qRT-PCR detected no expression of *NAV1* mRNA in vSMC of *NAV1*-deficient mice (KO) compared to wildtype (WT). *GAPDH* was used for normalization. Error bars represent SEM. (A-C) Initial generation of *NAV1*-knockout mice and verification of single integration site by Southern blot was performed by C. Klein.

We next analyzed if crossing of heterozygous mutant mice results in Mendelian distributions of the genotypes in the offspring. We expected 25 % of the newborn to be homozygous for *NAV1*-deficiency, but observed only around 14 % of the neonatal and adult mice to be homozygous for a mutation in the *NAV1* gene (Fig. 11A). This indicates that around 44 % of the *NAV1*-knockout mice died prenatally.

To clarify the exact timing and potential cause of death explaining the observed drop-out we next evaluated embryonic development at different time points. In the period embryonic day (E) 8.5 to E13.5 normal Mendalian distribution was observed. From E13.5 onward we noted strong deviation away from normal distribution. At E16.5 we detected only 64 % of the expected homozygous genotype (Fig. 11A). The *NAV1*-deficient embryos exhibited no obvious anatomical differences compared to wildtype.

We analyzed the *NAV1*-mutant mice that survived until postnatal stages in more detail. Weight was significantly reduced when compared to $NAV1^{+/-}$ or $NAV1^{+/+}$ littermates (Fig. 11B). The smaller weight of mutant mice was constant in 8 to 12 week old mice (data not shown). No difference in the distribution of female and males, as well as no additional lethality during adult stages was observed. Only male homozygous *NAV1*-knockout mice were fertile.

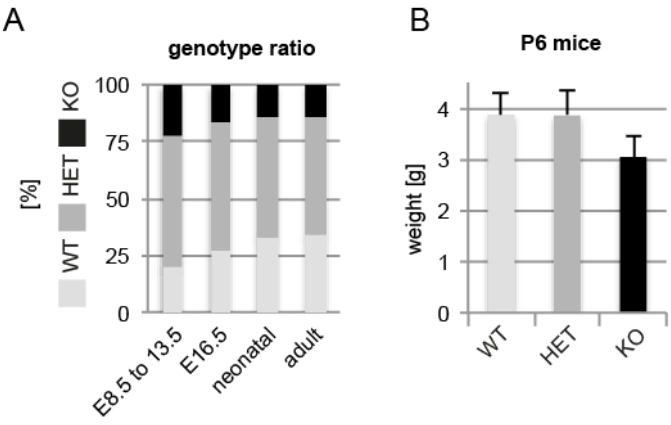

Figure 11. *NAV1*-knockout mice die during embryogenesis and the survivors have reduced weight.
(A) Around 22 % of embryos between E8.5 and E13.5 are homozygous for *NAV1*-deficiency (total amount of embryos n=72). This value decreases to 16 % at E16.5 (total number of embryos n=45) and further to 14 % after birth (neonatal n = 123 and adult n=392). **(B)** Neonatal *NAV1*-knockout (KO) mice have less body weight when compared to wildtype (WT) and heterozygous (HET) mice at postnatal day 6 (P6). Error bar represents standard deiviation.

Thus, we first verified the successful generation of the *NAV1*-knockout mice (Fig. 10). Analysis of Mendelian distributions showed that around 44 % of *NAV1*-deficient

animals die *in utero* during the last third of gestation (Fig. 11A) and the survivors seem to be underdeveloped, in respect to weight (Fig. 11B). As no obvious cause of the embryonic lethality could be detectable, the underlying biological reason remains to be clarified.

3.1.2 Characterization of NAV1 expression domains

We next investigated the expression domains of *NAV1* during embryogenesis and took advantage of the presence of the β-gal gene in the gene trap vector. We performed X-gal staining on whole mounts from *NAV1*-mutant mice. No intensity differences between heterozygous or knockout mice stainings were detectable.
Between E8 and E10 we observed expression domains in brain regions. At E9.5 the expression seems to be ubiquitous in the area of forebrain, midbrain and hindbrain, whereas at E11.5 the expression in the hindbrain was located more ventrally. Ubiquitous expression was detectable in the eye, somites and heart. Expression patterns in the eye resembled areas of the developing retinal tissues (Fig. 12A/B).

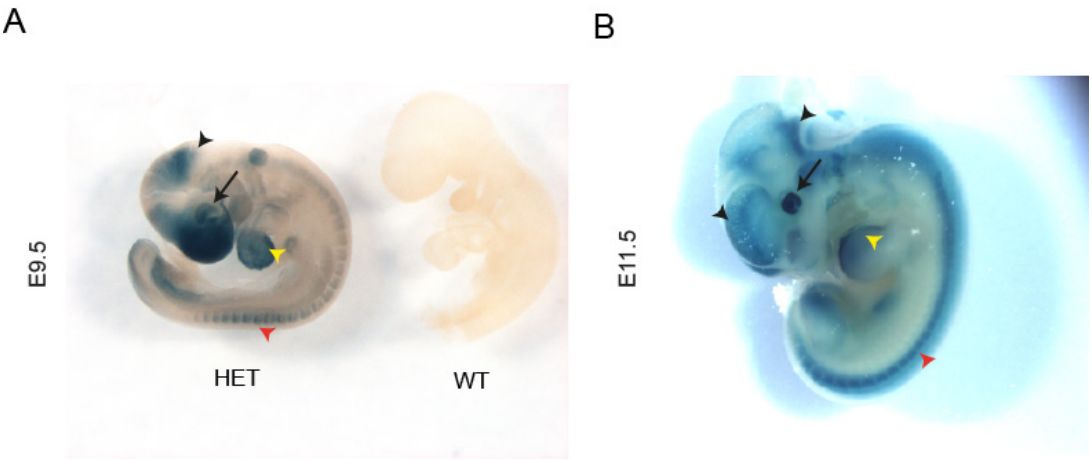

Figure 12. Characterization of *NAV1* expression during embryogenesis.
Representative images of X-gal stained embryos are depicted. Blue color represents β-gal activity, therefore *NAV1* expression. **(A)** Whole mount staining of embryonic day (E) 9.5 heterozygous (HET) and wildtype (WT) embryos (100x magnification). WT embryos routinely showed no staining. Expression domains can be monitored in brain regions (black arrowhead), eye (black arrow), heart and lung (yellow arrowhead), as well as in the somites (red arrowhead). **(B)** *NAV1* expression domains persists in E11.5 *NAV1*-heterozyous embryos (100x magnification)

As *NAV1*-knockout embryos die *in utero* after E13.5 we next analyzed expression domains at later stages. Careful analysis of E16.5 embryos showed expression in lung

(Fig. 13A) and heart (Fig. 13C). The expression in the fetal heart was ubiquitous at the surface of the ventricle and the atrium (Fig. 13C). The pulmonary expression resembled a network-like pattern located inwardly of the lung (Fig. 13A). *NAV1* was furthermore clearly expressed in embryonic kidney, in particular in the developing glomeruli (Fig. 14B/C). In contrast, in kidneys of 8-12 week old mice *NAV1* was not detectable in glomeruli by X-gal staining (Fig. 14 D-F).

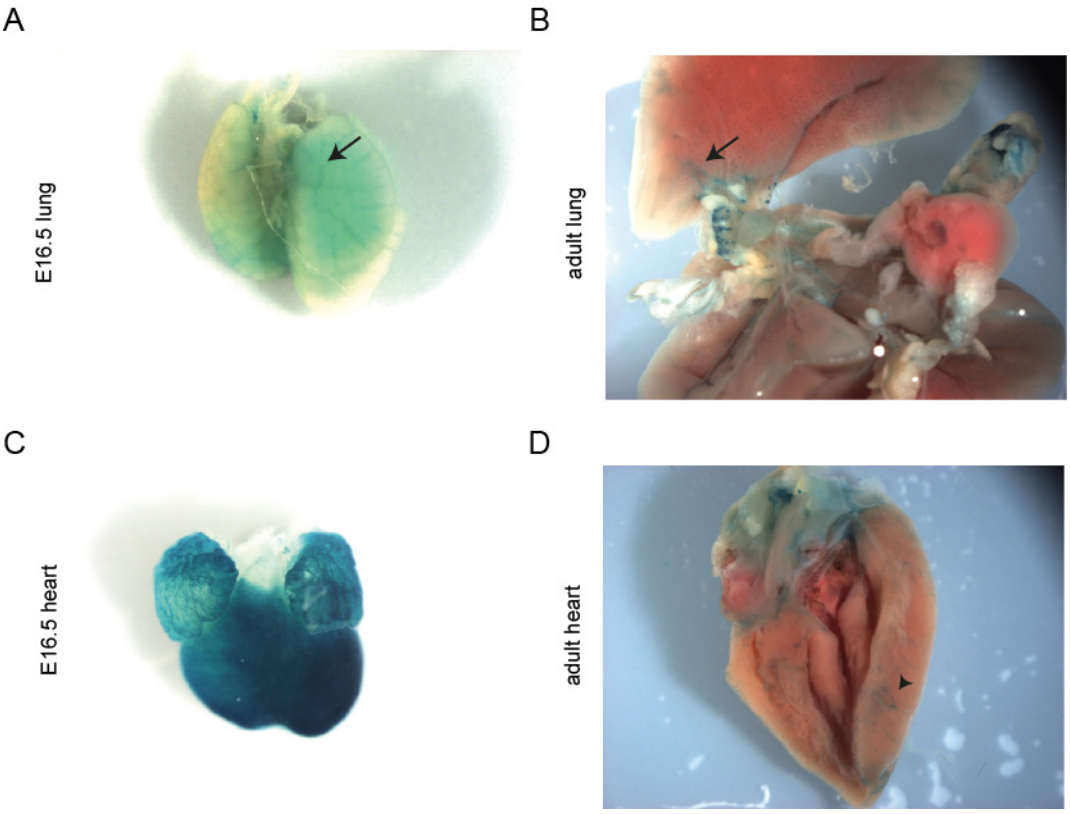

Figure 13. Branched vessel-like NAV1 expression domains in heart and lung tissues.
Representative images of whole mount X-gal staining of heart and lung are depicted. Blue staining shows β-gal activity, representative for *NAV1* expression **(A/B)** Whole mount X-gal staining of lungs in E16.5 embryos and adult mice revealed distinct branched tubular expression patterns (arrow) indicating that *NAV1* may be expressed in pulmonary vessels or the bronchial tree. **(C)** Strong ubiquitous NAV1 expression in the atria and ventricel of the embronic heart (E16.5). **(D)** In a longituidinal cut of an adult heart only vessel-like structures (arrowhead) at the epicardium persists, pointing to a specific expression in coronary vessels. Wildtype organs showed routinely no staining. Representative organs are depicted. (A/C 100x magnification) (B/D 70x magnification)

The network-like expression pattern of *NAV1* in the lung persisted in adult mice (Fig. 13B). In the heart the expression pattern at the ventricle changed from ubiquitous at embryonic stages to a vessel-like appearance at the endocardium in adult mice (Fig. 13D). These data suggests that expression of *NAV1* is predominantly restricted to, and important for, developmental stages.

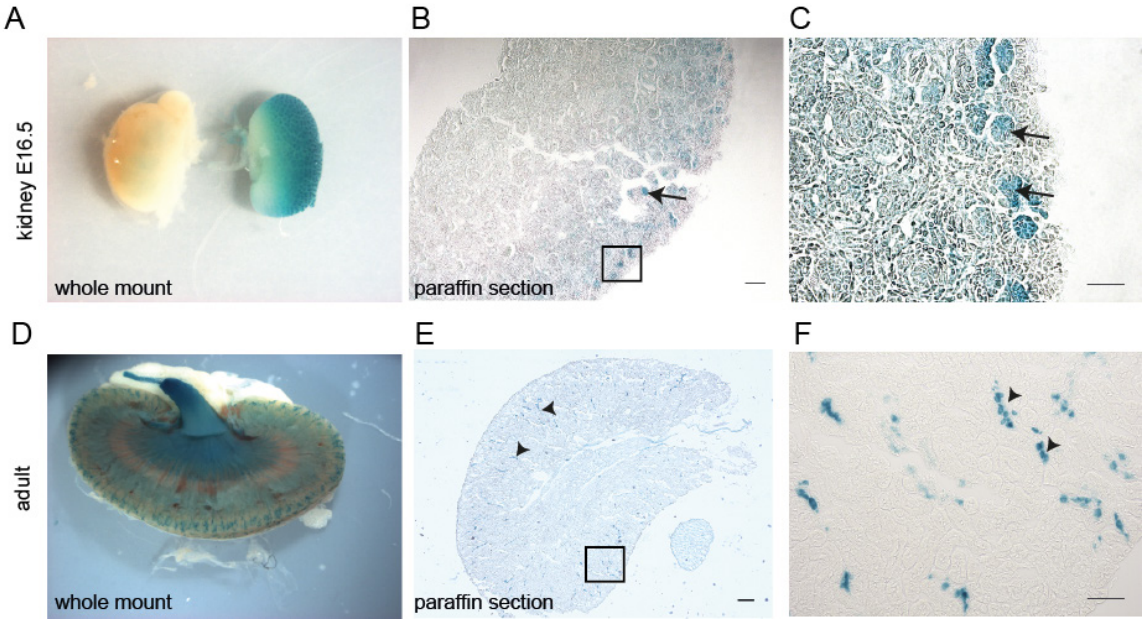

Figure 14. NAV1 is expressed in embryonic kidney glomeruli.

(A) X-gal stained kidney of E16.5 embryos are depicted. Mutant kidney (right) showed circular blue staining. Wildtype (left) exhibited routinely no staining. 100x magnification **(B/C)** Analysis of 15 µm thick kidney sections revealed *NAV1* expression in peripheral glomeruli (arrowhead). Black box indicates region taken for high magnification image shown in (C). **(D)** X-gal staining of adult kidney. Kidney is cut longitudinal. Blue staining can be observed in elongated structures. 70x magnification **(E/F)** The analysis of NAV1 expression in 15 µm thick kidney sections point to an expression in distale tubules (arrowheads). Black box indicates region taken for high magnification image shown in (F). **(B/E)** Scale bar 100 µm **(C/F)** Scale bar 50 µm

To substantiate the postnatal expression patterns of *NAV1* we performed qRT-PCR of different tissues from postnatal day (P)5 wildtype animals. Using this approach we detected *NAV1* expression in brain, lung, heart, kidney, retina and thoracic aorta (Fig. 15).

As expected for a neural gene, the highest expression was observed in the brain. However, highly vascularized organs like lung, heart and retina, as well as rings of the thoracic aorta expressed significant levels of *NAV1*. Expression in retina and thoracic aorta has not been reported before.

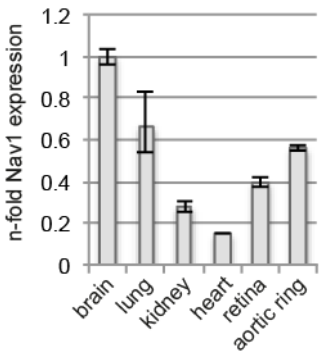

Figure 15. Neonatal expression of murine *NAV1* detected by qRT-PCR.

NAV1 expression was determined by qRT-PCR with Taqman expression assay in triplicates. Probes were normalized to *GAPDH*. Error bars represent SEM.

The retina is commonly used to investigate changes in angiogenesis and neuro-vascular interactions. Therefore, we decided to elucidate the expression pattern of *NAV1* in more detail. We dissected retinas from *NAV1*$^{+/-}$-mice at P5 and performed whole mount X-gal staining. We observed tubule-like expression domains in the area of the developing vessel network, with highest expression in regions of the vessel growth front (Fig. 16)

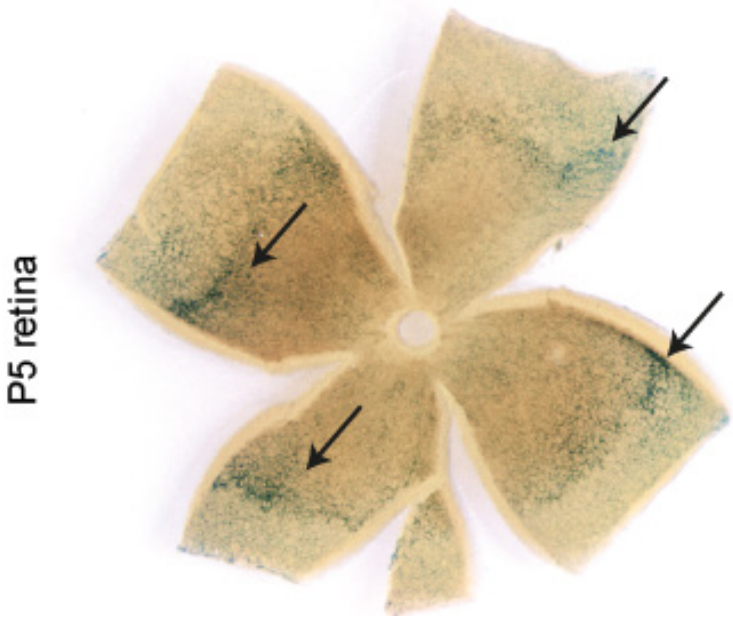

Figure 16. *NAV1* is expressed in vascular areas of neonatal retina.

Representative X-gal staining of neonatal retina taken from a postnatal day (P) 5 *NAV1*-heterozygous mouse (110x magnification). Blue staining can be observed over the whole retina in distinct domains, reminiscent of a vascular network. Staining intensity suggests strongest expression around the angiogenic front.

3.1.3 Murine NAV1 is expressed in a subset of mural cells

It is well established that neural guidance molecules expressed in the vascular system shape and remodel the developing retinal vasculature [27]. Given the almost two-dimensional nature of the vascular plexus in the retina, this model tissue is very suitable for imaging vascular remodeling at cellular resolution. We used X-gal staining to analyze *NAV1* expression domains in the retina. With this staining procedure it was not possible to draw definite conclusions about cellular localization of *NAV1* in retinal tissues. Therefore, we decided to perform immunofluorescent staining of the β-gal protein in mutant mice. In combination with isolectinB4 (IB4) staining to visualize the blood vessels, we were able to analyze the cellular expression domains of *NAV1* (Fig. 17).

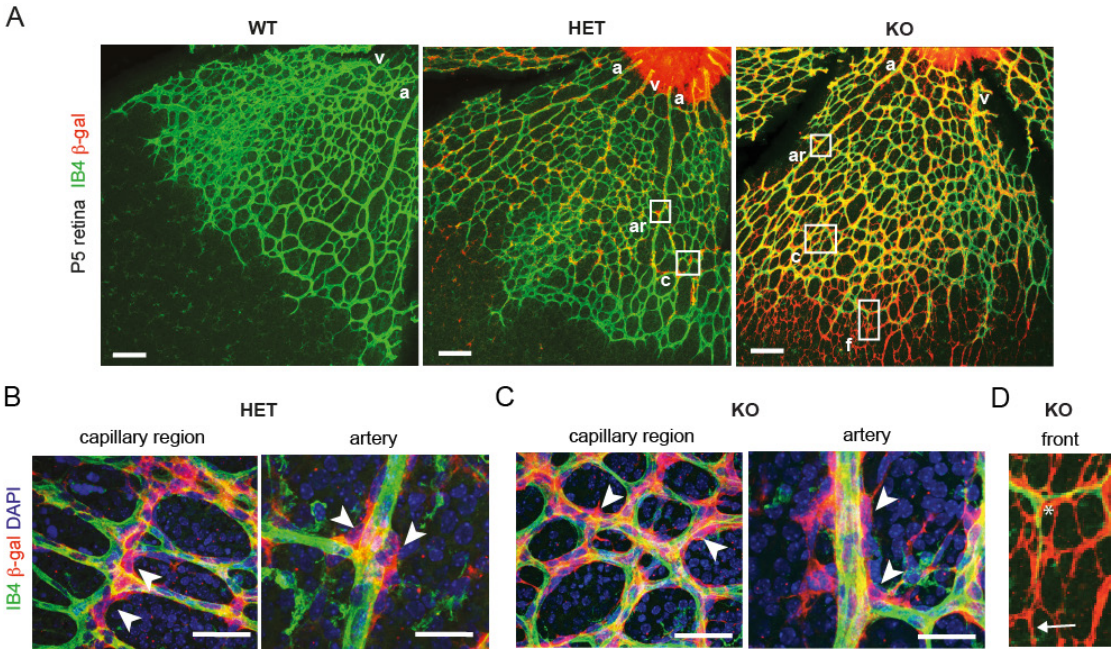

Figure 17. *NAV1* is expressed in perivascular cells of the retina.

(A) Representative images of retinas of P5 mice are shown. The endothelium (IB4, green) and β-galactosidase (β-gal, red) were immunofluorescently labeled. Wildtype mice (WT, left panel) showed no expression of β-gal in contrast to *NAV1*$^{+/-}$ (HET, middle panel) and *NAV1*$^{-/-}$ (KO, right panel). White boxes indicate higher magnifcation of capillary (c) and artery (ar) and front (f) regions depicted in B-D. a- artery; v – vein; Scale bar 200 µm **(B/C)** Higher magnification images of capillary region (left panel) and artery (right panel) region showed expression in cells adjacent to endothelium, due to morphology and location most likely mural cells (white arrowheads, Scale bar 50 µm). **(D)** In NAV1-KO mice addititional expression domains beyond the vascular front (white asterisk) can be detected (white arrow).

In retinas derived from *NAV1*-heteroygous mice we detected clear β-gal signals in distinct cells adjacent to the endothelium (Fig. 17A HET). The detectable expression in *NAV1*-knockout retinas seems to extend to a higher number of perivascular cells (Fig. 17A KO), as well as to cells behind the growing vascular front (Fig. 17D). The β-gal-positive cells in close proximity to the endothelium are localized at capillary regions, arteries and artery branch points (Fig. 17B/C). They exhibit typical morphology of mural cells (Fig. 17B/C arrowhead). Hence, we suggest that those cells resemble mural cells.

Astrocytes are glial cells closely associated with the vascular network of the neonatal retina and precede the vessel network [102]. The *NAV1* expression pattern in the avascular area is reminiscent of an astrocyte meshwork (Fig. 17A KO and 17D). Thus, *NAV1* might be also expressed in astrocytes.

We detected *NAV1* expression in thoracic aorta (Fig. 15). The aortic ring assay is commonly used to analyze angiogenesis *ex vivo* and no astrocytes are present. We therefore decided to substantiate *NAV1* expression in mural cells in the aortic ring assay.

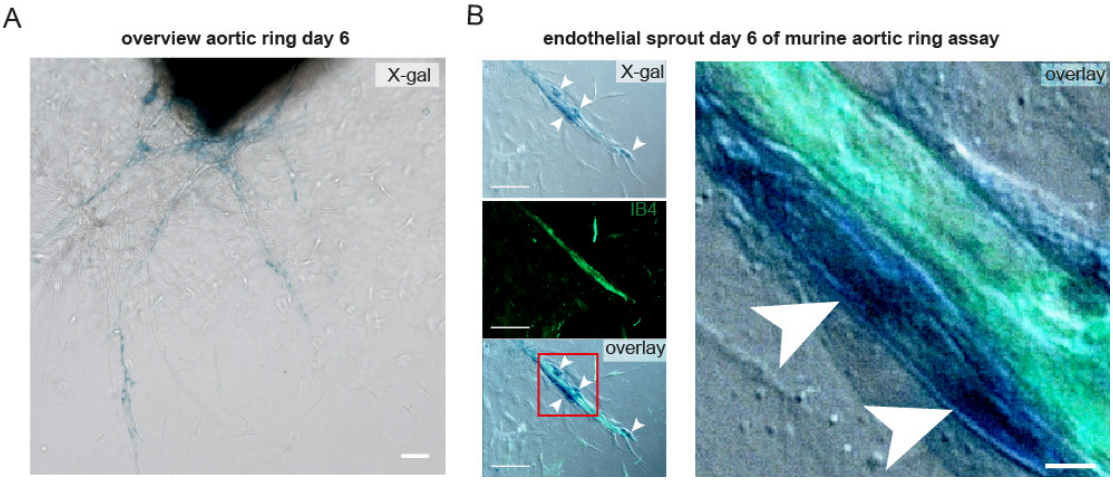

Figure 18. *NAV1* is expressed in cells adjacent to endothelial sprouts of an aortic ring assay.

(A) Aortic rings were embedded in Collagen I and allowed to sprout for six days under VEGF stimulus. Overview of a representative aortic ring stained with X-gal is shown (Scale bar 200 µm) **(B)** Combination of X-gal staining (blue colour, upper left panel) to visualize *NAV1* expression and isolectinB4 (IB4, green, middle left panel) for visualization of endothelial sprouts confirmed specific *NAV1* expression in perivascular cells (lower left panel, white arrowheads) but not in endothelium (Scale bar 50 µm). Right panel shows high magnification of a region in the lower left panel indicated by the red box (Scale bar 5 µm).

Rings of thoracic aorta are embedded in collagen I matrix and cultivated under the stimulus of VEGF. ECs from the intimal layer sprout into the surrounding accompanied by mural cells, resulting in the formation of a small lumenized micro-vessel network.

To detect *NAV1* expression domains we performed whole mount X-gal staining of the vascular networks derived from the aortic rings (Fig. 18A). Endothelial networks were counterstained with the ECs specific marker isolectinB4 (IB4). We detected β-gal-positive cells in close association to the developing vessel sprouts (Fig. 18B). Blue stained cells could be detected at the base and different positions along the vessel sprouts (Fig. 18B, overlay arrowheads), as well as at branch points. We neither could detect X-gal staining of ECs in the angiogenic sprouts nor detected co-localization with IB4 in other areas of the micro-vessel network. These data suggest that *NAV1* is expressed in cells that accompany the growing vessels sprouts at anatomical positions compatible with mural cells.

Taken together, these results showed in both the retina and aortic ring assay that distinct populations of mural cells express *NAV1*.

3.1.4 Loss of NAV1 results in reduced vessel branching complexity

Our data suggest that *NAV1* is expressed in a subset of mural cells. It is known that mural cells are frequently found at sites with active vascular remodeling and play a central role in vascular stabilization processes [33, 46]. We therefore determined if the loss of NAV1 affects mural cell behavior, abundance and distribution and whether vascular branching and maintenance is changed.

We first investigated the vascular formation characteristics in P6 retinas. We compared wildtype, *NAV1*-heterozygous and –knockout mice regarding branch point number, EC tip cell abundance and radial expansion of the vessel network (Fig. 19A). We counted the branch point numbers per defined capillary area (250μm^2) to examine the vessel branching complexity (Fig. 19B). We detected a statistically significant reduction of 24 % in *NAV1*-knockout mice when compared to wildtype (Fig. 19C). The heterozygous mice exhibited almost unaltered branch point numbers. To further confirm the vascular defect, the vascular density in these areas was measured by fluorescence intensity and showed 3.8 % reduction by comparison of wildtype and *NAV1*-knockout animals, but no change in heterozygous mice (Fig. 19D). We next

analyzed if the retinal vascular defect is due to an alteration in angiogenic sprouting behavior of ECs. We tested for vascular progression of the vessel network and amount of ECs sprout number at the angiogenic front. The radial expansion of the vessel network was measured as an indicator of vascular progression. No differences between all three genotypes could be detected (Fig. 19E). In addition, the endothelial sprout number per 1000 µm angiogenic front length was unaltered (Fig. 19F), indicating that the process of sprouting angiogenesis per se is not influenced.

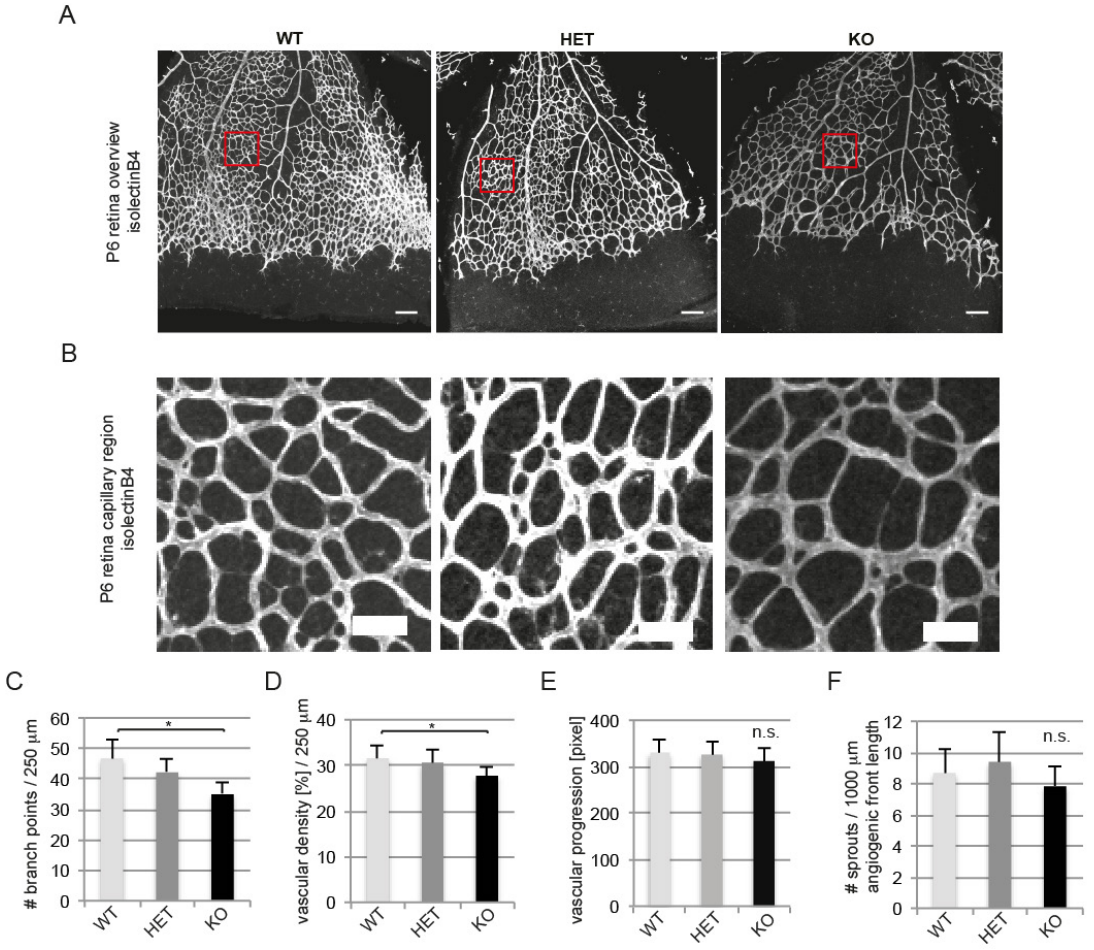

Figure 19. Less vessel branch points in neonatal retinas in the absence of *NAV1*.

(A) Retinas of postnatal day 6 (P6) mice were stained with isolectinB4 to visualize the vessel network. Representative images of wildtype (WT), *NAV1*-heterozygous (HET) and knockout (KO) mice are shown. Red boxes indicate the area taken for images depicted in (B). (Scale bar 150 µm) **(B)** High magnification images of capillary areas taken for quantification are depicted. (Scale bar 50 µm) **(C)** Branch point numbers were manually counted in 250 μm^2 areas shown in (B). Reduced branch point number in NAV1-knockout (KO) mice compared to wildtype (WT) and heterozygous (HET) mice. **(D)** Decreased vascular density only in *NAV1*-deficient mice. **(E/F)** Vascular progression of the vessel network and number of EC sprouts at the angiogenic front are not changed. **(C-F)** Error bars represent standard deviation * p<0,05, n=6 per genotype, n.s. not significant

Thus, these results point to a defect in vessel remodeling but not in EC sprouting, when *NAV1* is ablated.

The astrocyte network precedes the vascular network. It serves as scaffold and "guiding" structure for endothelial cell sprouts at the angiogenic front by secreting VEGF-A [123]. Our *NAV1* expression data implies that it is mainly expressed in mural cells, but also in astrocytes to a lesser degree (Fig. 17). We therefore analyzed the astrocyte network in capillary regions of the neonatal retina (Fig. 20A/B).

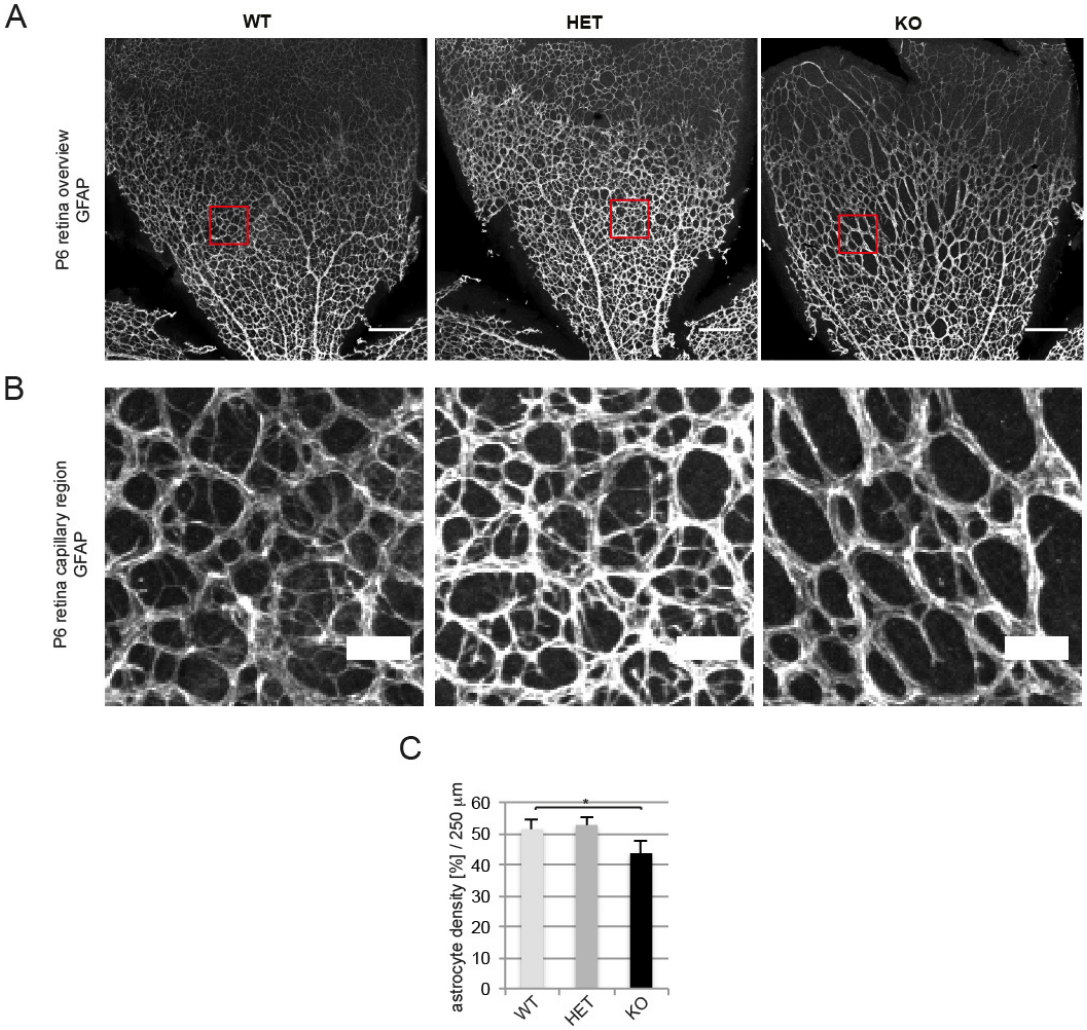

Figure 20. Reduced astrocyte density in *NAV1*-knockout retinas.

(A) Retinas of postnatal day 6 (P6) mice were stained with glial fibrillary acidic protein (GFAP) to visualize the astrocyte network. Representative images of wildtype (WT), *NAV1*-heterozygous (HET) and knockout (KO) mice are shown. Red boxes indicate the area used for quantification of astrocyte density. (Scale bar 150 µm) **(B)** High magnification images of areas taken for quantifaction of astrocyte density are depicted. (Scale bar 50 µm) **(C)** Astrocyte density in 250 μm^2 capillary regions are reduced in *NAV1*-deficient mice compared to wildtype, but not in *NAV1*-heterozygous mice. (error bars represent standard deviation, * $p<0,05$, n=6 per genotype)

We immunofluorescently labeled the astrocytes by the common marker glial fibrillary acidic protein (GFAP) and measured the astrocyte density by fluorescence intensity in identical acquired images. The astrocyte density decreased about 7.8 % by comparison of wildtype to *NAV1*-knockout retina, but showed no differences in heterozygous mice (Fig. 20C). Theoretically, this change in astrocyte network can be the cause for the vascular phenotype in *NAV1*-ablated mice.

To ensure that the detected vascular defect is not due to a change in the astrocyte network we analyzed the micro-vessel networks derived from aortic rings. Thoracic aortae from mice of all three genotypes were dissected and cut into 0.5 mm rings. These aortic rings were embedded in Collagen I matrix and subsequently cultivated under the stimulus of VEGF. At day six of cultivation the micro-vessel network was analyzed for branch point and vessel sprout number (Fig. 21A).

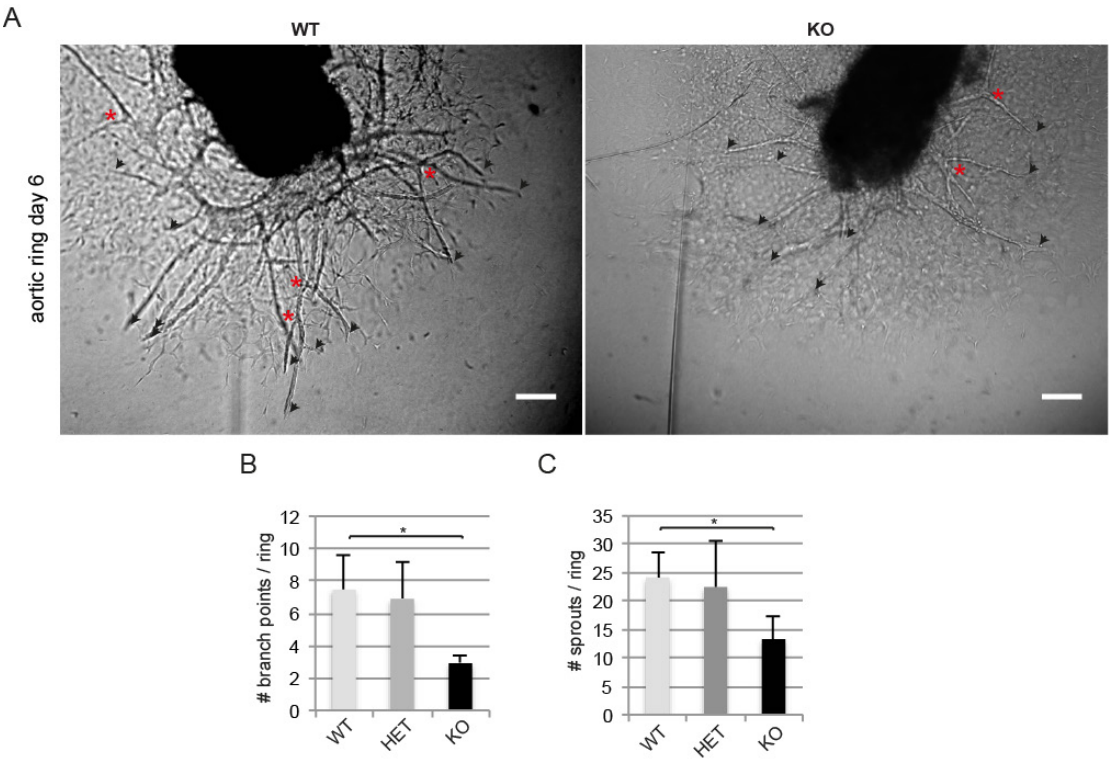

Figure 21. *NAV1*-knockout mice exhibt decreased number of branch points in an aortic ring assay.
(A) Representative phase contrast images of wildtype (WT) and *NAV1*-deficient (KO) aortic rings at day 6 of VEGF-treatment in Collagen I matrix are depicted (scale bar 250 µm). Endothelial sprouts are marked with black arrowheads and branch points with red asteriks. **(B)** Endothelial sprouts and branch points at day 6 were counted. *NAV1*-knockout rings (KO) showed less branch points and sprout number in comparison to wildtype (WT) or heterozygous (HET) rings (error bars represent standard deviation, n= 4 per genotype, * p>0,05).

Counting of branch point number per aortic ring revealed a strong reduction of approximately 63 % in *NAV1*-knockout mice when compared to wildtype, but no significant change in heterozygous animals (Fig. 21B). The amount of ECs sprouts in the absence of *NAV1* was diminished about 45 % (Fig. 21C) in comparison to wildtype. The aortic rings of heterozygous animals showed no difference to wildtype. These results suggest a strong defect in vessel branching of the micro-vessel network in the murine aortic ring assay.

The aortic ring assay underlines the defect in vessel branching in the absence of *NAV1*. Moreover, this implies, in combination with the unaltered ECs sprouting behavior in the neonatal retina that the change in astrocyte density is not causal for the reduction of vessel branching in *NAV1*-knockout mice.

In summary, our results demonstrated that loss of *NAV1* leads to less branched vessel networks.

3.1.5 Increased vessel regression in NAV1-deficient retina

We noted a reduction in the number of vessel branch points in *NAV1*-knockout retina. In contrast, our analysis of EC sprout number at the angiogenic front revealed no differences between *NAV1*-knockout mice and wildtype littermates. This suggests that the change in vessel morphology is not mediated by reduced angiogenic sprouting behavior. Fine-tuning of vascular remodeling processes is dependent on stabilization of vessels.

Newly formed vessels are stabilized by recruitment of mural cells and deposition of ECM components [16]. Destabilization of vessels lead to the regression of vessels. We therefore considered that the reduced vessel branch points might be related to an increase in vessel regression and asked if we could detect a change in vessel regression in neonatal retina of *NAV1*-deficient animals.

To test this, we examined so-called “empty sleeves” using Collagen IV staining. This staining is based on the principle that the basement membrane (BM) is left at the former place of the regressing vessel. The hallmark of an “empty sleeve” is that only remnants of the BM are detectable, in the absence of ECs (Fig. 22A/B). We manually counted the amount of “empty sleeves” per visual field in P6 retinas. The area taken for quantification included an arteriole with its surrounding capillary tree (Fig. 22A).

In line with increased regression we detected a significant 67 % increase in the amount of "empty sleeves" in *NAV1*-deficient retinas compared to wildtype littermates (Fig. 22C).

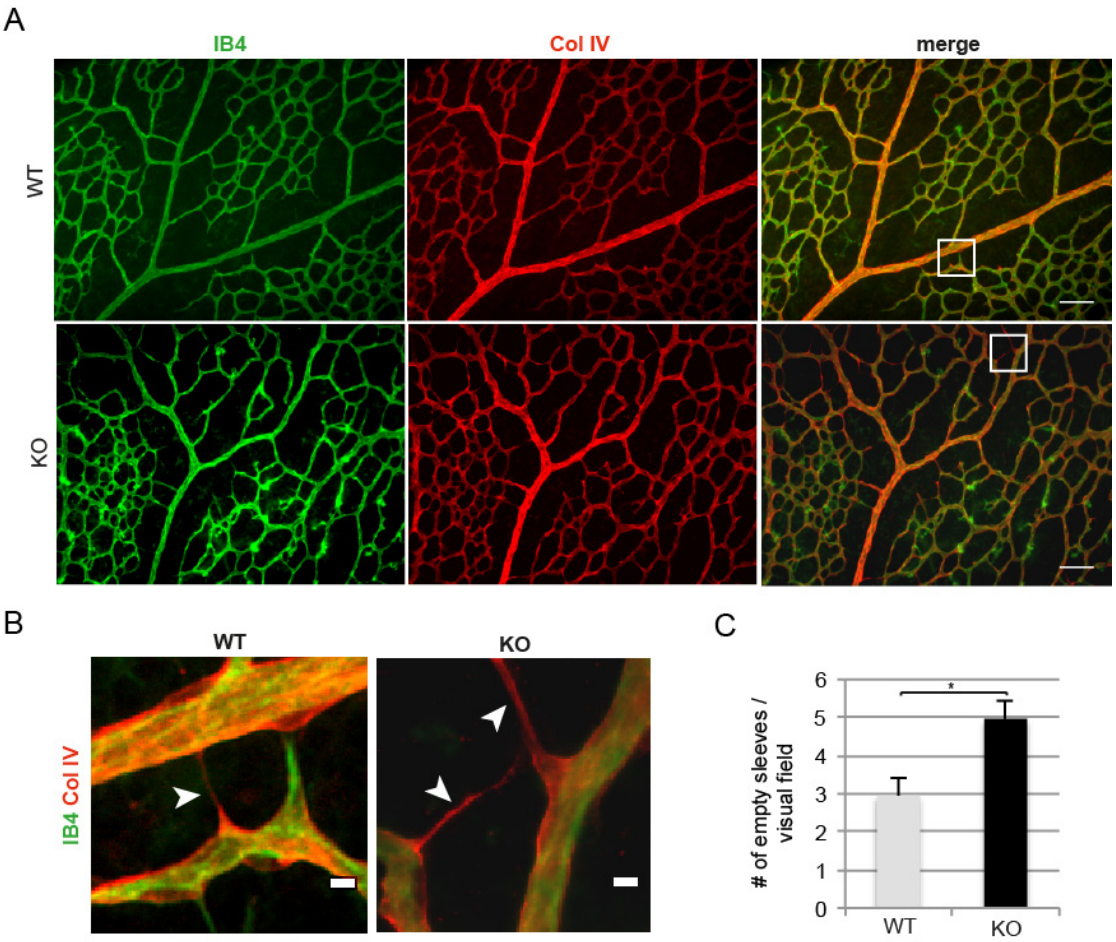

Figure 22. Increased vessel regression in *NAV1*-deficient retina.

Retinas of P6 mice were immunolabeled against Collagen IV (Col IV red) and isolectinB4 (IB4) to visualize basement membrane and endothelium, respectively. **(A)** Representative artery/capillary regions of wildtype (WT) and *NAV1*-knockout (KO) retinas are shown. White box indicates regions depicted in (B) (Scale bar 50 µm) **(B)** High magnification images highlight endothelial free Collagen IV sleeves (empty sleeves) that are marked with a white arrowhead. (Scale bar 50 µm) **(C)** Number of empty sleeves was calculated by manual counting per visual field in merged images as depicted in (A). *NAV1*-knockout mice exhibit an increase in the amount of empty sleeves compared to wildtype (error bars represent SEM, n=6 per genotype, * $p<0,05$).

Taken together, our data showed that the diminished vessel complexity in the *NAV1*-knockout mice associates with increased vessel regression.

3.1.6 Reduced mural cell coverage of vessels in NAV1-deficient mice

NAV1 is expressed in a subset of mural cells and our results demonstrated that the loss of *NAV1* accompanies with an increase in vessel regression. The recruitment of mural cells to the vessel wall is thought to protect vessels from regression [46]. Thus, we asked whether the increased pruning of vessels associates with a reduction in mural cell number covering retinal vessels.

We analyzed mural cell coverage in areas where vascular remodeling defects were detected, thus retinal arterioles and capillary vessels. The retina can be used to analyze different states of vascular remodeling. The more circumferential the vessel growth front gets, the more active is the state of angiogenesis [10, 102]. Thus, regions near the retinal periphery are more active in vascular remodeling processes and vessels near the optic disc are more stable.

We first counted the amount of mural cells per 50 µm artery length. To consider potential differences between mural cell numbers at different vessel positions we subdivided the artery in three different analysis areas (disc, middle, front; Fig. 23A). As mural cell marker we used the expression of the membrane protein neuron-glial antigen 2 (NG2) [43]. High magnification confocal z-stacks were taken for unambiguous identification of mural cells and cell number was counted manually (Fig. 23B).

Interestingly, we noted a change in mural cell coverage only in more peripheral regions (front and middle). In the front area we observed a 16 % reduction of mural cell number in *NAV1*-knockout mice when compared to wildtype, whereas this difference diminished to 12 % in the middle area. In the disc area no change in mural cell coverage could be determined (Fig. 23C). This indicates that the recruitment of mural cells is only disturbed at distinct positions of arterioles, where active vessel remodeling is occurring.

To substantiate the reduced mural cell number at sites of active vessel remodeling we examined the mural cell to vascular density ratio in capillary regions (Fig. 24A/B). Mural cells and ECs were immunofluorescently labeled and images of a defined area were taken under identical settings. The area of fluorescence intensity above a defined threshold was measured automatically and set as mural cell or vascular density, respectively. Subsequently, the mural cell to vascular density ratio was calculated.

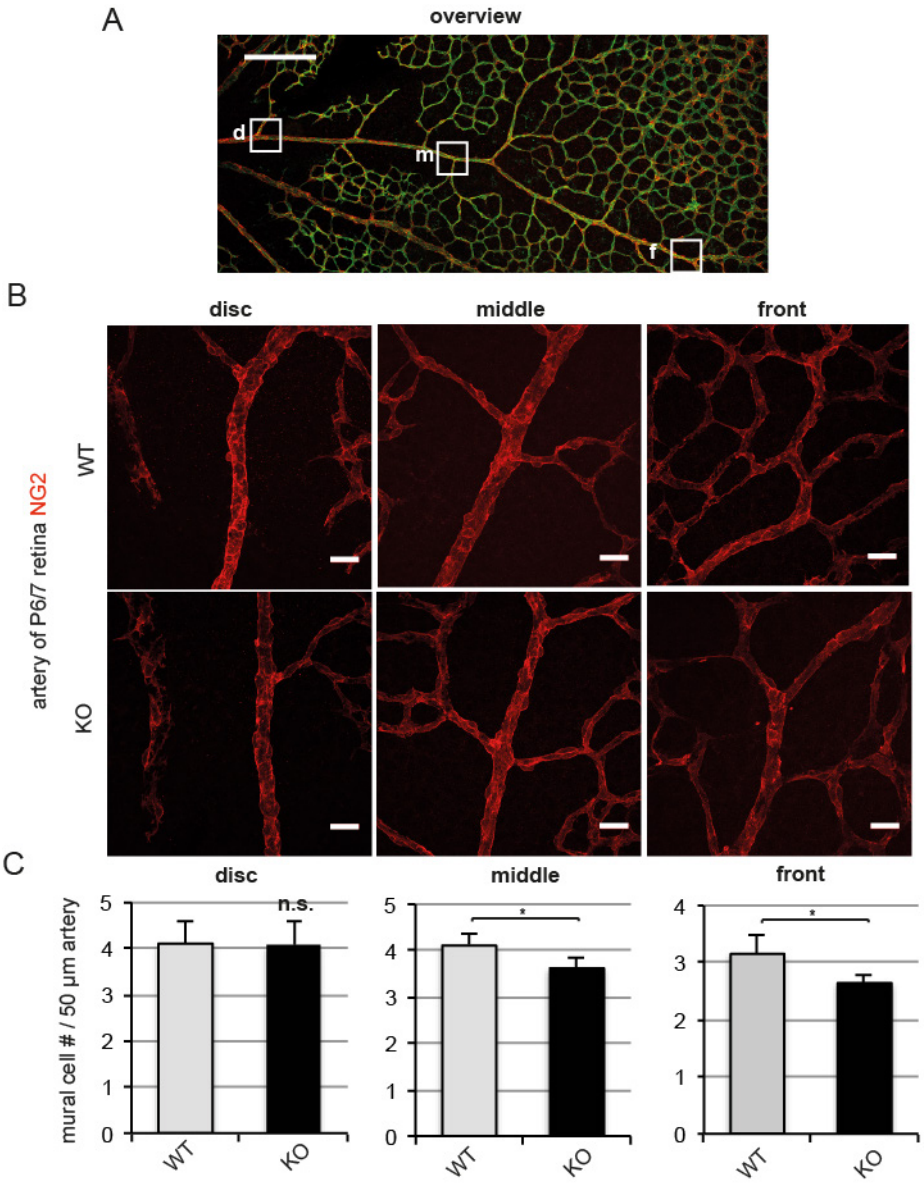

Figure 23. Reduced mural cell number on retinal arterioles in the absence of *NAV1*.
(A) Retinas of P6/7 were immunofluorescently labeled for the endothelium (IB4, green) and mural cells (NG2, red). Overview image of the vascular area of a retina is depicted. Three different areas were used for manually counting of mural cell coverage. disc area (d); middle area (m); front area (f) (Scale bar 200 µm) **(B)** Representative images of disc, middel and front region of wildtype (WT) and knockout (KO) arteries labeled for mural cells (NG2, red) are shown. (scale bar 50 µm) **(C)** Quantification of mural cell number per artery length showed a significant reduction in the middle and front region of the retina, but not in the disc region (Error bars represent SEM, n=6 per genotype, *p<0.05, n.s. not significant).

We detected a decrease in this ratio for *NAV1*-deficient mice in comparison to wildtype littermates (Fig. 24C), indicating reduced mural cell coverage of capillary vessels. This result confirms the decreased amount of mural cells at vessels in areas of active vessel remodeling.

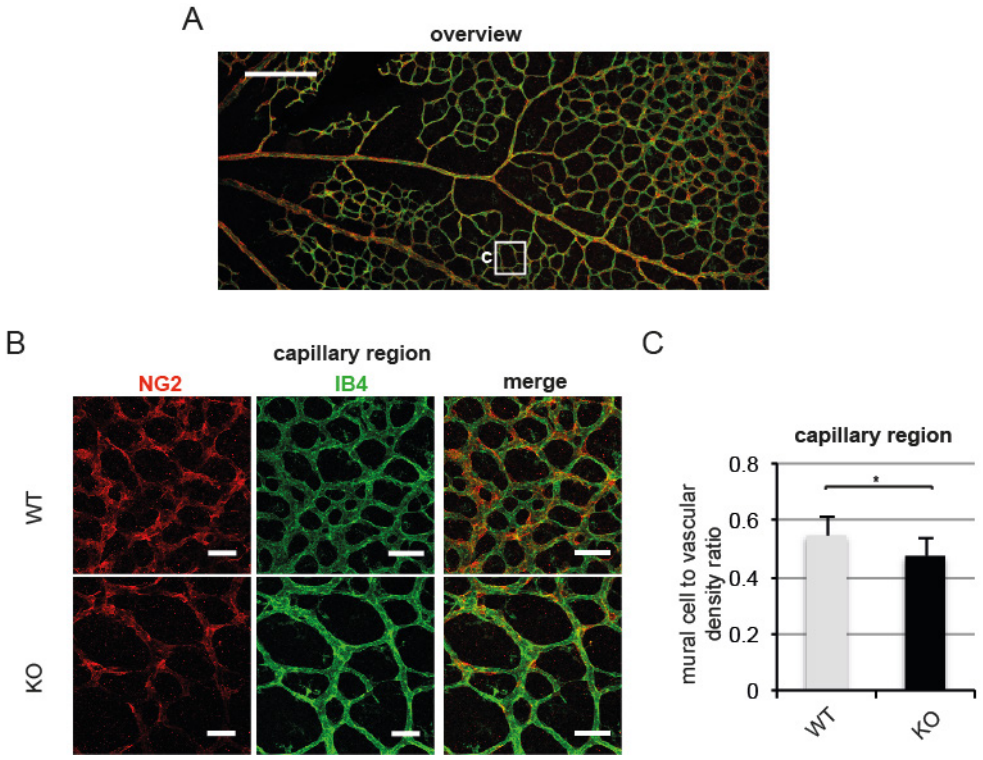

Figure 24. Decreased mural cell coverage of retinal capillaries in *NAV1*-knockout mice.
(A) Postnatal day 6/7 retinas were immunofluorescently labeled for endothelium (green) and mural cells (red). Overview image of the vascular area of a retina is depcited. White box indicates the representative capillary area (c) taken for quantification and shown in (B). (Scale bar 200 µm) **(B)** High magnification images of representative capillary areas in wildtype (WT) and knockout (KO) mice stained for mural cells (NG2, red) and endothelium (IB4, green) are shown. (Scale bar 50 µm) **(C)** Defined areas of capillary regions (250 μm^2) were used for determination of mural cell to vascular ratio. Here, the ratio decreased in *NAV1*-ablated mice compared to wildtype pointing to a reduced mural cell coverage of capillaries (Error bars represent SEM, n=6 per genotype, * $p<0.05$).

In addition, we decided to substantiate the mural cell recruitment defect in the aortic ring assay. The aortic ring was cultivated under identical conditions as before. The micro-vessel network emerged from the aortic ring was fixed and labeled with the mural cell marker NG2 (Fig. 25A). We counted the number of mural cells per 50 µm vessel length identical to the analysis procedure of the retinal arteries. The amount of mural cells per 50 µm vessel length significantly reduced about 26 % in *NAV1*-deficient aortic rings, when compared to wildtype (Fig. 25B).

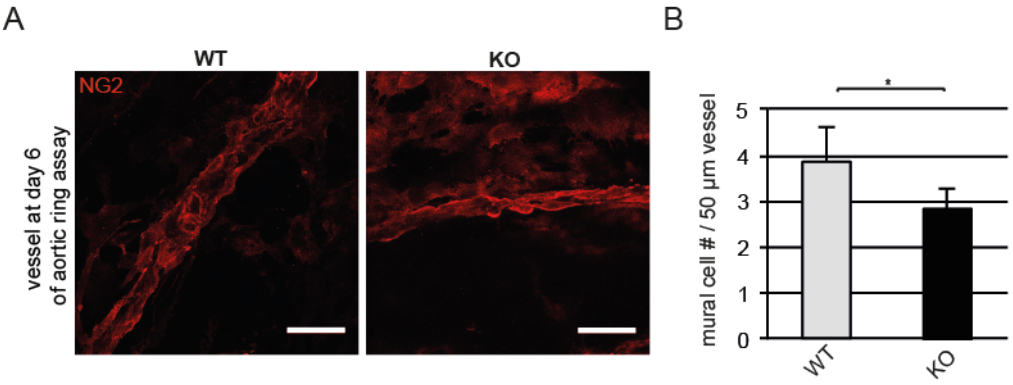

Figure 25. Reduced mural cell number at vessel sprouts of an aortic ring assay.
(A) Representative mural cell stainings (red, NG2) of vessel sprouts at day 6 of an aortic ring assay are depicted. WT-wildtype KO – *NAV1*-knockout mouse (Scale bar 50 µm) **(B)** Significant reduction of mural cell number per 50 µm vessel length can be detected in *NAV1*-knockout aortic rings compared to wildtype (Error bars represent SEM, n= 3 per genotype; *p<0.05,).

Taken together, these results indicate by an independent line of evidence that loss of *NAV1* leads to significantly reduced mural cell coverage of vessels.

3.1.7 Reduced adhesion and motility of NAV1-knockout vSMCs

The ablation of *NAV1* leads to less mural cell coverage of vessels and associates with increased vessel regression (Fig. 22-25). Increased pruning may account for reduced vessel branching as observed in the *NAV1*-knockout mice.
We next addressed why mural cell recruitment is disturbed and reasoned that, analogue to the function of NAV1 in the nervous system [92], [99], NAV1 in mural cells may be relevant for cell locomotion in response to guidance cues like platelet derived growth factor (PDGF)-B and Netrin-1.
Cell migration was examined in a scratch-assay with primary vSMCs. We isolated vSMCs from thoracic aorta as previously described [79]. *NAV1* expression in these primary cell cultures was verified by protein and mRNA detection (Fig. 10 D/E). Confluent cell layers of vSMCs were scratched with a pipette tip resulting in a cell free corridor (Fig. 26A 0 hours). In subsequent hours the cells migrated from the edge of the scratch wound toward the middle of the corridor, resulting finally in the closure of the scratch. The speed at which repopulation of the cell free area occurs is generally considered as an indicator of migratory potential.

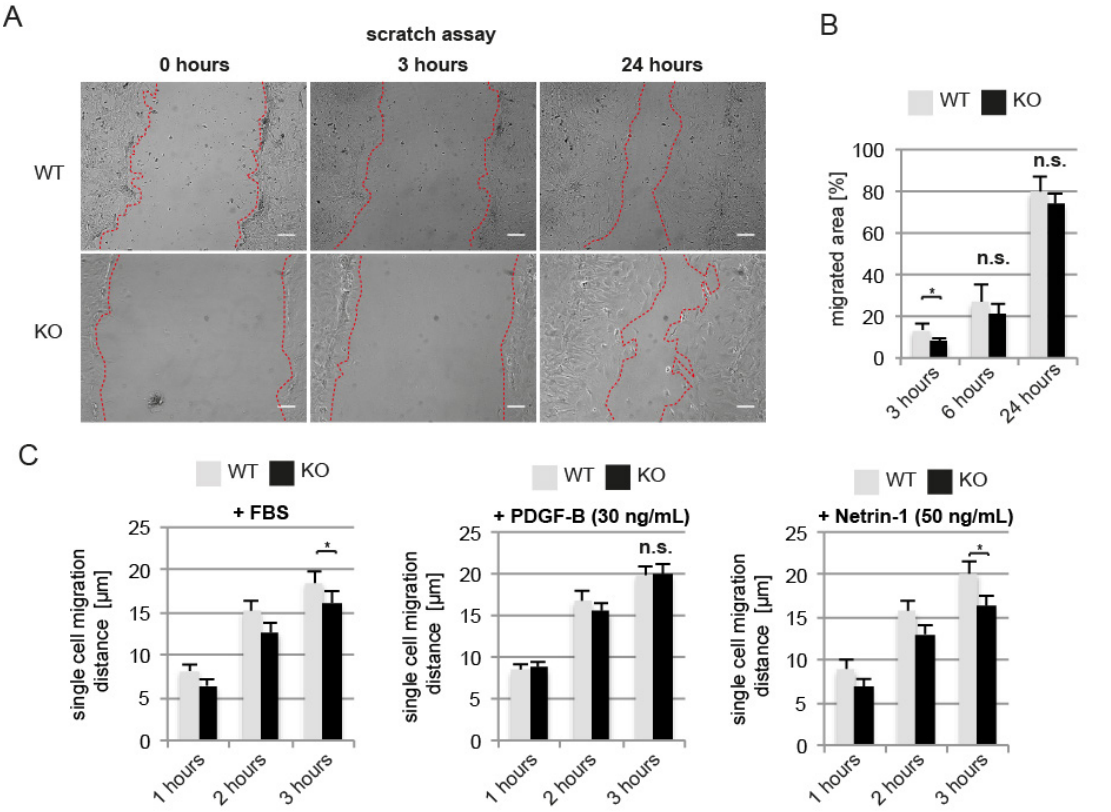

Figure 26. Loss of *NAV1* results in decreased cell motility.

Primary vSMC were grown to confluence. The confluent cell layer was scratched and migration of cells into the cell free area monitored over time. **(A)** Representative phase contrast microscopy images of primary vSMCs immediately after scratching the confluent cell layer (0 hours) and after 3 and 24 hours are depicted (WT wildtype KO *NAV1*-knockout; Scale bar 100 µm). Red dashed lines indicate migration front. **(B)** Quantification of the migrated area demonstrated an overall decreased cell migratory behaviour of *NAV1*-ablated cells in comparison to wildtype cells. (Error bars represent SEM, n=3 per genotype; * $p<0.05$, n.s. not significant) **(C)** Single cell migration distances were determined by single cell tracking of time lapse images in 5 min intervalls. Migration distances of three different time points and conditions are depicted. *NAV1*-deficient cells show reduced cell motility in medium conditioned solely with FBS or supplemented with Netrin-1, but no difference in presence of PDGF-B (Error bar represents SEM, each condition and genotype n = 60 of three independent experiments; *$p<0.05$).

Using time-lapse microscopy we measured the pace at which the cells close the scratch (Fig. 26A). *NAV1*-deficient mural cells moved significantly slower and as a consequence took longer to close the scratch (Fig. 26B). The most profound difference in cell motility was observed in the first three hours. We therefore tracked single cells and determined their migration distances in this time period. *NAV1*-

deficient cells moved slower when compared to wildtype and in any given time interval the migration distance was significantly reduced (Fig. 26C +FBS). Interestingly, this cell motility defect could be rescued by stimulation with PDGF-B (Fig. 26C +PDGF-B). It was recently proposed that Netrin-1 acts upstream of NAV1 [92] and is a positive modulator of vSMCs migration [124]. Conversely to PDGF-B, the addition of Netrin-1 did not rescue the cell motility defect of *NAV1*-knockout cells. In this setting the cells showed a reduction of 19 % in cell migration distance in comparison to wildtype cells. Hence, this points to a specific cell locomotion defect downstream of Netrin-1 in the absence of NAV1.

Cell motility in a physiological environment requires cell-to-cell and cell-to-extracellular matrix (ECM) interactions determining cell migration directionality and velocity. Netrin-1 belongs to a laminin-related protein family and is thought to modulate cell-ECM adhesion [125]. Therefore, we aimed to analyze cell adhesion properties of *NAV1*-deficient cells by a cell adhesion assay. The amount of adhered cells on a plastic surface coated with different protein components was counted manually (Fig. 27A).

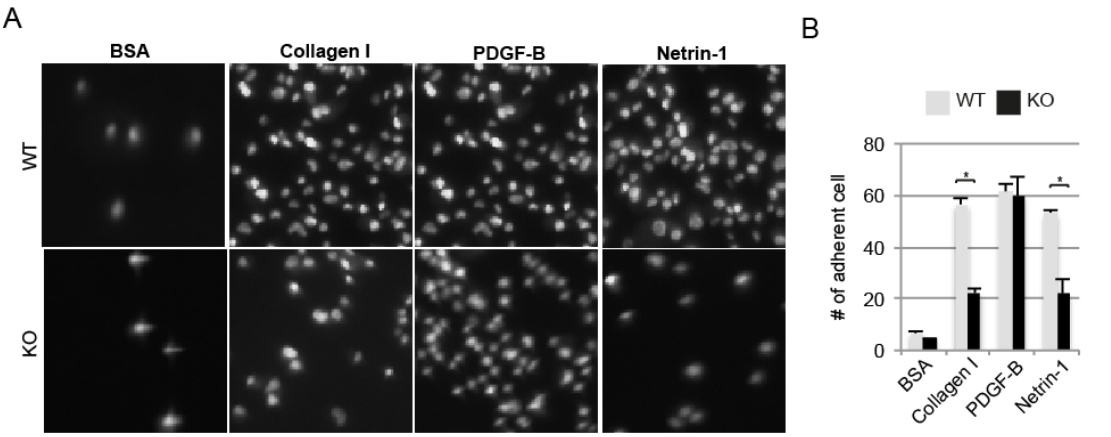

Figure 27. Reduced cell adhesion *of NAV1*-deficient primary vSMCs in response to Netrin-1 and Collagen I. Primary vSMCs were allowed to adhere on a plastic surface coated with BSA, Collagen I, PDGF-B or Netrin-1. Adherent cells were stained with DAPI to visualize cell nuclei. **(A)** Representative visual fields taken for quantification are depicted. **(B)** Amount of adherent cells was counted manually per visual field. *NAV1*-deficient cells exhibit reduced cell adhesion properties in response to Collagen I and Netrin-1 but not to PDGF-B. BSA served as negative control (Error bar represents SEM, cells were counted in triplicates of two independent experiments, *$p<0.05$).

BSA served as negative control showing hardly any cell adhesion (Fig. 27A/B). Interestingly, primary vSMCs deficient for NAV1 exhibit strong reduced adhesion to Netrin-1 and the ECM component Collagen I in comparison to wildtype cells (Fig. 27 A/B). In the presence of PDGF-B, cells showed no differences in adhesive behavior. This substantiates on the one hand the link of Netrin-1 acting upstream of NAV1 and suggests on the other hand that *NAV1*-ablated cells can only weakly adhere to ECM components.

In summary, we suggest that NAV1 is important for cell-ECM adhesion modulated by Netrin-1 ultimately leading to reduced mural cell locomotion.

3.2 *nav1* in vascular development of the zebrafish embryo

The murine loss-of-function data revealed the importance of NAV1 for vascular development (Section 3.1). We used the neonatal retina and the *ex vivo* aortic ring assay to study angiogenesis. Both assays have their limitations. The retina is a common *in vivo* angiogenesis assay, but lacks the dynamic aspect of vessel development. The *in vitro* aortic ring assay does not resemble the *in vivo* situation. To circumvent the limitations of these assays the zebrafish model system can be used. Transgenic zebrafish, expressing GFP under an endothelial specific promotor, can be used to track vascular development during embryogenesis. Knockdown strategies in zebrafish have resulted in similar phenotypes as in mouse. Therefore, we depleted *nav1* and analyzed vascular network remodeling to reveal conserved functions and substantiate the importance of NAV1 for vessel development.

3.2.1 Spatio-temporal regulation of zebrafish nav1 expression

We first identified the putative zebrafish *nav1* sequence. Based on the most recent genome database annotation (Ensembl zebrafish Zv9 assembly, Database version 73.9; GenBank Assembly ID GCA_000002035.2), three different *nav1* genes are predicted. One predicted form is located on chromosome 23 and the other two forms on chromosome 6 (Fig. 28A). Unfortunately, gene annotation of zebrafish genome is still incomplete and we therefore decided to confirm potential isoforms using RACE-PCR.

We first aimed to identify the bona fide gene sequence of *nav1* on chromosome 23. Therefore, we identified the 5´- and 3´-regions by RACE-PCR. 5´-RACE-PCR revealed the existence of two different *nav1* specific products (Fig. 28 B/C). Additionally, 3´-RACE-PCR identified two different 3´-ends pointing to four theoretical possible isoforms of *nav1* transcribed on chromosome 23, disregarding potential and likely alternative splicing products. Combination of the different 5´- and 3´-ends with the predicted database sequence (ENSDART00000115403) and an open-reading-frame-prediction confirms four different putative isoforms with two distinct translational start sites. We categorized those in two main isoforms: isoform A and B (Fig. 28C).

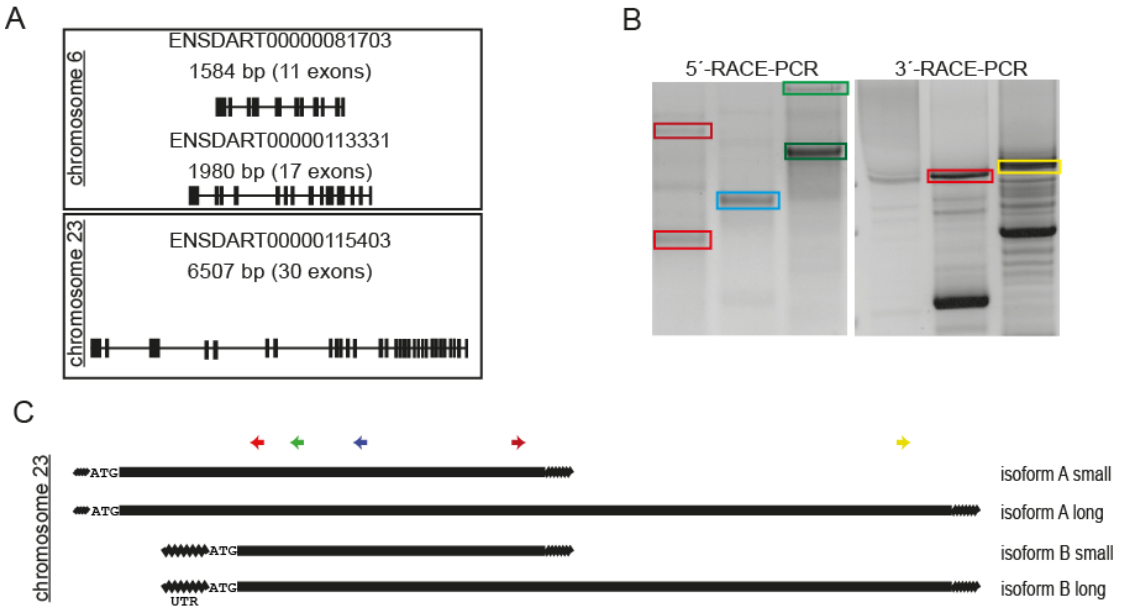

Figure 28. RACE-PCR revealed four potential nav1 isoforms on chromosome 23.

(A) Predicted *nav1* mRNA sequences according to Ensembl database **(B)** RACE-PCR with three different primers for 5´- and 3´- site revealed different *nav1* specific products indicated by coloured boxes. **(C)** *nav1* isoforms revealed by RACE-PCR in combination with data of Ensembl database. The colour of the arrows corresponds to the coloured boxes in (B) and indicate positions of primers used for RACE-PCR.

To identify the temporal expression patterns of *nav1* isoforms we designed specific qRT-PCR probes allowing detection of isoform A and B expression. Significant expression of isoform B starts at 12 hours post fertilization (hpf) culminating in highest expression at 72 hpf. Expression of isoform A starts later at 48 hpf and does not reach the expression level of isoform B (Fig. 29A).

To gain insight into the spatio-temporal expression pattern of *nav1* mRNA we performed whole mount in situ hybridization (WISH) of zebrafish embryos at different developmental stages. We used probes specific for isoform A and B (Fig. 29B). Both probes gave different expression patterns at various developmental stages. In line with qRT-PCR data we detected no expression of isoform A before 48 hpf. From 48 hpf onward, the expression of isoform A was restricted to the head surrounding the eye region (Fig. 29C).

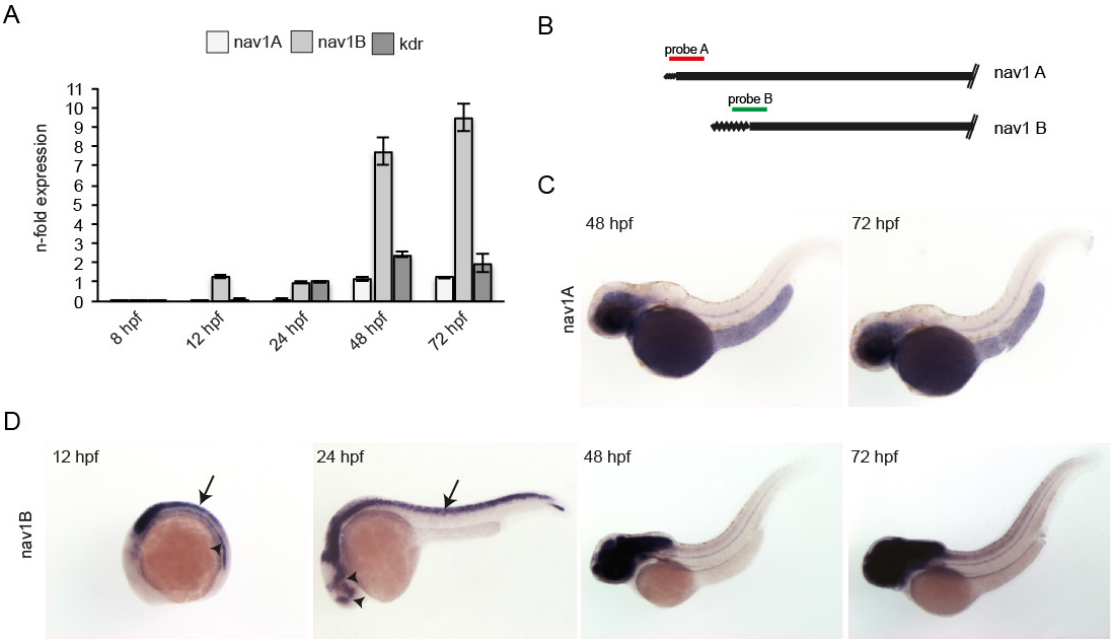

Figure 29. Zebrafish *nav1* isoforms are spatio-temporally expressed during development

(A) qRT-PCR of different developmental stages demonstrated temporal regulated expression of *nav1* isoform A and B. Endothelial specific marker (kdr) was used for comparison of expression levels. Probes were normalized against EF1-α **(B)** Scheme of *nav1* isoforms showing used probes for detection of *nav1A* (red) and *nav1B* (green) by whole mount in situ hybridization (WISH). Probes span 5´-untranslated region and coding region of isoforms. **(C/D)** Zebrafish embryos at 12, 24, 48 and 72 hpf were stained with antisense probes against *nav1* isoforms. Sense probes as negative control showed routinely no staining (not shown). **(C)** *nav1A* is first detectable at 48hpf in the head region surrounding the eye and persists at 72 hpf. **(D)** *nav1B* expression starts at 12 hpf in the notochord (arrowhead) and neural tube (arrow). At 24 hpf expression remains only in the neural tube (arrow) and additional staining patterns in the head region are detected (arrowhead). At 48 and 72 hpf strong expression can only be detected in the head.

Consistent with qRT-PCR, WISH showed expression of isoform B from 12 hpf onwards. Expression regions included the area of the developing neural tube and notochord (Fig. 29D 12 hpf). At 24 hpf expression in the neural tube maintained (Fig. 29D 24 hpf arrow) whereas the expression in the notochord seemed to be lost. Beside these expression patterns we started to observe expression in the head, particular in the hindbrain, midbrain and forebrain regions, as well as in the eye (Fig. 29D 24 hpf arrowheads). At 48 hpf and 72 hpf only strong ubiquitous expression over the whole head region remained (Fig. 29D 48 and 72 hpf).

In summary, we identified at least two novel *nav1* isoforms in zebrafish. Both are differentially expressed during the early embryonic development.

3.2.2 Molecular cloning of nav1 isoform B

We next aimed to identify the definitive isoforms of *nav1B* and therefore performed a nested PCR. In a first step, *nav1B* products were amplified with primer pairs lying in the untranslated regions of the, by RACE-PCR, beforehand identified sequence (Fig. 28B/C). Subsequently, we used primer pairs beginning at the potential start and stop sites of the predicted *nav1B* isoform diversity. The PCR products were analyzed by agarose gel electrophoresis and we could observe several bands, but only two corresponding to correct predicted sizes of around 2.5 and 6 kb (Fig. 30A). Sequencing of the PCR products verified that only the approximately 2.5 and 6 kb seized bands were specific *nav1* products (data not shown).

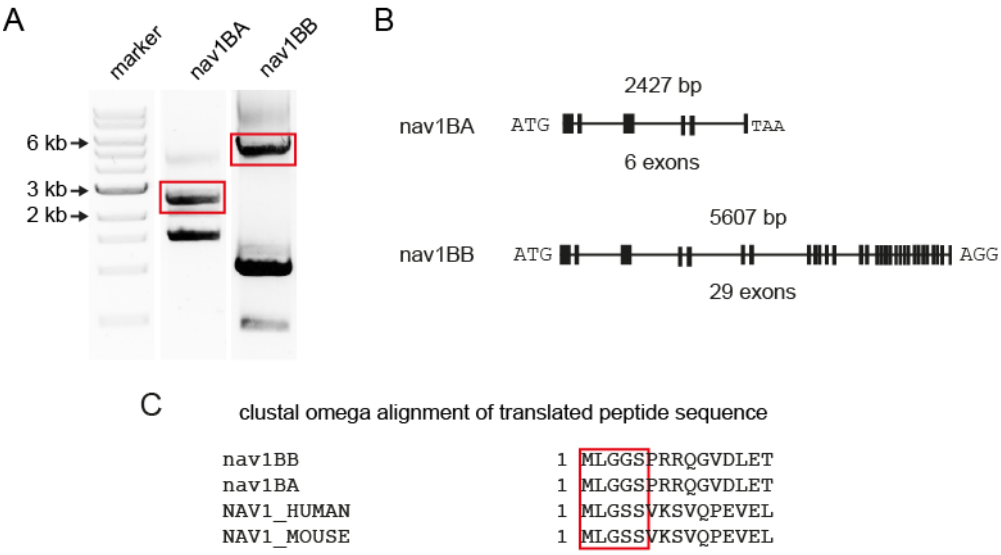

Figure 30. Identification of two distinct *nav1B* isoforms.

(A) Nested PCR with primer specific for *nav1BA* and *nav1BB* lead to two different products with sizes as expected. Verification of PCR products by sequencing revealed two different *nav1B* isoforms (marked with red boxes). **(B)** Model of cloned *nav1B* isoforms, named *nav1BA* and *nav1BB*. **(C)** Multiple sequence alignment of translated *nav1BA* and *nav1BB* isoforms shows homology of *nav1B* isoforms to human and mouse NAV1.

Detailed sequence alignment suggests that two different *nav1B* isoforms exist that we named *nav1BA* and *nav1BB*. They use the same translational start site but differ in length, maybe due to alternative splicing of the long isoform *nav1BB*. Open reading

frame analysis revealed a coding sequence of 5607 bp for *nav1BB,* encoding for a protein with 1807 amino acids and that has a predicted molecular weight of around 202 kDa. The *nav1BA* isoforms is 2427 bp long and encodes for a protein with 808 amino acids and that has a predicted molecular weight of around 86 kDa. To verify the identified *nav1* zebrafish mRNAs we translated the nucleotide sequence into the peptide sequence. Then, we performed a protein alignment with the peptide sequence of human and mouse NAV1 with an online multiple sequence alignment tool (Clustal Omega; http://www.ebi.ac.uk/Tools/msa/clustalo). Here, we monitored homology of Nav1 proteins between zebrafish, mouse and human (Fig. 30C).

Thus, we confirmed two different *nav1B* isoforms encoded by the *nav1* gene located at chromosome 23.

3.2.3 Loss of nav1 affects branching complexity of developing cerebral vascular networks

We used a morpholino approach to knockdown Nav1. Morpholino antisense oligonucleotids (MO) are small oligonucleotides complementary to translational start sites or splice acceptor sites of the corresponding mRNA effectively inhibiting protein synthesis of a desired gene [126].

Different isoforms of *nav1* on different chromosomes exist (Fig. 28A). We designed two different MOs, based on sequence information obtained by RACE-PCR and Ensembl database (Ensembl zebrafish Zv9 assembly, Database version 73.9). MO1 is directed against the translation start site of *nav1* on chromosome 6 and MO2 is directed against the translation start site of *nav1B* and additionally targets a splice site of *nav1A* (Fig. 31A). First, we analyzed if the mRNA expression pattern of *nav1A* and *nav1B* changes, when single MOs are used, to rule out for compensation effects and to verify the splice blocking characteristics of MO2 for *nav1A*.

We performed qRT-PCR to determine the expression levels of *nav1A* and *nav1B* in 24 hpf *nav1* morphants treated with MO1 alone. The expression pattern of both isoforms increased 2-fold when compared to control embryos pointing to possible compensation mechanisms between *nav1* isoforms (Fig. 31B). The use of MO2 resulted in a complete suppression of *nav1A*, but no change in *nav1B* expression compared to control embryos. The down-regulation of *nav1A* verified the splice-

blocking characteristic of MO2. The usage of both MO together lead to the loss of detectable *nav1A* expression levels, as expected, but only a very slight up-regulation of *nav1B* in contrast to control embryos (Fig. 31B).

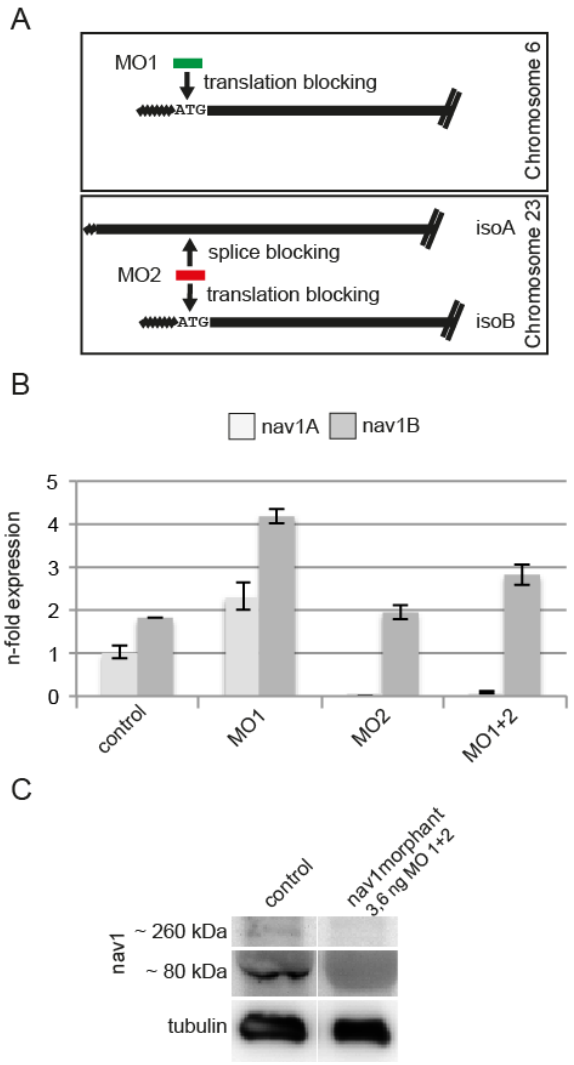

Figure 31. Use of two different morpholinos lead to efficent knockdown of *nav1*.

(A) Scheme of morpholinos (MOs) used for efficient knockdown of different *nav1* isoforms. MO1: translation blocking MO for *nav1* isoform on chromosome 6 ; MO2: translation blocking and splice blocking morpholino for *nav1* isoforms on chromosome 23. **(B)** Representative qRT-PCR of zebrafish embryos at 48 hpf treated with MO1, MO2 alone or both. Use of MO1 alone leads to 2-fold higher expression of *nav1A* and *nav1B* (MO1) in comparison to control (control). Treatment with MO2 leads to splice blocking of *nav1A* and subsequently to a detectable loss of *nav1A* mRNA, but no change in *nav1B* mRNA expression (MO2). Combination of both morpholinos showed no *nav1A* mRNA and a slight increase in *nav1B* expression (MO1+2). (Error bars represent SEM, representatives of three different experiments are shown) **(C)** Immunoblot with custom made antibody against Nav1 protein detected two specific bands for Nav1 with an approximately size of 260 kDa and 80 kDa. In *nav1* morphants treated with a combination of MO1 and 2 no Nav1 protein bands at this size were detectable. Tubulin was used as control for equal protein loading (representative of three independent experiments is shown).

These data suggests that only the use of both MOs lead to an efficient knockdown of *nav1* in zebrafish. We took advantage of a custom-made Nav1 antibody raised in rabbit against the peptide sequence KSDDDILSSKAKAS (Eurogentec, Belgium) to analyze the knockdown efficiency in more detail. We used protein lysates of 72 hpf embryos to determine protein levels by western blot and observed a reduction of two different bands at around 80 kDa and 260 kDa (Fig. 31C). We proposed, due to nucleotide sequence analysis, at least two different isoforms with corresponding protein size (see Section 3.2.2). Hence, this demonstrates on the one hand the functionality of both MOs to reduce Nav1 protein level and on the other hand verifies the existence of two different *nav1* isoforms on protein level. The use of both MOs results in efficient knockdown of *nav1* enabling us to analyze the vascular development in the absence of *nav1* in zebrafish embryos.

We performed knockdown of Nav1 in a transgenic zebrafish line in which eGFP is expressed under the promoter of the endothelial cell marker flk1 [Tg(flk1:EGFP)^{s483}] [113]. This allows *in vivo* inspection of vessel formation at different stages of development. We focused on vessel development in the head region of zebrafish, particular in the hindbrain region (Fig. 32A red box), based on *nav1* expression data determined by WISH (Fig. 29). Vessels in the area of the hindbrain develop in different steps. First, the primordial hindbrain channels (PMHC) are formed, followed by the formation of the basal artery (BA). Starting at around 36 hpf the central arteries (CtAs) sprout dorsally from the PMHC into the hindbrain. Those newly developing vessels interconnect with each other and/or the BA (Fig. 32B). This remodeling process is finished at around 60 hpf [127–129]. Thus, the analysis of the different steps of cerebral vessel development allows us to elucidate the potential role of *nav1* during zebrafish vessel formation.

We observed no differences in the formation of PMHC and BA (data not shown and Fig. 32C). Interestingly, visual analysis revealed a disordered appearance of the CtAs in *nav1* morphants, starting at 48 hpf (data not shown and Fig. 32C). This “disordered” phenotype, manifested by more random appearance of CtA interconnections among each other and connections with the BA, appeared in about 90 % of the analyzed *nav1* morphants at 72 hpf (Fig. 32D). This indicates a defect in remodeling of the CtAs in the absence of Nav1.

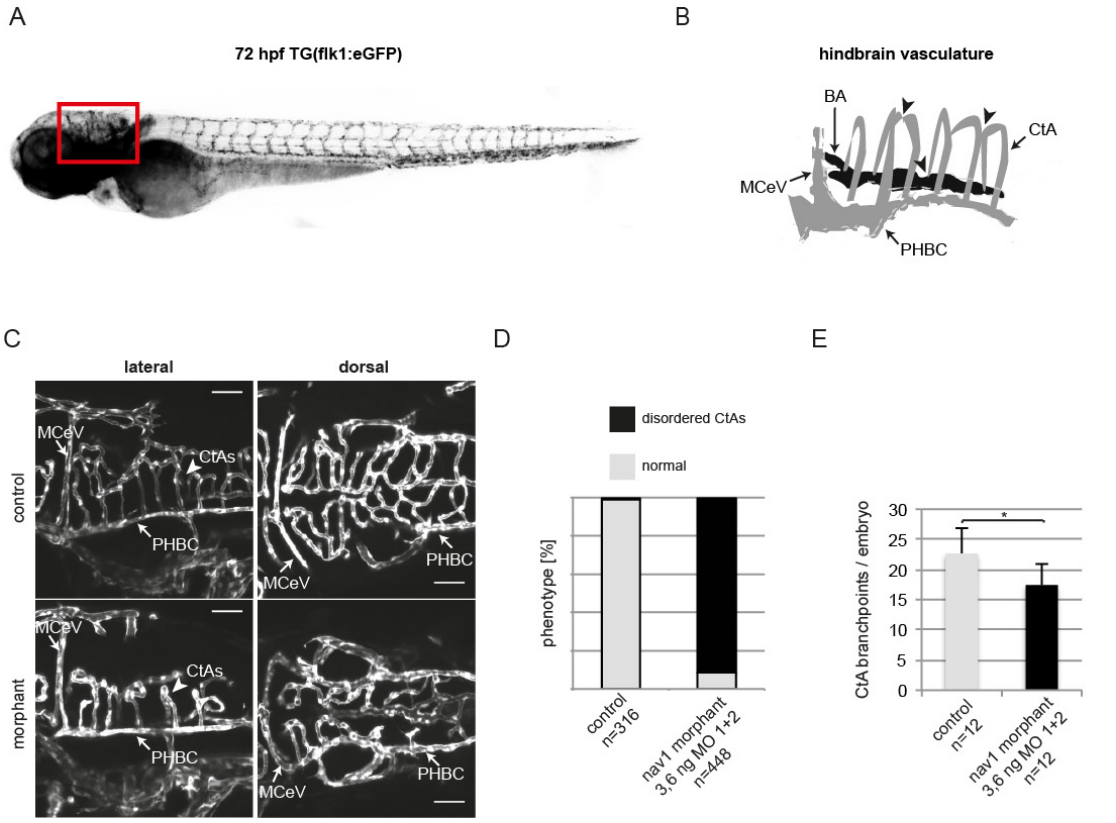

Figure 32. Decreased complexity of CtAs in *nav1* morphant zebrafish embryos.

(A) Vessel formation was analyzed in Tg(flk1:eGFP) zebrafish embryos. Overview images of 72 hpf old embryos are depicted in lateral view. Hindbrain region taken for analysis is marked with a red box. **(B)** Scheme of lateral view on hindbrain vessel architecture is depicted. The central arteries (CtAs) arise from the primordial hindbrain channel (PHBC) and interconnect with each other (arrowheads) or the basal artery (BA). MCeV middle cerebral vein **(C)** Representative images of hindbrain vasculature of control and *nav1* morphants are depicted. Note the 'disordered' pattern of CtAs (white arrowhead) in *nav1* morphants compared to control embryos. **(D)** Quantification of the CtA phenotype in *nav1* morphants compared to control embryos. **(E)** Branch points of CtAs were counted in the dorsal view of the hindbrain region as depicted in (C) dorsal view. (Error bar represents SEM, *p<0.05)

To substantiate the assumed vessel remodeling defect, we determined the branch point number of CtAs in maximum projections of z-stacks acquired by laser scanning confocal microscopy (Fig. 32C dorsal). Each interconnection between CtAs and/or connection with the BA artery was counted as branch point. The branch point number of CtAs decreased in *nav1* morphants about 26 % in comparison to control embryos (Fig. 32E).

In summary, these results demonstrated an efficient Nav1 knockdown by the use of two MOs. The loss of Nav1 results in a reduction of cerebral vessel branching, thus vessel branching complexity.

3.2.4 Reduced PDGFR-β signal in nav1 morphants

Murine *NAV1* loss-of-function data showed loss of branching complexity, potentially involving a defect in mural cell migration. To test whether this is also the case in the zebrafish model, we aimed to analyze mural cell recruitment.

To date no expression data for zebrafish mural cell markers in the hindbrain region exist. We screened different potential mural markers for expression near CtAs, but only the homologue to PDGFR-β was a promising candidate. The expression pattern at 24 hpf is consistent with a previous report [130] and revealed no obvious change of expression levels at this time point (Fig. 33A). PDGFR-β expression at 72 hpf could be observed in areas where CtA remodeling occurs (Fig. 33B control).

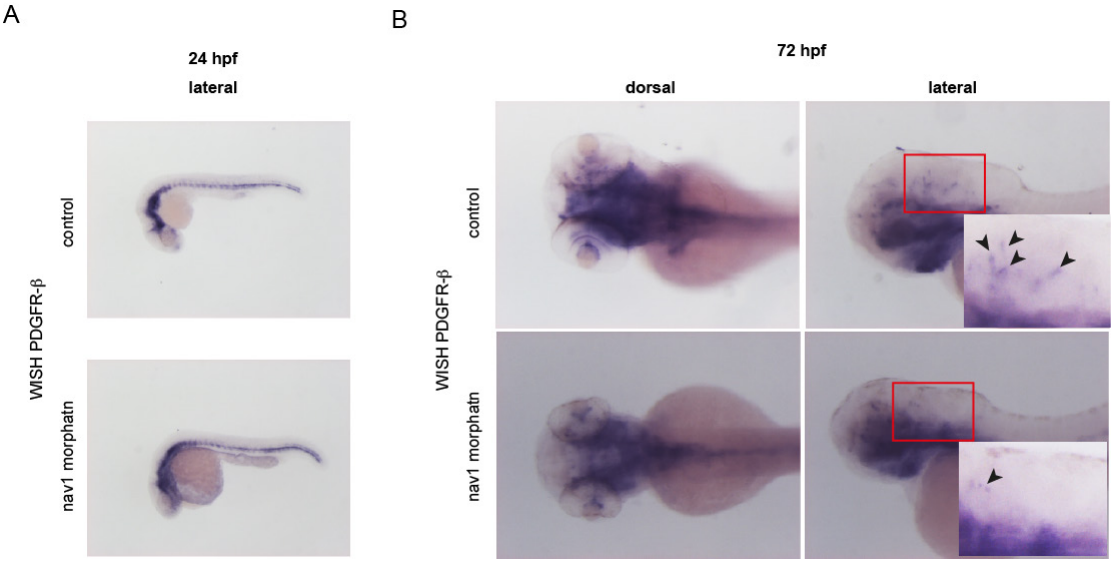

Figure 33. Reduced PDGFR-β signal in *nav1* morphants.

Zebrafish embryos were stained with antisense probes against PDGFR-β. **(A)** No change in expression levels of PDGFR-β at 24 hpf in *nav1* morphants compared to control embryos (315x magnification). **(B)** WISH of *nav1* morphants demonstrated reduced PDGFR–β signal in the hindbrain region in comparison to control animals at 72 hpf (630x magnification). 2x zoomed images of the hindbrain region are depicted in the insets. Black arrowheads mark expression domains anatomically located near CtAs (representatives of three independent experiments are shown).

The comparison of expression levels at 72 hpf between control embryos and *nav1* morphants revealed a slight reduction in PDGFR-β signal (Fig. 32 B dorsal). Importantly, single dots in close proximity to CtAs can be monitored in control embryos but not in *nav1* morphants (Fig. 72B lateral arrowheads).

In summary, these results point to a reduced PDGFR-β signal at defined positions at 72 hpf in the absence of *nav1* in zebrafish.

4. Discussion

In recent years the concept emerged that neurogenesis and angiogenesis share common growth principles. At the cellular level, both growing neurons and angiogenic sprouts use specialized cell types that can sense gradients of guidance cues directing branching morphogenesis. Neural guidance molecules like ephrins and neuropilins are expressed in the vascular system and are relevant for AV differentiation, as well as for vessel branching, whereas vascular growth factors like VEGF mediate neurogenesis [81]. Interestingly, functions of neural guidance molecules appear to be conserved from the nematode *C. elegans* to mouse, and mouse neural guidance genes mediate angiogenic remodeling events [27]. Therefore, it is postulated that during evolution the blood vascular system has co-opted growth control mechanisms from the nervous system in order to shape its structure.

Neural guidance genes have been identified by genetic mutation screens and studied systematically in C. elegans [84]. These mutation screens led to the discovery of several neural guidance genes also present in higher vertebrates. For example, the *C. elegans* genes uncoordinated (*unc*)*5* and *unc6* are named *Unc5* and *Netrin1* in mice. Pioneering work has shown that in mice, UNC5 and Netrin-1 mediate repulsive guidance of commissural axons [125]. More recently, it was demonstrated that in the vascular system Netrin-1 triggers repulsion of angiogenic sprouts involving UNC5B receptors expressed on endothelial tip cells. This was the first study to provide proof of principle that neural guidance molecule function is conserved in vessels and nerves [88]. Based on these studies and the assumption that neural guidance gene functions are conserved, we decided to investigate genes originally reported to mediate neural guidance events in *C. elegans* in higher vertebrates.

In *C.elegans* the neural guidance gene *unc53* has been implied to regulate movement of pioneering axons [91, 93, 99]. The vertebrate homologues of UNC53 are named Neuron Navigators (NAV) [93]. The NAVs family consists of three different members (NAV1, -2 and -3). Our group recently demonstrated that Nav3a controls hepatoblast migration in zebrafish embryos by interfering with actin remodeling [90]. The family member NAV1 has been implied to direct neuronal migration downstream

of Netrin-1 signaling [92]. We hypothesized that NAV1 plays a role in vascular development.

Using zebrafish and mouse loss-of-function models we showed in this thesis that NAV1 influences vascular branching morphogenesis. We identified *Nav1* expression in murine mural cells, and demonstrated that aberrant mural cell recruitment associates with increased vessel pruning culminating in less complex vessel networks. Our results suggest that NAV1 acts downstream of Netrin-1 to regulate cell motility and adhesion. Furthermore, we showed that cell adhesion to Collagen I is significantly decreased in the absence of NAV1, suggesting a profound defect in ECM-cell interaction contributing to the cell locomotion defect.

We conclude that a cell-autonomous function of NAV1 in mural cells is critical for directing mural cell migration, vessel stabilization and formation of a properly branched vascular system.

4.1 Murine NAV1 expression

4.1.1 Cellular localization

The *NAV1*-knockout mouse was generated by a gene-trap approach. The provider (German Gene Trap Consortium) of the ES cell clone showed that the gene trap cassette inserted into the intron 3 of the *NAV1* gene. Based on this information a Southern blot was performed to verify the single integration of the vector into the genome (Fig. 10). We ensured that the integration of the vector leads to a non-functional *NAV1* transcription and translation by western blot and qRT-PCR. In addition, we took advantage of the β-galactosidase (β-gal) activity of the inserted vector and used the β-gal activity to stain embryos and tissues with X-gal (Fig. 12-14). The compound X-gal is hydrolyzed by active β-gal into an insoluble blue product. Positive staining results can only be achieved by proper splicing of the vector into the exons of the *NAV1* gene. Hence, our successful X-gal staining of *NAV1*-mutant mice substantiates the loss of protein and mRNA data, and demonstrates an effective mutation of the *NAV1* gene.

Furthermore, we used X-gal stained tissues and embryos to track expression domains of *NAV1*. Our expression data are in line with previous described expression domains

regarding brain, heart, lung, kidney and somites. Recent reports characterized *NAV1* expression based on *in situ* hybridization data of embryo sections and Northern blot data of tissues samples [94, 96]. Both approaches limit insights considering expression architecture that we could circumvent by whole mount X-gal staining. With our approach we identified several expression domains that confirmed previously reported ones and in addition new domains not reported before.

We could show that *NAV1* is expressed in glomeruli of the embryonic kidney, but already during neonatal stages this expression domain changes to structures reminiscent of distal tubules (Fig. 14). Careful analysis of *NAV1* expression on cellular level and analysis of glomeruli morphology can be a subject of future studies.

The expression domains at the atrium and ventricle of the heart resembled a network of coronary blood vessels (Fig. 13). Whether the expression of *NAV1* is virtually located in these vessels is not clear.

In lung, the expression domain of *NAV1* resembles two different structures: the vessel or the bronchial tree. The analysis of adult lung sections suggest, that the expression is restricted to epithelial tissues, hence cells belonging to the respiratory tree (data not shown). But a vascular expression during embryogenesis cannot be excluded.

The eye is one novel identified expression domain of *NAV1*. During embryogenesis the expression pattern suggests that *NAV1* is located in areas of the prospective retinal tissues (Fig. 12). In neonatal mice the expression was pinpoint to retinal areas adjacent to the developing vessel network (Fig. 16). Moreover, careful analyses of cellular expression domains by immunofluorescent labeling of the β-gal indicates that subsets of perivascular cells, the mural cells, are positive for *NAV1* (Fig. 17). However, *NAV1* seems to be expressed also in a neuronal cell type, the astrocytes. Although double labeling of ECs marker and β-gal was successful, the use of antibodies against mural cell or astrocyte markers was not, when combined with β-gal labeling (data not shown). In addition, only one of different tested commercially available antibodies directed against NAV1 was adequate for protein detection by immunoblot (Fig. 10D), but not for immunofluorescent labeling of tissues. Thus, to verify the expression of *NAV1* in mural cells we decided to analyze gene expression by the murine aortic ring assay, in which astrocytes are absent. *NAV1* expression in the thoracic aorta was not reported before. Here, co-staining of β-gal and the ECs marker isolectinB4 substantiated the expression of *NAV1* in distinct mural cells (Fig. 18). Moreover, we

detected NAV1 in protein lysates of primary vSMCs isolated from thoracic aorta (Fig. 10D). Thus, our data clearly show that NAV1 is expressed in mural cells.
Mural cells influence vessel stability in vessel formation processes. The consequence of non-functional NAV1 for vessel development and particular for mural cells is discussed in section 4.2.1.

4.1.2 Sub-cellular localization

No definite information of native sub-cellular localization of NAV1 protein is so far available, but due to transfection of fibroblast-like cells with GFP-tagged NAV1 *in vitro* it is assumed that NAV1 is a cytoplasmic protein, [96, 98]. The use of β-gal labeling in *NAV1*-mutant mice does not allow us to draw conclusions about sub-cellular localization of NAV1 and available antibodies do not work in immunohistochemistry protocols. Nonetheless, it was shown that GFP-tagged NAV1 localizes specifically at plus ends of microtubules (MTs) via a distinct MT-binding domain. Overexpression of the GFP-NAV1 construct has lead to MT bundling in a fibroblast-like cell line suggesting a profound role of NAV1 in cytoskeletal dynamics [92]. The MT binding capacity has been also shown for NAV2 and NAV3 in other mammalian cell culture experiments [99]. Interestingly, one isoform of NAV3 in zebrafish, as well as UNC-53 in C. elegans, exhibit interaction with actin dynamics influencing cell migration properties [93, 100]. It is speculated that the NAV family in general may act as a link between actin and MT components of the cytoskeleton [91], but so far evidence for this presumption is missing. Based on our functional migration assay data it is conceivable that NAV1 is involved in cytoskeletal dynamics. The potential role of NAV1 on cytoskeletal dynamics and consequences for cellular behaviors are discussed in section 4.2.2.2.

4.2 The function of murine NAV1

4.2.1 NAV1 influences vessel formation in vivo

We could show that loss of NAV1 results in less complex vessel networks in the neonatal retina and in the aortic ring assay (Fig. 19 and 21). Vessel branching per se is dependent on sprouting angiogenesis, thus directed ECs migration [4, 5]. Deregulated ECs guidance can lead in consequence to increased or decreased vessel branching. Guidance of ECs is mainly driven by factors located in the extracellular environment, like the secreted vascular endothelial growth factor (VEGF). Netrin-1 is a neural guidance factor that can also influence vessel branching. It acts on UNC5B receptors expressed on ECs and induces vessel retraction [88]. Similar is true when the Notch-Delta Like 4 signaling pathway, triggered by VEGF, is abrogated [131]. These phenotypes are dependent on environmental cues influencing EC autonomous behavior. Since we detected no *NAV1* expression in ECs we exclude EC autonomous influences. Thus, expression of NAV1 in other cell types and subsequent cellular interactions must influence ECs behavior.

4.2.1.1 NAV1 and astrocytes

Angiogenesis is dependent on cellular interactions. Especially in the retina several cell types are important for correct vessel patterning [123]. One of those cell types is the astrocyte. Astrocytes grow, similar to blood vessels, from the retinal optic disc towards the periphery [102]. Importantly, this cell type precedes the blood vessels and guide vessel sprouts by secreting VEGF [132–134]. Furthermore, it is suggested that correct patterning of ECs and astrocytes in the retina is dependent on sequential reciprocal cellular interactions [123]. Primarily vessels receive signals from astrocytes for correct sprouting and subsequent provides negative feedback signals for astrocyte growth [134]. Interestingly, *NAV1* seems to be expressed in astrocytes (Fig. 17) and the density of the astrocyte network is reduced (Fig. 20). This can lead to the assumption that the cause for our observed vessel phenotype in *NAV1*-knockout mice is due to the change in astrocyte patterning. If this assumption is correct a strongly reduced vessel sprouting and growth should be detectable. However, loss of *NAV1* did

not lead to any differences in ECs sprout number and vascular progression compared to wildtype (Fig. 19). That makes it very unlikely that the change in astrocyte density is responsible for the reduced complexity of the vessel network in the *NAV1*-knockout retina. The use of the aortic ring assay to study branching morphogenesis substantiated this conclusion. Here, strong reduction in branch point number in the absence of astrocytes was observed (Fig. 21). This indicates that the change in the astrocyte network density is the consequence of the altered vessel network and not the cause of it.

4.2.1.2 NAV1 and mural cells

Another cellular relationship important for vascular patterning is the interaction between ECs and mural cells. We detected less mural cell coverage of retinal vessels and vessels formed in an aortic ring assay from *NAV1*-deficient animals (Fig. 22-24). Mural cell coverage of vessels is associated with vessel stability and maturation, but whether the actual presence of mural cells protect vessels from regression is controversial [46]. It was suggested that the coverage of vessels with α-smooth muscle actin (α -SMA) positive mural cells marks mature vessels in the retina, thus vessels that stopped to prune and remodel [47]. This assumption was furthermore supported by the observation that mural cell coverage in the retina correlated with protection from vessel regression [48]. In contrast, recently it was demonstrated that mural cells can selectively promote regression in the retina [50]. In this report endosialin, a transmembrane glycoprotein with mural cell specific expression was depleted. Intriguingly, the mutant mice showed no change in mural cell coverage. We detected less vessel density and reduced mural cell coverage of vessels in the absence of NAV1 (Fig.19 and 22). Our results are therefore contrary to the aforementioned vessel destabilization phenotype, but rather substantiate the vessel stabilization characteristics of mural cells.

Interestingly, both characteristics of mural cells may be feasible. Mural cells are a heterogeneous cell population thereby different functions are not unlikely. The expression pattern of *NAV1* suggests that it is expressed in subpopulations of mural cells (Fig. 17 and 18). The motility of mural cells lacking NAV1 is reduced *in vitro* (Fig. 26). Furthermore, missing or not correct positioned mural cells accompanies

with an increased vessel regression *in vivo* (Fig. 25). Thus, it is possible that NAV1 does not regulate recruitment of all mural cells, but rather seems to be important for distinct cell positioning on the endothelium; in consequence regulating vessel regression and thus vessel branching morphology. This points on the one hand to specific juxtacrine signaling between ECs and mural cells and/or mural cells to mural cells at certain positions and on the other hand support the notion of heterogeneous roles of mural cells in vessel development [46].

One explanation for diverse roles of mural cells – and maybe a key to identify different sub-populations - might be the heterogeneous ontogeny. At least for vSMCs it is clear that they arise from different origins, like mesoderm, neural crest, somites and others [32, 37]. However, little is known about the developmental origins of pericytes as very few lineage-mapping studies have addressed whether or not pericytes share common origins in the embryo with vSMCs. One exception to this is in the brain, where pericytes and cerebral vSMCs have been shown to originate from cephalic neural crest progenitor cells [135]. Moreover, studies *in vitro* and *in vivo* showed that vSMCs from different embryonic origins respond in lineage-specific ways to common stimuli [136, 137].

Thereby, based on their diverse developmental origin mural cells might facilitate different paracrine and autocrine signaling mechanisms even in one vessel tree like the retina. For mural cells of the retina no cell fate mapping studies have been performed so far. But under the assumption that retinal mural cells have a mosaic origin this can be one explanation for their divergent described roles.

To test whether different cell fates are responsible for variable influence on vessel development only mural cells from distinct anatomical positions can be used. Mural cells of the thoracic aorta are derived from the somites and is “segmental” insofar as the cells derive from individual somites [35]. Therefore, the aortic ring assay and/or the isolation of vSMCs from defined anatomical positions might be a practicable experimental setup to test for differences in mural cell behavior. Moreover, this approach can potentially give insights in differential function of NAV1 in mural cells.

4.2.2 Cell motility and signaling

Based on our results we propose that the absence of NAV1 leads to a reduction in mural cell motility that in turn causes less mural cell coverage of vessels triggering an increase in vessel regression ultimately resulting in less complex vessel networks (Fig. 36). We suggest that NAV1 is mainly regulating mural cell motility therefore we will discuss two main questions in the following sections: 1. What are the upstream factors influencing NAV1 and mural cell locomotion 2. What are the downstream factors influenced by NAV1 modulating cell migratory behavior.

4.2.2.1 Signaling upstream of NAV1

Knowledge of a distinct mechanism that can explain how the absence of mural cells may lead to a change in vessel patterning is thus far lacking [32, 33]. In recent years several signaling mechanisms were discovered that appear to be involved in mural cell recruitment processes. These include platelet derived growth factor B (PDGFB)/PDGFRB, angiopoietin-1 (ANG1)-TIE2 and Notch3 signaling. Ablation of the signaling pathway PDGF-B/PDGFR-β leads to less mural cell coverage [60, 61]. The degree of mural cell deficiency varies extensively between different organs [44], [57]. This suggests that other signaling components play similar important roles. The process of vascular remodeling and maturation seems to be strongly dependent on ANG1-TIE2 [5, 32]. ANG1 induces vessel stabilization via the TIE2 receptor [71]. Notch signaling is critical for angiogenic sprouting but also plays a role in mural cells and ECs-mural cell interactions. Notch3 is expressed in mural cells, seems to act via the ligand Jagged-1 (Jag-1) and induces vessel maturation in retinal vessels [76, 77]. Our *in vitro* experiments suggest that NAV1 controlled mural cell recruitment is rather Netrin-1 dependent than dependent on PDGF-B signaling (Fig. 26 and 27). The role of angiopoietins and notch signaling was not analyzed and therefore has to be considered in future experiments.

The role of Netrin-1 has been described as a positive modulator of mural cell migration [124], but Netrin-1 function in vascular development *in vivo* has been mainly illustrated for ECs so far. Here, it is known that it acts via its receptor UNC5B as repulsive cue [88]. Thus, one has to consider potential simultaneously action of

Netrin-1 on ECs and mural cells in general, but for the phenotype of the *NAV1*-knockout mice this dual role has not to be account for, as NAV1 is not expressed in ECs in the analyzed tissues. Nevertheless, it cannot be ruled out that NAV1 is expressed in ECs of other tissues.

Our *in vitro* experimental setup gives us information about general cell motility characteristics. Motility of cells can be regulated randomly (chemokinesis), guided by chemical soluble concentration gradients (chemotaxis) or by their adhesiveness to ECM itself or substrate-bound chemoattractants (haptotaxis). The comparison of the cell adhesion assay data (Fig. 27) with the cell motility data (Fig. 26) points to a stronger defect in cell adhesion properties when NAV1 is lacking. In addition, the adhesion defect was similar in response to Collagen I and Netrin-1. Thus, our results indicates that NAV1 in mural cells is more important for haptotactic migration downstream of Netrin-1 and/or the ECM component Collagen I (Fig. 27).

It was demonstrated previously that the haptotactic effect of ECM components on human vSMCs migration is more profound when compared to the chemotactic effect of PDGF [138]. Which is consistent with our data. We observed no change of cell adhesion and motility properties in *NAV1*-deficient mural cells in response to the chemotactic stimulator PDGF-B (Fig. 26 and 27). Thus, this substantiates the haptotactic defect of *NAV1*-deficient mural cells.

Cell adhesion can be facilitated by different receptors, like receptor tyrosine kinases, G-protein coupled receptors or integrins. Netrin-1 can bind to the UNC receptor family as well as the DCC and neogenin receptors [125]. Expression of the neogenin receptor in human and rat vSMCs was described [124], but evidence for murine mural cells is lacking so far. It was shown that Netrin-1 can bind $\alpha6\beta4$ and $\alpha3\beta1$ integrins and this is suggested to regulate epithelial cell adhesion and migration [139]. Furthermore, mural cell specific knockout of the integrin $\beta1$ subunit lead to discontinuous mural cell coverage of vessels [140]. Thus, signal transduction via integrins alone or even in combination with Netrin-1 can be one alternative pathway to regulate NAV1 activity. Furthermore, binding to ECM components is mediated by integrin receptors. Thus, it is also feasible that NAV1 modulated mural cell motility and adhesion is dependent on integrin receptors, but independent of Netrin-1.

Taken together, several possible upstream factors exist that might influence NAV1 and subsequently mural cell motility. Our data indicate that Collagen I and Netrin-1 are important signal transducers for NAV1 function and sequentially modulating mural cell locomotion. If other signaling cues exist that regulate NAV1 function remain to be clarified. Furthermore, we have given some receptor candidates, which might convey extracellular signals to the intracellular located NAV1. Overview of possible upstream signaling cues and receptors is given in Figure 34.

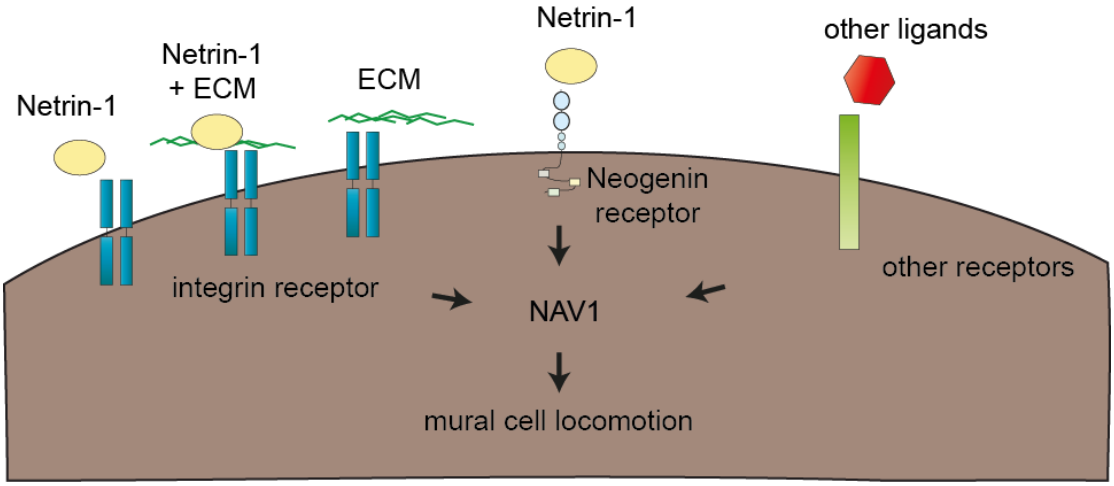

Figure 34. Potential upstream modulators of NAV1 during vascular development.
Scheme of different theoretic possible upstream signaling factors of NAV1 are depicted. Netrin-1 and the ECM component Collagen I are important for NAV1 dependent mural cell locomotion. Netrin-1 may act via the Neogenin receptor or with integrin receptors. ECM molecules alone can bind to integrins or in combination with Netrin-1. Other receptors like Notch-3 and ANG1 may also contribute to the signaling cascade regulating NAV1 function. In addition, so far unknown ligands and receptors may exert their influence on NAV1.

4.2.2.2 Downstream effectors of NAV1

The absence of NAV1 lead to reduced cell motility. Cell migration *in vivo* or *in vitro* begins with stimulation of cell surface receptors that transduce the external signal to series of remodeling events that alter the structure of the cytoskeleton. Early signaling events trigger actin polymerization, which causes protrusions of the cell toward a chemotactic stimulus or along a path of varying adhesiveness within the ECM. Transient focal contacts between the cell membrane and ECM are necessary for migration to proceed. Microtubules remodel actively during migration and dynamic instability is required for vSMC migration [141]. For all NAV family members it had

been shown *in vitro* that they bind to plus ends of microtubules (MTs) [96, 98]. Moreover, expression of GFP-tagged NAVs showed that they could dominantly alter cytoskeletal behavior. For NAV1 it was shown that this depends on its ATPase activity obtained from its ATPase activity associated with diverse cellular activities (AAA)-domain, thus its MT modulation is not achieved by classical bundling and stabilization processes [99]. If NAV1 influences MT dynamics in mural cells thereby modulating mural cell motility remains to be clarified. Preliminary results of MT stainings in NAV1-deficient primary vSMCs point to no change in MT filament appearance compared to wildtype (data not shown).

All NAVs harbor actin binding domains [93]. UNC-53, the homologue in *C. elegans*, was shown to interact with abelson kinase interactor (ABI-1), a regulator of Arp2/3 mediated actin filament nucleation [91]. In addition, the zebrafish isoform *nav3a* was co-localized with Abi-1 and actin filaments in protrusions of migrating cells [90]. Depletion of Nav3a *in vitro* resulted in strong migration defects in a cell scratch assay. In contrast, NAV1 ablation leads in similar experimental settings to significant but smaller migration defects. Furthermore, NAV1 lacks the calponin-homology domain thought to mainly mediate actin binding [90, 94]. This indicates that NAV1 is probably not directly involved in actin dynamics of mural cells. Nevertheless, acting binding properties of NAV1 cannot be excluded.

Static and dynamic structural interactions between MTs and actins have been documented in different systems [142]. It was proposed for the NAV family that they may act as scaffold between MT and actin [91].

A protein with similar properties like the NAVs is ACF7, a member of the spectraplakin family. It is a protein with MT and actin binding properties and harbors ATPase activity. This crosslinking protein is important in regulating dynamic interactions between MTs and F-actin to sustain directional cell movement [143]. In particular, it regulates MTs targeting along F-actin to focal adhesions (FAs). FAs are large dynamic protein complexes through which the cytoskeleton is connected with the ECM and are essential for cell migration and adhesion. Thus, given the parallels between ACF7 and NAVs, as well as the cell adhesion defects in the absence of NAV1 it would be interesting to examine the role of NAV1 in FA dynamics.

However, NAV1 harbors an AAA-domain. Proteins containing this domain belong to a functionally diverse protein family. Amongst others they are involved in signal transduction [97]. Thus, a potential direct influence of NAV1 on signal pathways

modulating cytoskeletal dynamics without direct protein-protein interactions should be considered.

The deficit of adequate antibodies to unravel subcellular localization and protein-protein-interactions of NAV1 makes it arguable to draw definite conclusions on those questions but has to be solved or circumvent for future studies.

Taken together, the diminished cell locomotion of *NAV1*-deficient mural cells *in vitro*, in combination with recent reports about MT binding abilities of NAV1, point to a prominent role of NAV1 on cytoskeletal dynamics. If NAV1 influences MT or actin directly, serve as scaffold between both or as regulator of MTs targeting to F-actin remains elusive. The several potential intracellular interaction partners downstream of NAV1 are summarized in Figure 35.

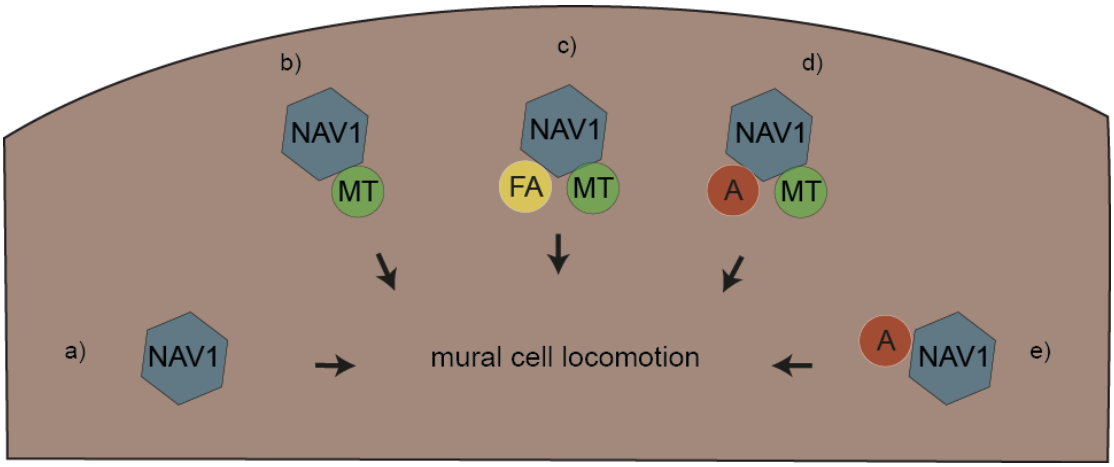

Figure 35. Potential downstream effectors of NAV1 modulating mural cell motility.

Scheme of different molecules potentially linked downstream of NAV1. NAV1 might influence mural cell locomotion by **a)** activation of signaling pathways influencing cytoskeletal dynamics **b)** directly modulating microtubule (MT) dynamics **c)** regulating MT and actin (A) at focal adhesions (FA) **d)** serving as independent scaffold for MT and actin **e)** directly influencing actin dynamics.

4.2.3 Loss of NAV1 causes embryonic lethality

In the last third of gestation a subset of *NAV1*-knockout embryos die. Surviving animals are decreased in size and weight (Fig. 11). One explanation of the prenatal death might be the vascular formation defect. For instance, loss or reduction of mural cells, induced by ablation of the signaling pathway PDGF-B/PDGFR-β , results in embryonic lethality due to vessel malformations leading to hemorrhages [45, 57, 60, 61]. However, in PDGF-B/PDGFR-β mutant mice loss of mural cells is in certain tissues near total. In contrast, *NAV1*-knockout mice exhibit only reduced mural cell number in the analyzed tissues and no obvious hemorrhages could be observed. Thus, vascular integrity is maybe only slightly disturbed (if at all). Nevertheless, correct formation of the vessel network is important for proper tissue oxygenation. The complexity of the vasculature in *NAV1*-deficient mice is diminished. An improper oxygenation of certain tissues may therefore be the cause for the embryonic lethality.
Alternatively, a specific vascular defect in the reproductive system can be the reason for embryonic lethality. NAV1 expression could be detected in placental regions during murine development (data not shown) and was reported for human placental tissue [93] pointing to a possible role of NAV1 in this tissue. The female *NAV1*-knockout mice are infertile. Whether a profound role in formation of the placenta is attributable to the infertility remains to be clarified.

4.3 The function of zebrafish nav1

We demonstrated that NAV1 is important for murine vessel development and sought to identify conserved roles in vertebrates by the use of the zebrafish model. Our zebrafish data indicate that Nav1 plays a conserved role on vessel branching. Here, central artery (CtA) connections in the hindbrain of the head are reduced (Fig. 32). Based on our WISH data this is most likely due to reduced amount of PDGFR-β signal (Fig. 33).

In zebrafish one drawback for the analysis of mural cells is that almost nothing is known about their role in early vessel formation. So far, one report had shown that PDGFR-β signal is important for correct intersegmental vessel growth in the trunk during early embryonic development at 24 hpf [130]. They propose that the PDGFR-β signal is not arising from mural cells due to an earlier study characterizing different mural cell marker [144] and their own electron microscopy study of intersegmental vessels at 72 hpf.

Santoro et al. reported different markers of mural cells to be expressed at 72 hpf surrounding the dorsal aorta in the trunk region [144]. Markers investigated were acta2 (homologue of α-SMA) and transgelin. Both markers identify only more differentiated mural cells, thereby potentially missing other populations of mural cells. Regarding expression domains of zebrafish *nav1* (Fig. 29) the mural cell markers acta2 and transgelin cannot be considered as regions with co-localization, therefore the alternate marker PDGFR-β was used (Fig. 33). Wiens et al did not report expression of PDGFR-β later then 24 hpf [130]. Our own expression data are consistent at this developmental stage, showing no change in the absence of *nav1*. In later stages we could demonstrate expression in the head with single expression domains in close proximity to CtAs (Fig. 33B). Even under the assumption that PDGFR-β expressing cells correspond per se not to mural cells in the zebrafish, the association of vascular malformation of CtAs and the reduction of PDGFR-β expression makes it tempting to speculate that here a mural cell like cell type is influencing vessel remodeling. The establishment of a PDGFR-β and nav1 reporter fish line can eventually circumvent the definite identification of mural cells expressing *nav1* and therefore allow definite conclusions about conserved functions of *nav1* in

mural cells. Nevertheless, a conserved role of Nav1 in vascular branching morphogenesis is unquestionable due to less complex cerebral vessels in the *nav1*-morphants.

4.4 NAV1 and pathology

Mural cells are intensely connected with various pathologies. To illustrate the diverse role of mural cells in pathological contexts and therefore possible implications of NAV1 we will distinguish between pericytes and vSMCs in these concluding paragraphs.

Selective pericyte loss is the earliest cellular deficiency noticed in diabetic retinopathy the main cause of vision loss of diabetic patients [41]. It is suggested that this "pericyte drop out" may have a causal role for this disease [28]. Pericyte death and BM thickening leads to microvascular changes, including altered blood flow and vascular leakage in the retinal capillaries. The cause of pericyte apoptosis in this setting is poorly understood [38]. Nevertheless, as NAV1 seems to play a major role in mural cell locomotion it is not promising that it is involved in this pathological process.

Cancer cells in solid tumors need to be equipped with blood vessels for growth and metastasis. Tumor blood vessels are both structurally and functionally abnormal compared with normal vessels [145]. Pericytes are attracted to tumor neovasculature by the same means as in developmental angiogenesis, thus recruitment is strongly dependent on PDGF-B [146]. Tumor vessels are heterogeneous in their pericyte coverage, but the amount is generally diminished. The exact cause of abnormal pericyte behavior in tumors is still unknown [32, 147]. A recent study suggested that NAV3 might be a novel cancer-associated gene in basal and squamous cell cancers [148]. Furthermore, another study postulated NAV3 as new prognostic biomarker for neuroblastomas [149]. In host study copy number changes of NAV3 were correlated with survival analysis. Information about cellular localization of NAV3 in this study is not given, as well as information about other NAV family members. Nonetheless, these studies indicate that NAV family members are an interesting novel protein family implicated in solid tumor diseases, in particular the potential role of NAV1 in mural cells could be analyzed in this context.

Mural cells/vSMCs are thought to play a key role in atherosclerosis [32], an extremely complex disease involving many cell types including macrophages, lymphocytes, neutrophils, ECs and vSMCs [150]. The role of the vSMCs seems to vary, depending on the stage of the disease, but is thought to include migration of cells into the intima of the blood vessel [32]. As NAV1 plays a role in mural cell motility it is tempting to speculate that it can play also a role in the progression of atherosclerosis.

4.5 Conclusions and perspectives

We initially hypothesized that NAV1 regulates cell migration processes during vascular development. Our loss-of-function data in the murine and zebrafish model confirmed this hypothesis. The absence of NAV1 results in less branched vessel networks in mouse and zebrafish. In the murine model the reduced vessel complexity accompanies with increased vessel regression and reduced mural cell coverage of vessels. In fact, our results showed that NAV1 is important for mural cell migration and adhesion *in vitro*. We suggest that this locomotion defect is causal for the reduced mural cell numbers *in vivo* (Fig. 36). NAV1 is a novel positive regulator of mural cell motility and vessel stability.

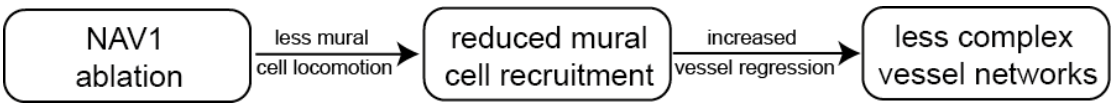

Figure 36. Causal chain of events resulting from NAV1 deficiency during vascular development.
NAV1 is expressed in mural cells. *NAV1*-deficiency leads to reduced mural cell locomotion. Less mural cell motility causes reduced mural cell recruitment, in consequence to reduced mural cell coverage of vessels. Newly formed vessels are therefore less stable and regression increases ultimately leading to a less complex vessel network.

NAV1-deficient murine primary vSMCs adhere less to Collagen I and Netrin-1 suggesting a profound role of NAV1 for conveying ECM-mural cell interactions. However, the precise mechanism how external stimuli modulate NAV1 action and finally regulates cell locomotion is unclear. Definite receptors and ligands upstream of NAV1 need to be clarified and intracellular interaction partners should be revealed for a better understanding of NAV1 working mechanisms.

The NAV proteins in general seem to be an interesting family to analyze in solid tumor diseases. Whether NAV1 is important for pathological angiogenesis can be analyzed in inducible tumor mouse models.

5. Abstract

Vessel development is a multistep process orchestrated by different cellular and signaling mechanisms. Mural cells are associated with the endothelium and thought to be important for vessel stabilization. Cell guidance is an essential factor during vascular development, accomplished by different attractive and repulsive factors. Some of these were originally described in neural development. The Neuron Navigator (NAV) protein family is a novel player in regulating cell migration events during neuron growth, but their potential impact in vessel development is unknown. We hypothesized that the family member NAV1 plays a role in cell migration events during angiogenesis and examined the function of NAV1 in vascular development using loss-of-function models in mouse and zebrafish.

Analysis of the vessel network phenotype in neonatal retina and an aortic ring assay of *NAV1*$^{-/-}$-mice revealed defective vessel remodeling in the absence of NAV1, indicated by reduced branch point numbers of vessels. Characterization of cellular expression domains point to a prominent, so far unknown, *NAV1* expression in mural cells and *NAV1*-knockout mice exhibited reduced mural cell numbers on vessels. Decreased mural cell recruitment accompanies with increased vessel regression in the retina that may be attributable for the vascular phenotype. *In vitro* data of primary mural cells indicate a cell-autonomous influence of NAV1 on cell locomotion in response to Netrin-1 and/or the extracellular matrix component Collagen I.

Analysis of Nav1 depleted zebrafish embryos revealed less complex vessel networks of specific cerebral vessels, the central arteries, suggesting that the impact of Nav1 on vessel development is conserved in vertebrates.

Taken together, we identified NAV1 as a novel cell-autonomous factor for mural cell motility that in consequence acts as a positive modulator of vascular patterning.

6. Zusammenfassung

Die Blutgefäßentwicklung ist ein mehrstufiger Prozess, der durch verschiedenste Signalwege und zelluläre Mechanismen bestimmt wird. Murale Zellen sind mit dem Endothel assoziiert und wichtig für die Stabilisierung von Blutgefäßen. Ein essentieller Faktor für die Blutgefäßentwicklung ist die Bestimmung der Zellmigrationsrichtung durch verschiedene anziehende und abstoßende Faktoren. Einige dieser Faktoren wurden ursprünglich für die neurale Entwicklung beschrieben. Die Proteinfamilie der "Neuron Navigators" (NAV) sind neue Akteure, die die Migration von Zellen während des Neuronenwachstums beeinflussen. Ein möglicher Einfluss auf die Blutgefäßentwicklung ist bisher unbekannt. Wir nehmen an, dass das Protein NAV1 in Zellmigrationsprozessen während der Angiogenese eine Rolle spielt und verwendeten zur Aufklärung der Funktion von NAV1 "loss-of-function" Modelle in der Maus und im Zebrafisch.

Das Blutgefäßnetzwerk in der Retina von neonatalen *NAV1*$^{-/-}$-Mäusen, als auch in einem "aortic ring assay" zeigte Defekte der Gefäßremodellierung durch eine verringerte Anzahl an Verzweigungspunkten der Blutgefäße auf. Es konnte erstmals eine Expression von *NAV1* in muralen Zellen gezeigt werden. Die *NAV1*-defizienten Mäuse zeigten eine verringerte Anzahl von muralen Zellen auf Blutgefäßen auf. Dieser Defekt ging mit einer verstärkten Regression von Blutgefäßen einher, welche für die geringere Verzweigung dieser verantwortlich sein kann. *In vitro* Experimente mit primären muralen Zellen deuten auf einen zellautonomen Einfluss von NAV1 auf die Bewegung von Zellen in Abhängigkeit von Netrin-1 und der extrazelluären Matrixkomponente Kollagen I hin.

Nav1-depletierte Zebrafische wiesen eine verringerte Komplexität von bestimmten zerebralen Blutgefäßen auf. Dies deutet darauf hin, dass der Einfluss von Nav1 auf die Blutgefäßausbildung konserviert ist.

Wir konnten NAV1 als einen neuen zelleigenen Faktor der Motilität von muralen Zellen identifizieren, der in Folge als positiver Modulator zur Regulation der Gefäßstrukturierung beiträgt.

7. References

[1] E. A. V Jones, F. le Noble, and A. Eichmann, "What determines blood vessel structure? Genetic prespecification vs. hemodynamics.," *Physiology (Bethesda).*, vol. 21, pp. 388–395, 2006.

[2] W. Risau and I. Flamme, "Vasculogenesis," *Annu Rev Cell Dev Biol*, vol. 11, pp. 73–91, 1995.

[3] W. Risau, "Mechanisms of angiogenesis," *Nature*, vol. 386, no. 6626, pp. 671–674, 1997.

[4] H. M. Eilken and R. H. Adams, "Dynamics of endothelial cell behavior in sprouting angiogenesis," *Curr Opin Cell Biol*, vol. 22, no. 5, pp. 617–625, 2010.

[5] I. Geudens and H. Gerhardt, "Coordinating cell behaviour during blood vessel formation," *Development*, vol. 138, no. 21, pp. 4569–4583, 2011.

[6] S. P. Herbert and D. Y. Stainier, "Molecular control of endothelial cell behaviour during blood vessel morphogenesis," *Nat Rev Mol Cell Biol*, vol. 12, no. 9, pp. 551–564, 2011.

[7] P. Carmeliet, "Angiogenesis in life, disease and medicine," *Nature*, vol. 438, no. 7070, pp. 932–936, 2005.

[8] A. N. Makanya, R. Hlushchuk, and V. G. Djonov, "Intussusceptive angiogenesis and its role in vascular morphogenesis, patterning, and remodeling," *Angiogenesis*, vol. 12, no. 2, pp. 113–123, 2009.

[9] C. Ruhrberg, H. Gerhardt, M. Golding, R. Watson, S. Ioannidou, H. Fujisawa, C. Betsholtz, and D. T. Shima, "Spatially restricted patterning cues provided by heparin-binding VEGF-A control blood vessel branching morphogenesis," *Genes Dev*, vol. 16, no. 20, pp. 2684–2698, 2002.

[10] H. Gerhardt, M. Golding, M. Fruttiger, C. Ruhrberg, A. Lundkvist, A. Abramsson, M. Jeltsch, C. Mitchell, K. Alitalo, D. Shima, and C. Betsholtz, "VEGF guides angiogenic sprouting utilizing endothelial tip cell filopodia," *J Cell Biol*, vol. 161, no. 6, pp. 1163–1177, 2003.

[11] F. De Smet, I. Segura, K. De Bock, P. J. Hohensinner, and P. Carmeliet, "Mechanisms of vessel branching: filopodia on endothelial tip cells lead the way," *Arter. Thromb Vasc Biol*, vol. 29, no. 5, pp. 639–649, 2009.

[12] L. Jakobsson, C. A. Franco, K. Bentley, R. T. Collins, B. Ponsioen, I. M. Aspalter, I. Rosewell, M. Busse, G. Thurston, A. Medvinsky, S. Schulte-Merker, and H. Gerhardt, "Endothelial cells dynamically compete for the tip

cell position during angiogenic sprouting," *Nat Cell Biol*, vol. 12, no. 10, pp. 943–953, 2010.

[13] V. W. van Hinsbergh and P. Koolwijk, "Endothelial sprouting and angiogenesis: matrix metalloproteinases in the lead," *Cardiovasc Res*, vol. 78, no. 2, pp. 203–212, 2008.

[14] R. H. Adams and K. Alitalo, "Molecular regulation of angiogenesis and lymphangiogenesis," *Nat Rev Mol Cell Biol*, vol. 8, no. 6, pp. 464–478, 2007.

[15] P. Carmeliet and R. K. Jain, "Molecular mechanisms and clinical applications of angiogenesis," *Nature*, vol. 473, no. 7347, pp. 298–307, 2011.

[16] R. K. Jain, "Molecular regulation of vessel maturation," *Nat Med*, vol. 9, no. 6, pp. 685–693, 2003.

[17] H. U. Wang, Z. F. Chen, and D. J. Anderson, "Molecular distinction and angiogenic interaction between embryonic arteries and veins revealed by ephrin-B2 and its receptor Eph-B4," *Cell*, vol. 93, no. 5, pp. 741–753, 1998.

[18] H. Gerhardt, C. Ruhrberg, A. Abramsson, H. Fujisawa, D. Shima, and C. Betsholtz, "Neuropilin-1 is required for endothelial tip cell guidance in the developing central nervous system.," *Dev. Dyn.*, vol. 231, no. 3, pp. 503–9, Nov. 2004.

[19] E. A. V Jones, L. Yuan, C. Breant, R. J. Watts, and A. Eichmann, "Separating genetic and hemodynamic defects in neuropilin 1 knockout embryos.," *Development*, vol. 135, no. 14, pp. 2479–88, Aug. 2008.

[20] T. Kawasaki, T. Kitsukawa, Y. Bekku, Y. Matsuda, M. Sanbo, T. Yagi, and H. Fujisawa, "A requirement for neuropilin-1 in embryonic vessel formation.," *Development*, vol. 126, pp. 4895–4902, 1999.

[21] Y.-S. Mukouyama, H.-P. Gerber, N. Ferrara, C. Gu, and D. J. Anderson, "Peripheral nerve-derived VEGF promotes arterial differentiation via neuropilin 1-mediated positive feedback.," *Development*, vol. 132, no. 5, pp. 941–52, Mar. 2005.

[22] M. R. Swift and B. M. Weinstein, "Arterial-venous specification during development," *Circ Res*, vol. 104, no. 5, pp. 576–588, 2009.

[23] I. Buschmann, A. Pries, B. Styp-Rekowska, P. Hillmeister, L. Loufrani, D. Henrion, Y. Shi, A. Duelsner, I. Hoefer, N. Gatzke, H. Wang, K. Lehmann, L. Ulm, Z. Ritter, P. Hauff, R. Hlushchuk, V. Djonov, T. van Veen, and F. le Noble, "Pulsatile shear and Gja5 modulate arterial identity and remodeling events during flow-driven arteriogenesis.," *Development*, vol. 137, pp. 2187–2196, 2010.

[24] F. le Noble, D. Moyon, L. Pardanaud, L. Yuan, V. Djonov, R. Matthijsen, C. Bréant, V. Fleury, and A. Eichmann, "Flow regulates arterial-venous

differentiation in the chick embryo yolk sac.," *Development*, vol. 131, pp. 361–375, 2004.

[25] J. L. Lucitti, E. A. Jones, C. Huang, J. Chen, S. E. Fraser, and M. E. Dickinson, "Vascular remodeling of the mouse yolk sac requires hemodynamic force," *Development*, vol. 134, no. 18, pp. 3317–3326, 2007.

[26] Q. Chen, L. Jiang, C. Li, D. Hu, J. W. Bu, D. Cai, and J. L. Du, "Haemodynamics-driven developmental pruning of brain vasculature in zebrafish," *PLoS Biol*, vol. 10, no. 8, p. e1001374, 2012.

[27] R. H. Adams and A. Eichmann, "Axon guidance molecules in vascular patterning," *Cold Spring Harb Perspect Biol*, vol. 2, no. 5, 2010.

[28] A. Armulik, A. Abramsson, and C. Betsholtz, "Endothelial/pericyte interactions," *Circ Res*, vol. 97, no. 6, pp. 512–523, 2005.

[29] V. Nehls and D. Drenckhahn, "The versatility of microvascular pericytes: from mesenchyme to smooth muscle?," *Histochemistry*, vol. 99, no. 1, pp. 1–12, 1993.

[30] G. Bergers and S. Song, "The role of pericytes in blood-vessel formation and maintenance," *Neuro Oncol*, vol. 7, no. 4, pp. 452–464, 2005.

[31] H. Gerhardt and C. Betsholtz, "Endothelial-pericyte interactions in angiogenesis," *Cell Tissue Res*, vol. 314, no. 1, pp. 15–23, 2003.

[32] G. K. Owens, M. S. Kumar, and B. R. Wamhoff, "Molecular regulation of vascular smooth muscle cell differentiation in development and disease.," *Physiol. Rev.*, vol. 84, pp. 767–801, 2004.

[33] S. A. Fisher, "Vascular smooth muscle phenotypic diversity and function," *Physiol Genomics*, vol. 42A, pp. 169–187, 2010.

[34] G. K. Owens, "Regulation of differentiation of vascular smooth muscle cells.," *Physiol. Rev.*, vol. 75, pp. 487–517, 1995.

[35] M. W. Majesky, "Developmental basis of vascular smooth muscle diversity," *Arter. Thromb Vasc Biol*, vol. 27, no. 6, pp. 1248–1258, 2007.

[36] D. Ribatti, B. Nico, and E. Crivellato, "The role of pericytes in angiogenesis.," *Int. J. Dev. Biol.*, vol. 55, pp. 261–268, 2011.

[37] D. E. Sims, "The pericyte--a review," *Tissue Cell*, vol. 18, no. 2, pp. 153–174, 1986.

[38] A. Armulik, G. Genove, and C. Betsholtz, "Pericytes: developmental, physiological, and pathological perspectives, problems, and promises," *Dev Cell*, vol. 21, no. 2, pp. 193–215, 2011.

[39] P. Cuevas, J. A. Gutierrez-Diaz, D. Reimers, M. Dujovny, F. G. Diaz, and J. I. Ausman, "Pericyte endothelial gap junctions in human cerebral capillaries," *Anat Embryol*, vol. 170, no. 2, pp. 155–159, 1984.

[40] H. Gerhardt, H. Wolburg, and C. Redies, "N-cadherin mediates pericytic-endothelial interaction during brain angiogenesis in the chicken," *Dev Dyn*, vol. 218, no. 3, pp. 472–479, 2000.

[41] G. Allt and J. G. Lawrenson, "Pericytes: cell biology and pathology," *Cells Tissues Organs*, vol. 169, no. 1, pp. 1–11, 2001.

[42] V. Nehls, K. Denzer, and D. Drenckhahn, "Pericyte involvement in capillary sprouting during angiogenesis in situ.," *Cell Tissue Res.*, vol. 270, pp. 469–474, 1992.

[43] U. Ozerdem, K. A. Grako, K. Dahlin-Huppe, E. Monosov, and W. B. Stallcup, "NG2 proteoglycan is expressed exclusively by mural cells during vascular morphogenesis.," *Dev. Dyn.*, vol. 222, pp. 218–227, 2001.

[44] P. Lindahl, B. R. Johansson, P. Leveen, and C. Betsholtz, "Pericyte loss and microaneurysm formation in PDGF-B-deficient mice," *Science (80-.).*, vol. 277, no. 5323, pp. 242–245, 1997.

[45] K. Gaengel, G. Genove, A. Armulik, and C. Betsholtz, "Endothelial-mural cell signaling in vascular development and angiogenesis," *Arter. Thromb Vasc Biol*, vol. 29, no. 5, pp. 630–638, 2009.

[46] D. von Tell, A. Armulik, and C. Betsholtz, "Pericytes and vascular stability," *Exp Cell Res*, vol. 312, no. 5, pp. 623–629, 2006.

[47] L. E. Benjamin, I. Hemo, and E. Keshet, "A plasticity window for blood vessel remodelling is defined by pericyte coverage of the preformed endothelial network and is regulated by PDGF-B and VEGF," *Development*, vol. 125, no. 9, pp. 1591–1598, 1998.

[48] T. Chan-Ling, M. P. Page, T. Gardiner, L. Baxter, E. Rosinova, and S. Hughes, "Desmin ensheathment ratio as an indicator of vessel stability: evidence in normal development and in retinopathy of prematurity.," *Am. J. Pathol.*, vol. 165, pp. 1301–1313, 2004.

[49] M. Enge, M. Bjarnegard, H. Gerhardt, E. Gustafsson, M. Kalen, N. Asker, H. P. Hammes, M. Shani, R. Fassler, and C. Betsholtz, "Endothelium-specific platelet-derived growth factor-B ablation mimics diabetic retinopathy," *EMBO J*, vol. 21, no. 16, pp. 4307–4316, 2002.

[50] N. Simonavicius, M. Ashenden, A. van Weverwijk, S. Lax, D. L. Huso, C. D. Buckley, I. J. Huijbers, H. Yarwood, and C. M. Isacke, "Pericytes promote selective vessel regression to regulate vascular patterning," *Blood*, vol. 120, no. 7, pp. 1516–1527, 2012.

[51] U. Ozerdem and W. B. Stallcup, “Early contribution of pericytes to angiogenic sprouting and tube formation,” *Angiogenesis*, vol. 6, no. 3, pp. 241–249, 2003.

[52] R. O. Schlingemann, F. J. Rietveld, F. Kwaspen, P. C. van de Kerkhof, R. M. de Waal, and D. J. Ruiter, “Differential expression of markers for endothelial cells, pericytes, and basal lamina in the microvasculature of tumors and granulation tissue,” *Am J Pathol*, vol. 138, no. 6, pp. 1335–1347, 1991.

[53] A. N. Witmer, B. C. van Blijswijk, C. J. van Noorden, G. F. Vrensen, and R. O. Schlingemann, “In vivo angiogenic phenotype of endothelial cells and pericytes induced by vascular endothelial growth factor-A,” *J Histochem Cytochem*, vol. 52, no. 1, pp. 39–52, 2004.

[54] D. Virgintino, F. Girolamo, M. Errede, C. Capobianco, D. Robertson, W. B. Stallcup, R. Perris, and L. Roncali, “An intimate interplay between precocious, migrating pericytes and endothelial cells governs human fetal brain angiogenesis.,” *Angiogenesis*, vol. 10, pp. 35–45, 2007.

[55] J. Andrae, R. Gallini, and C. Betsholtz, “Role of platelet-derived growth factors in physiology and medicine,” *Genes Dev*, vol. 22, no. 10, pp. 1276–1312, 2008.

[56] C. Betsholtz, “Insight into the physiological functions of PDGF through genetic studies in mice,” *Cytokine Growth Factor Rev*, vol. 15, no. 4, pp. 215–228, 2004.

[57] M. Hellstrom, M. Kalen, P. Lindahl, A. Abramsson, and C. Betsholtz, “Role of PDGF-B and PDGFR-beta in recruitment of vascular smooth muscle cells and pericytes during embryonic blood vessel formation in the mouse,” *Development*, vol. 126, no. 14, pp. 3047–3055, 1999.

[58] A. Ostman, M. Andersson, U. Hellman, and C. H. Heldin, “Identification of three amino acids in the platelet-derived growth factor (PDGF) B-chain that are important for binding to the PDGF beta-receptor,” *J Biol Chem*, vol. 266, no. 16, pp. 10073–10077, 1991.

[59] K. K. Hirschi, S. A. Rohovsky, L. H. Beck, S. R. Smith, and P. A. D’Amore, “Endothelial cells modulate the proliferation of mural cell precursors via platelet-derived growth factor-BB and heterotypic cell contact,” *Circ Res*, vol. 84, no. 3, pp. 298–305, 1999.

[60] P. Leveen, M. Pekny, S. Gebre-Medhin, B. Swolin, E. Larsson, and C. Betsholtz, “Mice deficient for PDGF B show renal, cardiovascular, and hematological abnormalities,” *Genes Dev*, vol. 8, no. 16, pp. 1875–1887, 1994.

[61] P. Soriano, “Abnormal kidney development and hematological disorders in PDGF beta-receptor mutant mice,” *Genes Dev*, vol. 8, no. 16, pp. 1888–1896, 1994.

[62] M. Bjarnegard, M. Enge, J. Norlin, S. Gustafsdottir, S. Fredriksson, A. Abramsson, M. Takemoto, E. Gustafsson, R. Fassler, and C. Betsholtz, "Endothelium-specific ablation of PDGFB leads to pericyte loss and glomerular, cardiac and placental abnormalities," *Development*, vol. 131, no. 8, pp. 1847–1857, 2004.

[63] M. Thomas and H. G. Augustin, "The role of the Angiopoietins in vascular morphogenesis," *Angiogenesis*, vol. 12, no. 2, pp. 125–137, 2009.

[64] S. Davis, T. H. Aldrich, P. F. Jones, A. Acheson, D. L. Compton, V. Jain, T. E. Ryan, J. Bruno, C. Radziejewski, P. C. Maisonpierre, and G. D. Yancopoulos, "Isolation of angiopoietin-1, a ligand for the TIE2 receptor, by secretion-trap expression cloning," *Cell*, vol. 87, no. 7, pp. 1161–1169, 1996.

[65] C. Sundberg, M. Kowanetz, L. F. Brown, M. Detmar, and H. F. Dvorak, "Stable expression of angiopoietin-1 and other markers by cultured pericytes: phenotypic similarities to a subpopulation of cells in maturing vessels during later stages of angiogenesis in vivo," *Lab Invest*, vol. 82, no. 4, pp. 387–401, 2002.

[66] L. Eklund and P. Saharinen, "Angiopoietin signaling in the vasculature," *Exp Cell Res*, vol. 319, no. 9, pp. 1271–1280, 2013.

[67] S. Patan, "TIE1 and TIE2 receptor tyrosine kinases inversely regulate embryonic angiogenesis by the mechanism of intussusceptive microvascular growth," *Microvasc Res*, vol. 56, no. 1, pp. 1–21, 1998.

[68] T. N. Sato, Y. Tozawa, U. Deutsch, K. Wolburg-Buchholz, Y. Fujiwara, M. Gendron-Maguire, T. Gridley, H. Wolburg, W. Risau, and Y. Qin, "Distinct roles of the receptor tyrosine kinases Tie-1 and Tie-2 in blood vessel formation.," *Nature*, vol. 376, no. 6535, pp. 70–4, Jul. 1995.

[69] D. J. Dumont, G. Gradwohl, G. H. Fong, M. C. Puri, M. Gertsenstein, A. Auerbach, and M. L. Breitman, "Dominant-negative and targeted null mutations in the endothelial receptor tyrosine kinase, tek, reveal a critical role in vasculogenesis of the embryo," *Genes Dev*, vol. 8, no. 16, pp. 1897–1909, 1994.

[70] M. C. Puri, J. Rossant, K. Alitalo, A. Bernstein, and J. Partanen, "The receptor tyrosine kinase TIE is required for integrity and survival of vascular endothelial cells.," *EMBO J.*, vol. 14, no. 23, pp. 5884–91, Dec. 1995.

[71] C. Suri, P. F. Jones, S. Patan, S. Bartunkova, P. C. Maisonpierre, S. Davis, T. N. Sato, and G. D. Yancopoulos, "Requisite role of angiopoietin-1, a ligand for the TIE2 receptor, during embryonic angiogenesis," *Cell*, vol. 87, no. 7, pp. 1171–1180, 1996.

[72] N. W. Gale, G. Thurston, S. F. Hackett, R. Renard, Q. Wang, J. McClain, C. Martin, C. Witte, M. H. Witte, D. Jackson, C. Suri, P. A. Campochiaro, S. J. Wiegand, and G. D. Yancopoulos, "Angiopoietin-2 is required for postnatal angiogenesis and lymphatic patterning, and only the latter role is rescued by Angiopoietin-1.," *Dev. Cell*, vol. 3, no. 3, pp. 411–23, Sep. 2002.

[73] P. C. Maisonpierre, C. Suri, P. F. Jones, S. Bartunkova, S. J. Wiegand, C. Radziejewski, D. Compton, J. McClain, T. H. Aldrich, N. Papadopoulos, T. J. Daly, S. Davis, T. N. Sato, and G. D. Yancopoulos, "Angiopoietin-2, a natural antagonist for Tie2 that disrupts in vivo angiogenesis," *Science (80-.).*, vol. 277, no. 5322, pp. 55–60, 1997.

[74] M. J. Goumans, G. Valdimarsdottir, S. Itoh, A. Rosendahl, P. Sideras, and P. ten Dijke, "Balancing the activation state of the endothelium via two distinct TGF-beta type I receptors," *EMBO J*, vol. 21, no. 7, pp. 1743–1753, 2002.

[75] V. Domenga, P. Fardoux, P. Lacombe, M. Monet, J. Maciazek, L. T. Krebs, B. Klonjkowski, E. Berrou, M. Mericskay, Z. Li, E. Tournier-Lasserve, T. Gridley, and A. Joutel, "Notch3 is required for arterial identity and maturation of vascular smooth muscle cells," *Genes Dev*, vol. 18, no. 22, pp. 2730–2735, 2004.

[76] H. Liu, S. Kennard, and B. Lilly, "NOTCH3 expression is induced in mural cells through an autoregulatory loop that requires endothelial-expressed JAGGED1," *Circ Res*, vol. 104, no. 4, pp. 466–475, 2009.

[77] H. Liu, W. Zhang, S. Kennard, R. B. Caldwell, and B. Lilly, "Notch3 is critical for proper angiogenesis and mural cell investment.," *Circ. Res.*, vol. 107, pp. 860–870, 2010.

[78] A. Joutel, C. Corpechot, A. Ducros, K. Vahedi, H. Chabriat, P. Mouton, S. Alamowitch, V. Domenga, M. Cécillion, E. Marechal, J. Maciazek, C. Vayssiere, C. Cruaud, E. A. Cabanis, M. M. Ruchoux, J. Weissenbach, J. F. Bach, M. G. Bousser, and E. Tournier-Lasserve, "Notch3 mutations in CADASIL, a hereditary adult-onset condition causing stroke and dementia.," *Nature*, vol. 383, pp. 707–710, 1996.

[79] S. S. Foo, C. J. Turner, S. Adams, A. Compagni, D. Aubyn, N. Kogata, P. Lindblom, M. Shani, D. Zicha, and R. H. Adams, "Ephrin-B2 controls cell motility and adhesion during blood-vessel-wall assembly," *Cell*, vol. 124, no. 1, pp. 161–173, 2006.

[80] O. Salvucci, D. Maric, M. Economopoulou, S. Sakakibara, S. Merlin, A. Follenzi, and G. Tosato, "EphrinB reverse signaling contributes to endothelial and mural cell assembly into vascular structures," *Blood*, vol. 114, no. 8, pp. 1707–1716, 2009.

[81] B. Larrivée, C. Freitas, S. Suchting, I. Brunet, and A. Eichmann, "Guidance of vascular development: lessons from the nervous system.," *Circ. Res.*, vol. 104, pp. 428–441, 2009.

[82] Y. Mukouyama, D. Shin, S. Britsch, M. Taniguchi, and D. J. Anderson, "Sensory nerves determine the pattern of arterial differentiation and blood vessel branching in the skin.," *Cell*, vol. 109, no. 6, pp. 693–705, Jun. 2002.

[83] P. Carmeliet, "Blood vessels and nerves: common signals, pathways and diseases.," *Nat. Rev. Genet.*, vol. 4, no. 9, pp. 710–20, Sep. 2003.

[84] S. Brenner, "The genetics of Caenorhabditis elegans.," *Genetics*, vol. 77, pp. 71–94, 1974.

[85] E. M. Hedgecock, J. G. Culotti, and D. H. Hall, "The unc-5, unc-6, and unc-40 genes guide circumferential migrations of pioneer axons and mesodermal cells on the epidermis in C. elegans," *Neuron*, vol. 4, no. 1, pp. 61–85, 1990.

[86] T. Serafini, S. A. Colamarino, E. D. Leonardo, H. Wang, R. Beddington, W. C. Skarnes, and M. Tessier-Lavigne, "Netrin-1 is required for commissural axon guidance in the developing vertebrate nervous system.," *Cell*, vol. 87, pp. 1001–1014, 1996.

[87] V. Cirulli and M. Yebra, "Netrins: beyond the brain," *Nat Rev Mol Cell Biol*, vol. 8, no. 4, pp. 296–306, 2007.

[88] X. Lu, F. Le Noble, L. Yuan, Q. Jiang, B. De Lafarge, D. Sugiyama, C. Breant, F. Claes, F. De Smet, J. L. Thomas, M. Autiero, P. Carmeliet, M. Tessier-Lavigne, and A. Eichmann, "The netrin receptor UNC5B mediates guidance events controlling morphogenesis of the vascular system," *Nature*, vol. 432, no. 7014, pp. 179–186, 2004.

[89] B. Larrivee, C. Freitas, M. Trombe, X. Lv, B. Delafarge, L. Yuan, K. Bouvree, C. Breant, R. Del Toro, N. Brechot, S. Germain, F. Bono, F. Dol, F. Claes, C. Fischer, M. Autiero, J. L. Thomas, P. Carmeliet, M. Tessier-Lavigne, and A. Eichmann, "Activation of the UNC5B receptor by Netrin-1 inhibits sprouting angiogenesis," *Genes Dev*, vol. 21, no. 19, pp. 2433–2447, 2007.

[90] C. Klein, J. Mikutta, J. Krueger, K. Scholz, J. Brinkmann, D. Liu, J. Veerkamp, D. Siegel, S. Abdelilah-Seyfried, and F. le Noble, "Neuron navigator 3a regulates liver organogenesis during zebrafish embryogenesis," *Development*, vol. 138, no. 10, pp. 1935–1945, 2011.

[91] E. G. Stringham and K. L. Schmidt, "Navigating the cell: UNC-53 and the navigators, a family of cytoskeletal regulators with multiple roles in cell migration, outgrowth and trafficking," *Cell Adh Migr*, vol. 3, no. 4, pp. 342–346, 2009.

[92] M. J. Martinez-Lopez, S. Alcantara, C. Mascaro, F. Perez-Branguli, P. Ruiz-Lozano, T. Maes, E. Soriano, and C. Buesa, "Mouse neuron navigator 1, a novel microtubule-associated protein involved in neuronal migration," *Mol Cell Neurosci*, vol. 28, no. 4, pp. 599–612, 2005.

[93] T. Maes, A. Barcelo, and C. Buesa, “Neuron navigator: a human gene family with homology to unc-53, a cell guidance gene from Caenorhabditis elegans,” *Genomics*, vol. 80, no. 1, pp. 21–30, 2002.

[94] S. Hekimi and D. Kershaw, “Axonal guidance defects in a Caenorhabditis elegans mutant reveal cell-extrinsic determinants of neuronal morphology,” *J Neurosci*, vol. 13, no. 10, pp. 4254–4271, 1993.

[95] E. B. Chen, C. S. Branda, and M. J. Stern, “Genetic enhancers of sem-5 define components of the gonad-independent guidance mechanism controlling sex myoblast migration in Caenorhabditis elegans hermaphrodites,” *Dev Biol*, vol. 182, no. 1, pp. 88–100, 1997.

[96] K. L. Schmidt, N. Marcus-Gueret, A. Adeleye, J. Webber, D. Baillie, and E. G. Stringham, “The cell migration molecule UNC-53/NAV2 is linked to the ARP2/3 complex by ABI-1,” *Development*, vol. 136, no. 4, pp. 563–574, 2009.

[97] T. Frickey and A. N. Lupas, “Phylogenetic analysis of AAA proteins,” *J Struct Biol*, vol. 146, no. 1–2, pp. 2–10, 2004.

[98] P. D. Muley, E. M. McNeill, M. A. Marzinke, K. M. Knobel, M. M. Barr, and M. Clagett-Dame, “The atRA-responsive gene neuron navigator 2 functions in neurite outgrowth and axonal elongation,” *Dev Neurobiol*, vol. 68, no. 13, pp. 1441–1453, 2008.

[99] J. van Haren, K. Draegestein, N. Keijzer, J. P. Abrahams, F. Grosveld, P. J. Peeters, D. Moechars, and N. Galjart, “Mammalian Navigators are microtubule plus-end tracking proteins that can reorganize the cytoskeleton to induce neurite-like extensions,” *Cell Motil Cytoskelet.*, vol. 66, no. 10, pp. 824–838, 2009.

[100] E. Stringham, N. Pujol, J. Vandekerckhove, and T. Bogaert, “unc-53 controls longitudinal migration in C. elegans,” *Development*, vol. 129, no. 14, pp. 3367–3379, 2002.

[101] P. Carmeliet and R. K. Jain, “Angiogenesis in cancer and other diseases,” *Nature*, vol. 407, no. 6801, pp. 249–257, 2000.

[102] M. Fruttiger, “Development of the retinal vasculature,” *Angiogenesis*, vol. 10, no. 2, pp. 77–88, 2007.

[103] A. Stahl, K. M. Connor, P. Sapieha, J. Chen, R. J. Dennison, N. M. Krah, M. R. Seaward, K. L. Willett, C. M. Aderman, K. I. Guerin, J. Hua, C. Lofqvist, A. Hellstrom, and L. E. Smith, “The mouse retina as an angiogenesis model,” *Invest Ophthalmol Vis Sci*, vol. 51, no. 6, pp. 2813–2826, 2010.

[104] A. Uemura, S. Kusuhara, H. Katsuta, and S. Nishikawa, “Angiogenesis in the mouse retina: a model system for experimental manipulation,” *Exp Cell Res*, vol. 312, no. 5, pp. 676–683, 2006.

[105] M. E. Pitulescu, I. Schmidt, R. Benedito, and R. H. Adams, “Inducible gene targeting in the neonatal vasculature and analysis of retinal angiogenesis in mice,” *Nat Protoc*, vol. 5, no. 9, pp. 1518–1534, 2010.

[106] R. F. Nicosia and A. Ottinetti, “Growth of microvessels in serum-free matrix culture of rat aorta. A quantitative assay of angiogenesis in vitro,” *Lab Invest*, vol. 63, no. 1, pp. 115–122, 1990.

[107] A. C. Aplin, E. Fogel, P. Zorzi, and R. F. Nicosia, “The aortic ring model of angiogenesis,” *Methods Enzym.*, vol. 443, pp. 119–136, 2008.

[108] M. Baker, S. D. Robinson, T. Lechertier, P. R. Barber, B. Tavora, G. D’Amico, D. T. Jones, B. Vojnovic, and K. Hodivala-Dilke, “Use of the mouse aortic ring assay to study angiogenesis,” *Nat Protoc*, vol. 7, no. 1, pp. 89–104, 2011.

[109] R. F. Nicosia, “The aortic ring model of angiogenesis: a quarter century of search and discovery,” *J Cell Mol Med*, vol. 13, no. 10, pp. 4113–4136, 2009.

[110] Y. Blum, H. G. Belting, E. Ellertsdottir, L. Herwig, F. Luders, and M. Affolter, “Complex cell rearrangements during intersegmental vessel sprouting and vessel fusion in the zebrafish embryo,” *Dev Biol*, vol. 316, no. 2, pp. 312–322, 2008.

[111] S. Childs, J. N. Chen, D. M. Garrity, and M. C. Fishman, “Patterning of angiogenesis in the zebrafish embryo,” *Development*, vol. 129, no. 4, pp. 973–982, 2002.

[112] S. Isogai, N. D. Lawson, S. Torrealday, M. Horiguchi, and B. M. Weinstein, “Angiogenic network formation in the developing vertebrate trunk,” *Development*, vol. 130, no. 21, pp. 5281–5290, 2003.

[113] S. W. Jin, D. Beis, T. Mitchell, J. N. Chen, and D. Y. Stainier, “Cellular and molecular analyses of vascular tube and lumen formation in zebrafish,” *Development*, vol. 132, no. 23, pp. 5199–5209, 2005.

[114] N. D. Lawson and B. M. Weinstein, “In vivo imaging of embryonic vascular development using transgenic zebrafish,” *Dev Biol*, vol. 248, no. 2, pp. 307–318, 2002.

[115] A. F. Siekmann and N. D. Lawson, “Notch signalling and the regulation of angiogenesis,” *Cell Adh Migr*, vol. 1, no. 2, pp. 104–106, 2007.

[116] P. Carmeliet and M. Tessier-Lavigne, “Common mechanisms of nerve and blood vessel wiring,” *Nature*, vol. 436, no. 7048, pp. 193–200, 2005.

[117] A. Gossler, A. L. Joyner, J. Rossant, and W. C. Skarnes, “Mouse embryonic stem cells and reporter constructs to detect developmentally regulated genes,” *Science (80-.).*, vol. 244, no. 4903, pp. 463–465, 1989.

[118] W. L. Stanford, J. B. Cohn, and S. P. Cordes, “Gene-trap mutagenesis: past, present and beyond,” *Nat Rev Genet*, vol. 2, no. 10, pp. 756–768, 2001.

[119] M. R. Capecchi, “Gene targeting in mice: functional analysis of the mammalian genome for the twenty-first century,” *Nat Rev Genet*, vol. 6, no. 6, pp. 507–512, 2005.

[120] E. Hanneman and M. Westerfield, “Early expression of acetylcholinesterase activity in functionally distinct neurons of the zebrafish.,” *J. Comp. Neurol.*, vol. 284, pp. 350–361, 1989.

[121] T. Jowett, “Double in situ hybridization techniques in zebrafish.,” *Methods*, vol. 23, pp. 345–358, 2001.

[122] Y. Zhang and M. A. Frohman, “Cloning cDNA Ends Using RACE.,” *Methods Mol. Med.*, vol. 13, pp. 81–105, 1998.

[123] R. F. Gariano and T. W. Gardner, “Retinal angiogenesis in development and disease,” *Nature*, vol. 438, no. 7070, pp. 960–966, 2005.

[124] K. W. Park, D. Crouse, M. Lee, S. K. Karnik, L. K. Sorensen, K. J. Murphy, C. J. Kuo, and D. Y. Li, “The axonal attractant Netrin-1 is an angiogenic factor,” *Proc Natl Acad Sci U S A*, vol. 101, no. 46, pp. 16210–16215, 2004.

[125] K. Lai Wing Sun, J. P. Correia, and T. E. Kennedy, “Netrins: versatile extracellular cues with diverse functions.,” *Development*, vol. 138, pp. 2153–2169, 2011.

[126] A. Nasevicius and S. C. Ekker, “Effective targeted gene ‘knockdown’ in zebrafish.,” *Nat. Genet.*, vol. 26, pp. 216–220, 2000.

[127] J. Bussmann, S. A. Wolfe, and A. F. Siekmann, “Arterial-venous network formation during brain vascularization involves hemodynamic regulation of chemokine signaling.,” *Development*, vol. 138, pp. 1717–1726, 2011.

[128] M. Fujita, Y. R. Cha, V. N. Pham, A. Sakurai, B. L. Roman, J. S. Gutkind, and B. M. Weinstein, “Assembly and patterning of the vascular network of the vertebrate hindbrain.,” *Development*, vol. 138, pp. 1705–1715, 2011.

[129] F. Ulrich, L.-H. Ma, R. G. Baker, and J. Torres-Vázquez, “Neurovascular development in the embryonic zebrafish hindbrain.,” *Dev. Biol.*, vol. 357, pp. 134–151, 2011.

[130] K. M. Wiens, H. L. Lee, H. Shimada, A. E. Metcalf, M. Y. Chao, and C.-L. Lien, “Platelet-derived growth factor receptor beta is critical for zebrafish intersegmental vessel formation.,” *PLoS One*, vol. 5, p. e11324, 2010.

[131] S. Suchting, C. Freitas, F. le Noble, R. Benedito, C. Bréant, A. Duarte, and A. Eichmann, "The Notch ligand Delta-like 4 negatively regulates endothelial tip cell formation and vessel branching.," *Proc. Natl. Acad. Sci. U. S. A.*, vol. 104, pp. 3225–3230, 2007.

[132] B. Jiang, M. A. Bezhadian, and R. B. Caldwell, "Astrocytes modulate retinal vasculogenesis: effects on endothelial cell differentiation.," *Glia*, vol. 15, pp. 1–10, 1995.

[133] J. Stone, A. Itin, T. Alon, J. Pe'er, H. Gnessin, T. Chan-Ling, and E. Keshet, "Development of retinal vasculature is mediated by hypoxia-induced vascular endothelial growth factor (VEGF) expression by neuroglia," *J Neurosci*, vol. 15, no. 7 Pt 1, pp. 4738–4747, 1995.

[134] H. West, W. D. Richardson, and M. Fruttiger, "Stabilization of the retinal vascular network by reciprocal feedback between blood vessels and astrocytes," *Development*, vol. 132, no. 8, pp. 1855–1862, 2005.

[135] H. C. Etchevers, C. Vincent, N. M. Le Douarin, and G. F. Couly, "The cephalic neural crest provides pericytes and smooth muscle cells to all blood vessels of the face and forebrain," *Development*, vol. 128, no. 7, pp. 1059–1068, 2001.

[136] T. H. Rosenquist, M. L. Kirby, and L. H. van Mierop, "Solitary aortic arch artery. A result of surgical ablation of cardiac neural crest and nodose placode in the avian embryo.," *Circulation*, vol. 80, pp. 1469–1475, 1989.

[137] M. W. Majesky and S. Topouzis, "Smooth Muscle Lineage Diversity in the Chick Embryo," *Developmental Biology*, vol. 178. pp. 430–445, 1996.

[138] P. R. Nelson, S. Yamamura, and K. C. Kent, "Extracellular matrix proteins are potent agonists of human smooth muscle cell migration.," *J. Vasc. Surg.*, vol. 24, pp. 25–32; discussion 32–3, 1996.

[139] M. Yebra, A. M. P. Montgomery, G. R. Diaferia, T. Kaido, S. Silletti, B. Perez, M. L. Just, S. Hildbrand, R. Hurford, E. Florkiewicz, M. Tessier-Lavigne, and V. Cirulli, "Recognition of the neural chemoattractant Netrin-1 by integrins alpha6beta4 and alpha3beta1 regulates epithelial cell adhesion and migration.," *Dev. Cell*, vol. 5, pp. 695–707, 2003.

[140] S. Abraham, N. Kogata, R. Fässler, and R. H. Adams, "Integrin beta1 subunit controls mural cell adhesion, spreading, and blood vessel wall stability.," *Circ. Res.*, vol. 102, pp. 562–570, 2008.

[141] W. T. Gerthoffer, "Mechanisms of vascular smooth muscle cell migration.," *Circ. Res.*, vol. 100, pp. 607–21, 2007.

[142] O. C. Rodriguez, A. W. Schaefer, C. A. Mandato, P. Forscher, W. M. Bement, and C. M. Waterman-Storer, "Conserved microtubule-actin interactions in cell movement and morphogenesis.," *Nat. Cell Biol.*, vol. 5, pp. 599–609, 2003.

[143] X. Wu, A. Kodama, and E. Fuchs, “ACF7 regulates cytoskeletal-focal adhesion dynamics and migration and has ATPase activity.,” *Cell*, vol. 135, pp. 137–148, 2008.

[144] M. M. Santoro, G. Pesce, and D. Y. Stainier, “Characterization of vascular mural cells during zebrafish development.,” *Mech. Dev.*, vol. 126, no. 8–9, pp. 638–49.

[145] R. K. Jain, “Antiangiogenic therapy for cancer: current and emerging concepts.,” *Oncol. {(Williston} Park.*, vol. 19, pp. 7–16, 2005.

[146] A. Abramsson, O. Berlin, H. Papayan, D. Paulin, M. Shani, and C. Betsholtz, “Analysis of mural cell recruitment to tumor vessels.,” *Circulation*, vol. 105, pp. 112–117, 2002.

[147] P. Baluk, H. Hashizume, and D. M. McDonald, “Cellular abnormalities of blood vessels as targets in cancer.,” *Curr. Opin. Genet. Dev.*, vol. 15, pp. 102–111, 2005.

[148] P. Maliniemi, E. Carlsson, A. Kaukola, K. Ovaska, K. Niiranen, O. Saksela, L. Jeskanen, S. Hautaniemi, and A. Ranki, “NAV3 copy number changes and target genes in basal and squamous cell cancers,” *Exp. Dermatol.*, vol. 20, pp. 926–931, 2011.

[149] E. Carlsson, K. Krohn, K. Ovaska, P. Lindberg, V. Häyry, P. Maliniemi, A. Lintulahti, M. Korja, R. Kivisaari, S. Hussein, S. Sarna, K. Niiranen, S. Hautaniemi, H. Haapasalo, and A. Ranki, “Neuron navigator 3 alterations in nervous system tumors associate with tumor malignancy grade and prognosis.,” *Genes. Chromosomes Cancer*, 2012.

[150] R. Ross, “The pathogenesis of atherosclerosis: a perspective for the 1990s.,” *Nature*, vol. 362, pp. 801–809, 1993.

8. Appendix

8.1 Selbstständigkeitserklärung

Hiermit versichere ich, Stefan Kunert, die vorliegende Arbeit selbstständig verfasst und keine anderen, als die angegebenen Quellen und Hilfsmittel benutzt zu haben. Daten und Abbildungen, die in Zusammenarbeit entstanden sind, wurden als solche gekennzeichnet.

Die vorgelegte Arbeit wurde in gleicher oder ähnlicher Form keiner anderen Prüfungskommission vorgelegt.

Die dem angestrebten Promotionsverfahren an der Mathematisch-Naturwissenschaftlichen Fakultät I der Humboldt-Universität zu Berlin zugrunde liegende Promotionsordnung ist mir bekannt.

Berlin, im Dezember 2013

8.3 Publikationsliste

Originalpublikationen

Kunert S , et al. (2013)
Neuron Navigator 1 is a positive modulator of mural cell motility influencing vessel branching morphology (Manuskript in Vorbereitung)

Meyer I, **Kunert S**, et al. (2012)
Altered microtubule equilibrium and impaired thrombus stability in mice lacking RanBP10 Blood **120**(17): 3594-60

Kunert S, et al. (2009)
The microtubule modulator RanBP10 plays a critical role in regulation of platelet discoid shape and degranulation. Blood **114**(27): 5532-5540.

Kongressbeiträge

1st French-UK Platelet Meeting, Toulouse, 9. - 10.10.2009
"The microtubule modulator RanBP10 plays a critical role in regulation of platelet discoid shape and degranulation" (**Poster**)

XXIInd European Platelet Meeting, Wittenberg, 11. – 13.10.2007
"RanBP10 is a beta1-tubulin binding protein that plays a role in microtubule assembly during platelet biogenesis" (**Vortrag**)